SIAM REVIEW
Vol. 48, No. 2, pp. 207–304

The Dynamics of Legged Locomotion: Models, Analyses, and Challenges*

Philip Holmes†
Robert J. Full‡
Dan Koditschek§
John Guckenheimer¶

Abstract. Cheetahs and beetles run, dolphins and salmon swim, and bees and birds fly with grace and economy surpassing our technology. Evolution has shaped the breathtaking abilities of animals, leaving us the challenge of reconstructing their targets of control and mechanisms of dexterity. In this review we explore a corner of this fascinating world. We describe mathematical models for legged animal locomotion, focusing on rapidly running insects and highlighting past achievements and challenges that remain. Newtonian body–limb dynamics are most naturally formulated as piecewise-holonomic rigid body mechanical systems, whose constraints change as legs touch down or lift off. Central pattern generators and proprioceptive sensing require models of spiking neurons and simplified phase oscillator descriptions of ensembles of them. A full neuromechanical model of a running animal requires integration of these elements, along with proprioceptive feedback and models of goal-oriented sensing, planning, and learning. We outline relevant background material from biomechanics and neurobiology, explain key properties of the hybrid dynamical systems that underlie legged locomotion models, and provide numerous examples of such models, from the simplest, completely soluble "peg-leg walker" to complex neuromuscular subsystems that are yet to be assembled into models of behaving animals. This final integration in a tractable and illuminating model is an outstanding challenge.

Key words. animal locomotion, biomechanics, bursting neurons, central pattern generators, control systems, hybrid dynamical systems, insect locomotion, Lagrangians, motoneurons, muscles, neural networks, periodic gaits, phase oscillators, piecewise holonomic systems, preflexes, reflexes, robotics, sensory systems, stability, templates

AMS subject classifications. 34C15, 34C25, 34C29, 34E10, 70E, 70H, 92B05, 92B20, 92C10, 92C20, 93C10, 93C15, 93C85

DOI. 10.1137/S0036144504445133

1. Introduction.

The question of how animals move may seem a simple one. They push against the world, with legs, fins, tails, wings, or their whole bodies, and

*Received by the editors July 12, 2004; accepted for publication (in revised form) April 28, 2005; published electronically May 2, 2006. This work was supported by DARPA/ONR through grant N00014-98-1-0747, the DoE through grants DE-FG02-95ER25238 and DE-FG02-93ER25164, and the NSF through grants DMS-0101208 and EF-0425878.
http://www.siam.org/journals/sirev/48-2/44513.html

†Department of Mechanical and Aerospace Engineering, and Program in Applied and Computational Mathematics, Princeton University, Princeton, NJ 08544 (pholmes@math.princeton.edu).
‡Department of Integrative Biology, University of California, Berkeley, CA 94720 (rjfull@socrates.berkeley.edu).
§Department of Electrical and Systems Engineering, University of Pennsylvania, Philadelphia, PA 19104 (kod@ese.upenn.edu).
¶Department of Mathematics and Center for Applied Mathematics, Cornell University, Ithaca, NY 14853 (gucken@cam.cornell.edu).

the rest is Newton's third and second laws. A little reflection reveals, however, that locomotion, like other animal behaviors, emerges from complex interactions among animals' neural, sensory, and motor systems, their muscle–body dynamics, and their environments [101]. This has led to three broad approaches to locomotion. Neurobiology emphasizes studies of central pattern generators (CPGs): networks of neurons in spinal cords of vertebrates and invertebrate thoracic ganglia, capable of generating muscular activity in the absence of sensory feedback (e.g., [142, 79, 260]). CPGs are typically studied in preparations isolated *in vitro*, with sensory inputs and higher brain "commands" removed [79, 163], and sometimes in neonatal animals. A related, reflex-driven approach concentrates on the role of proprioceptive[1] feedback and inter- and intralimb coordination in shaping locomotory patterns [258]. Finally, biomechanical studies focus on body–limb environment dynamics (e.g., [8]) and usually ignore neural detail. No single approach can encompass the whole problem, although each has amassed vast amounts of data.

We believe that mathematical models, at various levels and complexities, can play a critical role in synthesizing parts of these data by developing unified *neuromechanical* descriptions of locomotive behavior, and that in this exercise they can guide the modeling and understanding of other biological systems, as well as bio-inspired robots. This review introduces the general problem and, taking the specific case of rapidly running insects, describes models of varying complexity, outlines analyses of their behavior, compares their predictions with experimental data, and identifies a number of specific mathematical questions and challenges. We shall see that, while biomechanical and neurobiological models of varying complexity are individually relatively well developed, their integration remains largely open. The latter part of this article will therefore move from a description of work done to a prescription of work that is mostly yet to be done.

Guided by previous experience with both mathematical and physical (robot) models, we postulate that successful locomotion depends upon a hierarchical family of control loops. At the lowest end of the neuromechanical hierarchy, we hypothesize the primacy of mechanical feedback or *preflexes*[2]: neural clock-excited and tuned muscles acting through chosen skeletal postures. Here biomechanical models provide the basic description, and we are able to get quite far using simple models in which legs are represented as passively sprung, massless links. Acting above and in concert with this preflexive bottom layer, we hypothesize feedforward muscle activation from the CPG, and above that, sensory, feedback-driven reflexes that further increase an animal's stability and dexterity by suitably adjusting CPG and motoneuron outputs. Here modeling of neurons, neural circuitry, and muscles is central. At the highest level, goal-oriented behaviors such as foraging or predator-avoidance employ environmental sensing and operate on a stride-to-stride timescale to "direct" the animal's path. More abstract notions of connectionist neural networks and information and learning theory are appropriate at this level, which is perhaps the least well developed mathematically.

Some personal history may help to set the scene. This paper, and some of our recent work on which it draws, has its origins in a remarkable IMA workshop on

[1]Proprioceptive: activated by, related to, or being stimuli produced within the organism (as by movement or tension in its own tissues) [157]; thus: sensing of the body, as opposed to exteroceptive sensing of the external environment.

[2]Brown and Loeb [48, section 3] define a preflex as "the zero-delay, intrinsic response of a neuromusculoskeletal system to a perturbation" and they note that they are programmable via preselection of muscle activation.

gait patterns and symmetry held in June 1998, which brought together biologists, engineers, and mathematicians. At that workshop, one of us (RJF) pointed out that insects can run stably over rough ground at speeds high enough to challenge the ability of proprioceptive sensing and neural reflexes to respond to perturbations "within a stride." Motivated by his group's experiments on, and modeling of, the cockroach *Blaberus discoidalis* [135, 136, 317, 216] and by the suggestion of Brown and Loeb that, in rapid movements, "detailed" neural feedback (reflexes) might be partially or wholly replaced by largely mechanical feedback (preflexes) [49, 227, 48], we formulated simple mechanical models within which such hypotheses could be made precise and tested. Using these models, examples of which are described in section 5 below, we confirmed the preflex hypothesis by showing that simple, energetically conservative systems with passive elastic legs can produce asymptotically stable gaits [291, 292, 290]. This prompted "controlled impulse" perturbation experiments on rapidly running cockroaches [192] that strongly support the preflex hypothesis in *Blaberus*, as well as our current development of more realistic multilegged models incorporating actuated muscles. These allow one to study the differences between static and dynamic stability, and questions such as how hexapedal and quadrupedal runners differ dynamically (see sections 3.2 and 5.3).

Workshop discussions in which we all took part also inspired the creation of RHex, a six-legged robot whose unprecedented mobility suggests that engineers can aspire to achieving the capabilities of such fabulous runners as the humble cockroach [284, 208]. In turn, since we know (more or less) their ingredients, robots can help us better understand the animals that inspired them. Mathematical models allow us to translate between biology and engineering, and our ultimate goal is to produce a model of a "behaving insect" that can also inform the design of novel legged machines. More specifically, we envisage a range of models, of varying complexity and analytical tractability, that will allow us to pose and probe, via simulation and physical machine and animal experimentation, the mechanisms of locomotive control.

Biology is a broad and rich science, collectively producing vast amounts of data that may seem overwhelming to the modeler. (In [270], Michael Reed provides a beautifully clear perspective directed to mathematicians in general, sketching some of the difficulties and opportunities.) Our earlier work has nonetheless convinced us that simple models, which, in an exercise of creative neglect, ignore or simplify many of these data, can be invaluable in uncovering basic principles. We call such a model, containing the smallest number of variables and parameters that exhibits a behavior of interest, a *template* [131]. In robotics applications, we hypothesize the template as an attracting invariant submanifold on which the restricted dynamics takes a form prescribed to solve the specific task at hand (e.g., [53, 279, 254, 334]). In both robots and animals, we imagine that templates are composed [205] to solve different tasks in various ways by a supervisory controller in the central nervous system (CNS). The spring-loaded inverted pendulum (SLIP), introduced in section 2.2 and described in more detail in section 4.4, is a classical locomotion template that describes the center of mass behavior of diverse legged animals [68, 34]. The SLIP represents the animal's body as a point mass bouncing along on a single elastic leg that models the action of the legs supporting each stance phase: muscles, neurons, and sensing are excluded. (Acronyms such as CNS, CPG, and SLIP are common in biology, and so for the reader's convenience we list those used in this review in Table 1.)

Most of the models described below are templates, but we shall develop at least some ingredients of a more complete and biologically realistic model: an *anchor* in the terminology of [131]. A model representing the neural circuitry of a CPG, mo-

Table 1 *Acronyms commonly used in this article.*

AP	action potential	EMG	electromyograph
CNS	central nervous system	LLS	lateral leg spring
COM	center of mass	ODE	ordinary differential equation
COP	center of pressure	PRC	phase response curve
CPG	central pattern generator	RHex	name of hexapedal robot
DAE	differential-algebraic equation	SLIP	spring-loaded inverted pendulum
DOF(s)	degree(s) of freedom		

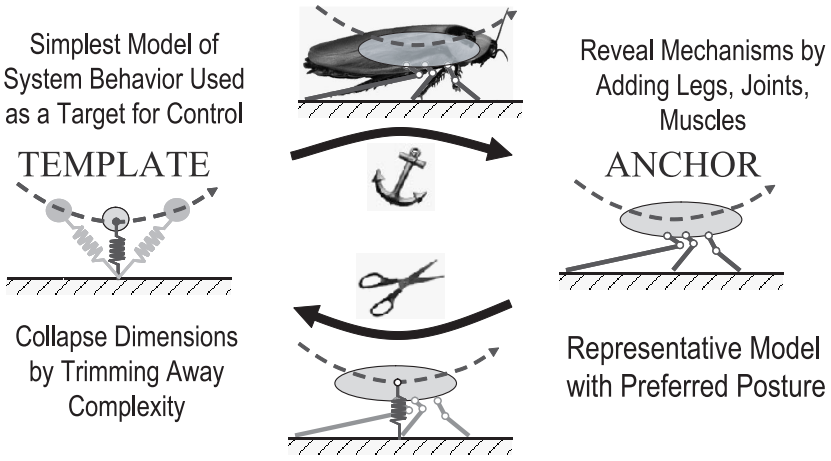

Fig. 1 *Templates and anchors: a preferred posture leads to collapse of dimension. The SLIP is shown at left, and a multilegged and jointed model at right. Both share the mass center dynamics of the insect (top). Reprinted from* [208] *with permission from Elsevier.*

toneurons, muscles, individual limb segments and joints, and ground contact effects, would exemplify an anchor. However, in spite of such complexity, we shall argue in section 3 that, under suitable conditions, animals with diverse morphologies and leg numbers, and many mechanical and yet more neural degrees of freedom (DOFs), run as if their mass centers were following SLIP dynamics [68, 34, 130]. Part of our challenge is to explain how their preflexive dynamics and reflexive control circuits cause their complex anchors to behave like this simple template, and to understand why nature should exercise such a mathematically attractive reduction of complexity, a process sketched in Figure 1. In dynamical systems terminology, this is a collapse of dimension in state space, which would follow from the existence of a center or inertial manifold with a strong stable foliation [89, 166]. While experimental evidence for a principle that selects postures for stereotyped movements has emerged from analyses of kinematic data, as noted in section 2.4.1, the complexity of detailed models has thus far largely prevented its theoretical analysis, but we shall give an example for an insect CPG in section 5.4.

Posture principles and the resulting collapse of dimension are examples of motor control policies. A key instance is gait selection in quadrupeds such as horses, which is normally explained in terms of minimization of metabolic cost [8] (gait changes for insects will be discussed in section 3.2). Such reduction and optimization ideas are central to the development of control and design principles in robotics and also seem likely to play a helpful role in elucidating biological principles. There is a vast

literature on motor control, parts of which are reviewed in section 2.4, where we describe both experimental evidence of and models for neuromechanical coupling via both reflexive and prereflexive feedback. However, as we shall see in section 5.4, for our main example, this integration still remains to be done.

Legged locomotion appears to be more tractable than swimming or flying, especially at moderate or high Reynolds numbers, since discrete reaction forces from a (relatively) rigid substrate are involved, rather than fluid forces requiring integration of the unsteady Navier–Stokes equations (but see the comments on foot-contact forces in section 2.3). Nonetheless, even at the simplest level, legged locomotion models have unusual features. Idealizing to a rigid body with massless elastic legs or to a linkage of rigid elements with torsional springs at the joints, we produce a mechanical system, but these systems are not classical. As feet touch down and lift off, the constraints defining the Lagrangians change. The resulting ordinary differential equations (ODEs) of motion describe *piecewise-holonomic*[3] mechanical systems, examples of more general *hybrid dynamical systems* [19], in which evolution switches among a finite set of vector fields, driven by event-related rules determined by the location of solutions in phase space. We shall meet our first example in section 2.1, and we discuss some properties of these systems in more detail in sections 4–5.

This paper's contents are as follows. Section 2 reviews earlier work on locomotion and movement modeling, introducing the relevant mechanical, biomechanical, neurobiological, and robotics background, and section 3 summarizes key experimental work on walking and running animals that inspires and informs previous and current modeling efforts. In section 4 we digress to describe an important class of hybrid dynamical systems that are central to locomotion models, and we describe some features of their analytical description and numerical issues that arise in simulations, ending with a sketch of the classical SLIP model. Section 5 constitutes a gallery of examples drawn from our own work, concentrating on models of horizontal plane dynamics of sprawled-posture animals, and of insects in particular. We start with a simple model of passive bipedal walking, special cases of which are (almost) soluble in closed form. We successively add more realistic features, culminating in our current hexapedal models that include CPG, motoneuron, and muscle models, and demonstrating throughout that the basic features of stable periodic gaits, possessed by the simplest templates, persist. We summarize and outline some major challenges in section 6.

We shall draw on a broad range of "whole animal" integrative biology, biomechanics, and neurobiology, as well as control and dynamical systems theory, including perturbation methods. We introduce relevant ideas from these disparate fields as they are needed, mostly via simple explicit examples, but the reader wishing to consult the biological literature might start with the reviews of Dickinson et al. [101] and Delcomyn [100]; the former is general, while the latter covers both insect locomotion per se and the use of ideas from insect studies in robotics. A recent special issue of *Arthropod Structure and Development* [278] collects several papers on insect locomotion, sensing, and bio-inspired robot design. For more general background, Alexander's monograph [8] provides an excellent introduction to, and summary of, the biomechanical literature on legged locomotion, flight, and swimming, going considerably beyond the scope of this article. We cite other texts and reviews in section 2.

Unlike genomics, locomotion studies are relatively mature: recent progress in neurophysiology, biomechanics, and nonlinear control and systems theory has poised

[3]This term was introduced by Ruina [282].

us to unlock how complex, dynamical, musculosketelal systems create effective behaviors, but a substantial task of synthesis remains. We believe that the language and methods of dynamical systems theory in particular, and mathematics in general, can assist that synthesis. Thus, our main goal is to introduce an emerging field in biology to applied mathematicians, drawing on relatively simple models as both examples of successful approaches and sources of interesting mathematical problems, some of which we highlight as "Questions." Our presentation therefore differs from that of many Survey and Review articles appearing in this journal in that we focus on modeling issues rather than mathematical methods per se. The models are, of course, formulated with the tools available for their analysis in mind; we sketch results that these tools afford, and we provide an extensive bibliography wherein mathematical results and biological details may be found.

We hope that this review will encourage the sort of multidisciplinary collaboration that we—a biologist, two applied mathematicians, and an engineer—have enjoyed over the past six years and that it will stimulate others to go beyond our own efforts.

2. Three Traditions: Biomechanics, Neurobiology, and Robotics. In developing our initial locomotion models, we discovered some relevant parts of three vast literatures. The following selective survey may assist the reader who wishes to acquire working background knowledge.

2.1. Holonomic, Nonholonomic, and Piecewise-Holonomic Mechanics. Before introducing a key locomotion model in section 2.2, the SLIP, we recall some basic facts concerning conservative mechanical and Hamiltonian systems. Holonomically constrained mechanical systems, such as linkages and rigid bodies, admit canonical Lagrangian and Hamiltonian descriptions [151]. (Holonomic constraints are equalities expressed entirely in terms of configuration—position—variables; nonholonomic constraints involve velocities in an essential—"nonintegrable"—manner, or are expressed via inequalities.) The symplectic structures [16] of holonomic systems strongly constrain the possible stability types of fixed points and periodic orbits: eigenvalues of the linearized ODEs occur in pairs or quartets [16, 2]: if λ is an eigenvalue, then so are $-\lambda$, $\bar{\lambda}$, and $-\bar{\lambda}$, where $\bar{\cdot}$ denotes complex conjugate. Thus, any "stable" eigenvalue in the left-hand complex half-plane has an "unstable" partner in the right-hand half-plane. Similar results hold for symplectic (Poincaré) mappings obtained by linearizing around closed orbits: an eigenvalue λ within the unit circle implies a partner $1/\lambda$ outside. Hence holonomic, conservative systems can at best exhibit neutral (Liapunov) stability; asymptotic stability is impossible.

Before proceeding to two simple examples, we remark that there is an elegant differential-geometric framework for treating nonholonomically constrained mechanical systems, based on ideas of Arnold [16] (cf. [234, 235]) and developed by Bloch, Crouch, Marsden, and others [38, 39, 40, 36, 54]. It provides unified Lagrangian and Hamiltonian descriptions for stability and control [41, 37, 71] and has been used to derive equations of motion, identify conserved quantities, and analyze equilibria and periodic orbits and their stability for such problems as the "snakeboard" [224], segmented crawlers [256], and underwater vehicles [340]. However, the mathematical machinery is rather technical, and we shall not require it for the models described in this article.

2.1.1. Nonholonomic Constraints and Partial Asymptotic Stability. Nonholonomic constraints, in contrast to holonomic ones, can lead to partial asymptotic stability. The Chaplygin sled [255] is an instructive example that also introduces other

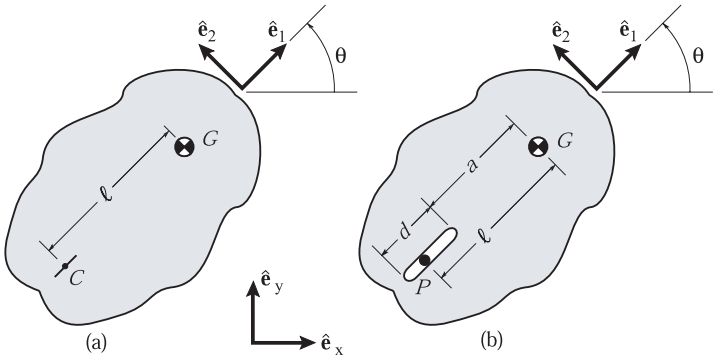

Fig. 2 (a) *The Chaplygin sled and* (b) *a piecewise-holonomic pegleg walker. The basis vectors* $(\hat{\mathbf{e}}_1, \hat{\mathbf{e}}_2)$ *specify body coordinate frames and* $(\hat{\mathbf{e}}_x, \hat{\mathbf{e}}_y)$ *span the inertial frame. Schematic adapted from Ruina* [282].

ideas that will recur. Here we shall follow the analysis of Ruina [282] using straightforward Newtonian force and moment balances, although the constrained Lagrangian framework can also be used, as described in [36, section 1.7].

Consider an "ice-boarder": a two-dimensional rigid body of mass m and moment of inertia I, free to move on a frictionless horizontal plane, equipped with a skate blade C, at a distance ℓ from the center of mass (COM) G, that exerts a force normal to the body axis (Figure 2(a)). The velocity vector at C is thereby constrained to lie along the body axis ($\mathbf{v}_C = v\hat{\mathbf{e}}_1$), although the body may turn about this point and v may take either sign (the skate can reverse direction). The angle θ specifies orientation in the inertial plane and the absolute velocity of G in terms of the body coordinate system is $\mathbf{v}_G = v\,\hat{\mathbf{e}}_1 + \ell\dot{\theta}\,\hat{\mathbf{e}}_2$.

Using the relations $\dot{\hat{\mathbf{e}}}_1 = \dot{\theta}\,\hat{\mathbf{e}}_2, \dot{\hat{\mathbf{e}}}_2 = -\dot{\theta}\,\hat{\mathbf{e}}_1$, for the rotating body frame, we first balance linear momentum,

$$\mathbf{F} = F_c\,\hat{\mathbf{e}}_2 = m\mathbf{a}_G = m(\dot{v} - \ell\dot{\theta}^2)\,\hat{\mathbf{e}}_1 + m(\ell\ddot{\theta} + \dot{\theta}v)\,\hat{\mathbf{e}}_2, \tag{1}$$

and then angular momentum about C', the nonaccelerating point in an inertial frame instantaneously coincident with C,

$$0 = (\mathbf{r_G} - \mathbf{r_{C'}}) \times m\mathbf{a}_G + I\ddot{\theta}\hat{\mathbf{e}}_z \;\Rightarrow\; m\ell(\ell\ddot{\theta} + v\dot{\theta}) + I\ddot{\theta} = 0\,. \tag{2}$$

The three (scalar) equations (1)–(2) determine the constraint force and the equations of motion:

$$F_c = m(\ell\ddot{\theta} + \dot{\theta}v)\,, \tag{3a}$$

$$\dot{s} = v\ ,\ \dot{\theta} = \omega\,, \tag{3b}$$

$$\dot{v} = l\omega^2\ ,\ \dot{\omega} = \frac{-m\ell v\omega}{m\ell^2 + I}\,, \tag{3c}$$

where s denotes arclength (distance) traveled by the skate and ω is the body angular velocity.

Equations (3) have a three-parameter family of constant speed straight-line motion solutions: $\bar{\mathbf{q}} = \{\bar{s} + \bar{v}t, \bar{\theta}, \bar{v}, 0\}^T$. Linearizing (3) at $\bar{\mathbf{q}}$ yields eigenvalues $\lambda_{1-3} = 0$ and $\lambda_4 = -(\frac{m\ell\bar{v}}{m\ell^2+I})$. The first three correspond to a family of solutions parameterized

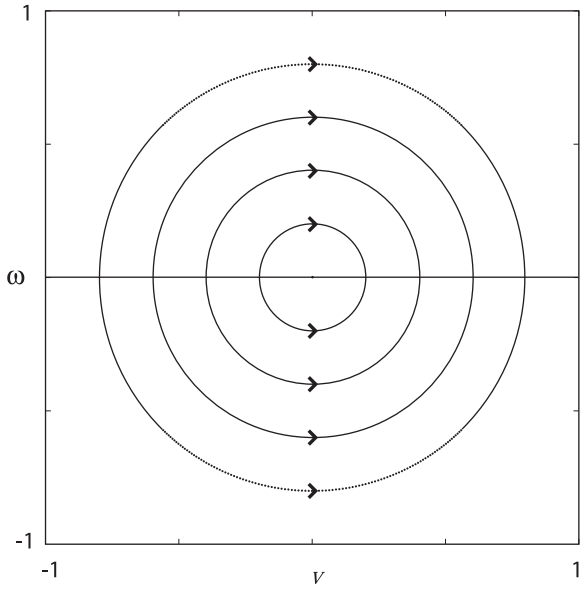

Fig. 3 *A phase portrait for the Chaplygin sled in appropriately scaled coordinates (in general, the solutions lie on ellipses* $T = \text{const.}$*).*

by starting point $\bar{s}$, velocity $\bar{v}$, and heading $\bar{\theta}$; λ_4 indicates asymptotic stability for $\ell\bar{v} > 0$ and instability for $\ell\bar{v} < 0$: stable motions require that the mass center precede the skate.

The global behavior is perhaps best appreciated via a phase portrait in the *reduced* phase space (v, ω) of linear and angular velocity (Figure 3). Noting that total kinetic energy,

$$T = \frac{m(v^2 + l^2\omega^2)}{2} + \frac{I\omega^2}{2}\,, \tag{4}$$

is conserved (since the constraint force $F_c\,\hat{\mathbf{e}}_1$ is normal to $\mathbf{v}_C$ and does no work), solutions of (3c) lie on the (elliptical) level sets of (4). The direction of the vector field, toward positive v, follows from the first equation of (3c). Explicit solutions as functions of time may be found in [83]. Taking $\ell > 0$ (skate behind COM), the line of fixed points $(\bar{v}, 0)$ with $\bar{v} < 0$ are unstable, while those with $\bar{v} > 0$ are stable. Typical solutions start with nonzero angular velocity, which may further grow, but which eventually decays exponentially as the solution approaches a fixed point on the positive v-axis. Angular momentum about the mass center G is *not* conserved since the constraint force exerts moments about G.

Figure 3 also shows that the $\bar{v} > 0$ equilibria are only *partially* asymptotically stable; as noted above, they belong to a continuum of such equilibria, and the eigenvalue with eigenvector in the $\bar{v}$ direction is zero. Indeed, the system is invariant under the group SE(2) of planar translations and rotations, and COM position $\mathbf{x}_G = (x, y)$ and orientation θ are cyclic coordinates [151].[4] This accounts for the other two direc-

[4]However, Noether's theorem [16] does *not* apply here: due to the constraint force neither linear nor angular momenta are conserved for general motions.

tions of neutral stability: $\bar{s}$ and $\bar{\theta}$. Such translation and rotation invariance will be a recurring theme in our analyses of horizontal plane motions.

The full three-DOF dynamics may be reconstructed from solutions $(v(t), \omega(t))$ of the reduced system (3c) by integration of (3b) to determine $(s(t), \theta(t))$, followed by integration of

$$\dot{x} = -v \sin\theta\,, \;\; \dot{y} = -v\cos\theta \tag{5}$$

to determine the path in inertial space.

2.1.2. Piecewise-Holonomic Constraints: Peg-Leg Walking. While the details of foot contact and joint kinematics, involving friction, deformation, and possible slipping, are extremely complex and poorly understood, one may idealize limb–body dynamics within a stance phase as a holonomically constrained system. As stance legs lift off and swing legs touch down, the constraint geometry changes; hence, legged locomotion models are piecewise-holonomic mechanical systems. Here we describe perhaps the simplest example of such a system.

Ruina [282] devised a discrete analog of Chaplygin's sled, in which the skate is replaced by a peg, fixed in the inertial frame and moving along a slot of length d, whose front end lies a distance a behind the COM. When it reaches one end of the slot, it is removed and instantly replaced at the other. Figure 2(b) shows the geometry: the coordinate system of 2(a) is retained. Ruina was primarily interested in the limit in which $d \to 0$ and the system approaches the continuous Chaplygin sled, but we noticed that the device constitutes a rudimentary and completely soluble, single-leg locomotion model: a peg-leg walker [83, 291]. The stance phase occurs while the peg is fixed, and (coincident) liftoff and touchdown correspond to peg removal and insertion. During stance the peg may slide freely, as in Ruina's example [282], move under prescribed forces or displacements $l(t)$, or move in response to an attached spring or applied force [291]. Here we take the simplest case, supposing that $l(t)$ is prescribed and increases monotonically (the peg moves backward relative to the body, thrusting it forward). The models of sections 4–5 will include both passive springs and active muscle forces; see also [291, section 2].

Pivoting about the (fixed) peg, the body's kinetic energy may be written as

$$T = \frac{1}{2} m(\dot{l}^2 + l^2\dot{\theta}^2) + \frac{1}{2} I\dot{\theta}^2\,, \tag{6}$$

so the Lagrangian is simply $L = T$, and since $l(t)$ is prescribed, there is but one DOF. Moreover, θ is a cyclic variable and Lagrange's equation simply states that

$$p_\theta = \frac{\partial L}{\partial \dot{\theta}} = (ml^2 + I)\,\dot{\theta} = \text{const.}: \tag{7}$$

angular momentum is conserved about P during each stride. However, at peg insertion, p_θ may suffer a jump due to the resulting angular impulse. Indeed, letting $\dot{\theta}(n^-)$ and $\dot{\theta}(n^+)$ denote the body angular velocities at the end of the $(n-1)$st and the beginning of the nth strides, and performing an angular momentum balance about the *new* peg position at which the impulsive force acts, we obtain the angular momentum in the nth stride as

$$p_{\theta_n} = (ma^2 + I)\,\dot{\theta}(n^+) = ma(a+d)\,\dot{\theta}(n^-) + I\,\dot{\theta}(n^-)\,.$$

Here the last expression includes the moment of linear momentum of the mass center at the end of the $(n-1)$st stride, computed about the *new* peg position: $a \times m(a+d)\,\dot{\theta}(n^-)$. Replacing angular velocities by momenta via (7), this gives

$$p_{\theta_n} = \left[\frac{ma(a+d)+I}{m(a+d)^2+I}\right] p_{\theta_{n-1}} \stackrel{\text{def}}{=} A p_{\theta_{n-1}}\,. \tag{8}$$

Thus, provided $A \neq 1$, angular momentum changes from stride to stride, unless $p_\theta = 0$, in which case the body is moving in a straight line along its axis. The change in body angle during the nth stride is obtained by integrating (7):

$$\theta((n+1)^-) = \theta(n^+) + p_{\theta_n} \int_0^\tau \frac{dt}{(ml^2(t)+I)} \stackrel{\text{def}}{=} \theta(n^+) + B p_{\theta_n}\,, \tag{9}$$

where τ is the stride duration.

Equations (8)–(9) form the (linear) stride-to-stride Poincaré map

$$\begin{pmatrix} \theta_{n+1} \\ p_{\theta_{n+1}} \end{pmatrix} = \begin{bmatrix} 1 & B \\ 0 & A \end{bmatrix} \begin{pmatrix} \theta_n \\ p_{\theta_n} \end{pmatrix}, \tag{10}$$

whose eigenvalues are simply the diagonal matrix elements. Echoing the ODE example of (3c) above, with its zero eigenvalue, one eigenvalue is unity, corresponding to rotational invariance, and asymptotic behavior is determined by the second eigenvalue A: if $|A| < 1$, $p_{\theta_n} \to 0$ as $n \to \infty$ and θ approaches a constant value; the body tends toward motion in a straight line at average velocity $v = \frac{1}{\tau}\int_0^\tau \dot{l}(t)dt = d/\tau$, with final orientation θ determined by the initial data. From (8), $A < 1$ for all $I, m, d > 0$ and $a > -d$, and $A > -1$ provided that $I > md^2/16$; for $a < -d$, $A > 1$. Hence, if the back of the slot lies behind G and the body shape and mass distribution are "reasonable," we have $|A| < 1$ (e.g., a uniform elliptical body with major and minor axes b, c has $I = m(b^2+c^2)/16$ and $b > d$ is necessary to accommodate the slot, implying that $I > md^2/16$).

Unlike the original Chaplygin sled, this discrete system is not conservative: energy is lost due to impacts at peg insertion (except in straight line motion), and energy may be added or removed by the prescribed displacement $l(t)$. However, regardless of this, the angular momentum changes induced by peg insertion determine stability with respect to angular velocity, and, if $|A| < 1$, the discrete sled asymptotically "runs straight." We shall see similar behavior in the energetically conservative models of sections 4.4 and 5.1. Here the stance dynamics is trivially summarized by conservation of angular momentum (7), and the stride-to-stride angular momentum mapping (8) determines stability. In more complex models, combinations of continuous dynamics within stance and touchdown/liftoff switching or impact maps are involved, resulting in higher-dimensional Poincaré maps (e.g., [237, 239, 238, 240, 138, 82, 249] and see section 5), but while coupled equations of motion must be integrated through stance to derive these maps, the stability properties of their fixed points are still partly determined by trading of angular momentum from stride to stride, much as in this simple example.

2.2. Mechanical Models and Legged Machines. As noted in the introduction, diverse species that differ in leg number and posture, while running fast, exhibit COM motions approximating that of a SLIP in the sagittal (vertical) plane [32, 244, 34, 130]. The same model also describes the gross dynamics of legged machines such as RHex [13, 11, 208], and as we shall show in section 5, a second template model

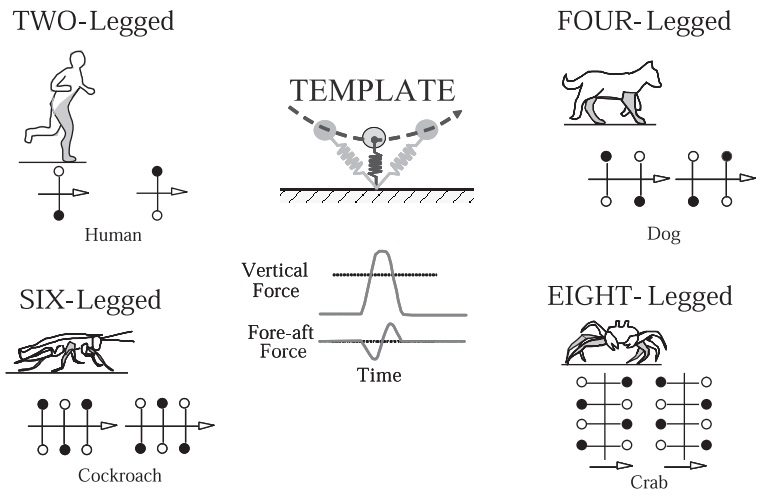

Fig. 4 *COM dynamics for running animals with two to eight legs. Groups of legs act in concert so that the runner is an effective biped, and mass center falls to its lowest point at midstride. Stance legs are shown shaded, with qualitative vertical and fore-aft force patterns through a single stance phase at bottom center. The SLIP, which describes these dynamics, is shown in the center of the figure.*

inspired by SLIP, the lateral leg spring (LLS) [291, 290], accounts equally well for horizontal plane dynamics. We shall briefly describe the SLIP and summarize some of the relevant mathematical work on it, returning to it in more detail in section 4. Further details of the biological data summarized below can be found in section 3.

At low speeds animals walk by vaulting over stiff legs acting like inverted pendula, exchanging gravitational and kinetic energy. At higher speeds, they bounce like pogo sticks, exchanging gravitational and kinetic energy with elastic strain energy [8, Chapters 6–7]. In running humans, dogs, lizards, cockroaches, and even centipedes, the COM falls to its lowest position at midstance as if compressing a virtual or effective leg spring, and rebounds during the second half of the step as if recovering stored elastic energy. In species with more than a pair of legs, the virtual spring represents the set of legs on the ground in each stance phase: typically two in quadrupeds, three in hexapods such as insects, and four in octopods such as crabs [124, 130] (Figure 4). This prompts the idealized mechanical model for motion in the sagittal (fore-aft/vertical) plane shown in the center of Figure 4, consisting of a massive body contacting the ground during stance via a massless elastic spring-leg [32, 244] (a point mass is sometimes added at the foot). The SLIP generalizes an earlier, simpler model: a rigid inverted pendulum, the "compass-walker" [247, 248] (cf. [242, 8]), which is more appropriate to low-speed walking. In running, a full stride divides into a stance phase, with one foot on the ground, and an entirely airborne flight phase, and the model employs a single leg to represent both left and right stance support legs. More complex running models have also been considered, starting with McGeer's study of a point mass body with a pair of massive legs attached to massless sprung feet [236].

Although the SLIP has appeared widely in the locomotion literature, we have found precise descriptions and mathematical analyses elusive. This prompted some of our own studies [297, 296, 298], including a recent paper in which we derived

analytical gait approximations and proved that the "uncontrolled" SLIP has stable gaits [145]. This fact was simultaneously, and independently, discovered via numerical simulation by Seyfarth et al. [306], who also matched SLIP parameters to human runners and proposed control algorithms [304, 305, 307]. We shall therefore spend some time setting up this model and sketching its analysis in section 4.4, both to exemplify issues involved in integrating hybrid dynamical systems and to prepare for more detailed accounts of LLS models in section 5. Here we informally review the main ideas.

In flight, the equations of ballistic motion are trivially integrated to yield the parabolic COM trajectory, assuming that resistance forces are negligible at the speeds of interest. Moreover, as we show in section 4.4, if the spring force developed in the leg dominates gravitational forces during stance, we may neglect the latter and reduce the two-DOF point mass SLIP to a single DOF system that may also be integrated in closed form. However, even in this approximation, the quadrature integrals typically yield special functions that are difficult to use, and asymptotic or numerical evaluations are required [298]. For small leg angles, one can linearize about the vertical position and obtain expressions in terms of elementary functions [143].

No matter how the stance phase trajectories are obtained, they must be matched to appropriate flight phase trajectories to generate a *full stride* Poincaré return map P. One then seeks fixed and periodic points of P which correspond to steady gaits, and investigates their bifurcations and stability. It is often possible to invoke bilateral (left–right) symmetry; for example, in seeking a symmetric period-1 gait of a biped modeled by a SLIP, it suffices to compute a fixed point of P, since although P includes only one stance phase, both right and left phases satisfy identical equations. However, there may be additional reflection- and time-shift–symmetric periodic orbits that would correspond to period-2 points of P.

More realistic models of legged locomotion, with extended body and limb components requiring rotational as well as translational DOFs, generally demand entirely numerical solutions, and merely deriving their Lagrangians may be a complex procedure, requiring intensive computer algebra. Nonetheless, fifteen years ago McGeer [237, 238, 239, 240] designed, built, and (with numerical assistance) analyzed passive-dynamic walking machines with rigid links connected by knee joints, in which the dynamics was restricted to the sagittal plane. These machines walk in a human-like manner down a shallow incline, the gravitational energy thus gained balancing kinetic energy lost in foot impacts. Ruina and his colleagues have recently carried out rather complete studies of simplified models of these machines [81, 138], as well as of a three-dimensional version, which they have shown is dynamically stable but statically unstable [84, 82, 87]. They and other groups have also studied energetic costs of passive walking and built powered walkers inspired by the passive machines [86].

In the robotics literature there are many numerical and a growing number of empirical studies of legged locomotion, incorporating varying degrees of actuation and sensory feedback to achieve increasingly useful gaits. Slow walking machines whose limited kinetic energies cannot undermine their quasi-static stability (i.e., with gaits designed to insure that the mass center always projects within the convex hull of a tripod of legs) have been successfully deployed in outdoor settings for years [329]. The first dynamically stable machines were SLIP devices built by Raibert two decades ago [268], but their complexity limited initial stability analyses to single DOF simplifications [207]. The more detailed analysis of SLIP stability that we will pursue in section 4.4 is directly relevant to these machines. More recently, in laboratory settings, completely actuated and sensed mechanisms have realized dynamical gaits

whose stability can be established and tuned analytically [334], using inverse dynamics control.[5] However, the relevance of such approaches to rapid running of powered autonomous machines is unclear, since they require a very high degree of control authority. In contrast, the analytically messier, "low-affordance" controlled robot RHex, introduced in section 1, is the first autonomous, dynamically stable, legged machine to successfully run over rugged and broken outdoor terrain [284]. Its design was inspired by preflexively stabilized arthropods and the notion of centralized/decentralized feedforward/feedback locomotion control architectures to be outlined in section 2.4 [208].

Extensions of the analysis introduced in section 4.4 are relevant to RHex's behavior [12, 11], but a gulf remains between the performance we can elicit empirically and what mathematical analyses or numerical simulations can explain. Modeling is still too crude to offer detailed design insights for dynamically stable autonomous machines in physically interesting settings. For example, in even the most anchored models, complicated natural foot–ground contacts are typically idealized as frictionless pin joints or smooth surfaces that roll without slipping. Similarly, in the models cited above and later in this paper, motion typically occurs over idealized horizontal or uniformly sloping flat terrain.

Accounting for inevitable foot slippage and loss of contact on level ground is necessary for simulations relevant to tuning physical robot controls [285], but far from sufficient for gaining predictive insight into the likely behavior of real robots traveling on rough terrain. It is still not even clear which details of internal leg and actuator mechanics must be included in order to achieve predictive correspondence with the physical world. For example, numerical studies of more realistically underactuated and incompletely sensed autonomous runners, similar to RHex, fail to predict gait stability even in the laboratory, if motor torque and joint compliance models are omitted [266, 267]. Modeling foot contacts over more complex topography in a manner that is computationally feasible and physically revealing is an active area of mechanics research [341] that does not yet seem ripe for exploitation in robot controller design, much less amenable to mathematical analysis. In any case, since the bulk of this paper is confined to template models such as the SLIP, we shall largely ignore these issues.

We regard the SLIP and similar templates as passive systems, since energy is neither supplied nor dissipated, although in practice some effort must be expended to repoint the leg during flight. In the case of McGeer's and Ruina's passive walkers, energy lost in foot impacts and friction is replaced by gravitational energy supplied as the machine moves down a slight incline. As noted above, more aggressively active hopping robots have been built by Raibert and colleagues [268, 207]. In that work, however, it was generally *assumed* that state variable feedback would be needed, not just to replace lost energy, but to achieve stable motions at all. The studies of [306] and [145], summarized above, and a recent numerical study of an actuated leg–body linkage [249], suggest that this is not necessary.

The nature of directly sensed information required for stabilization—the so-called "static output feedback stabilization" problem—is a central question of control theory that is in general algorithmically intractable even for linear, time-invariant dynamical systems [42]. In the very low dimensional setting of present interest, where algorithmic

[5] Inverse dynamics employs high-power joint actuators to inject torques computed as functions of the complete sensed state, together with an accurate kinematic and dynamical model and high-speed computation. These torques cancel the natural dynamics and replace them with more analytically tractable terms designed to yield desired closed-loop behavior.

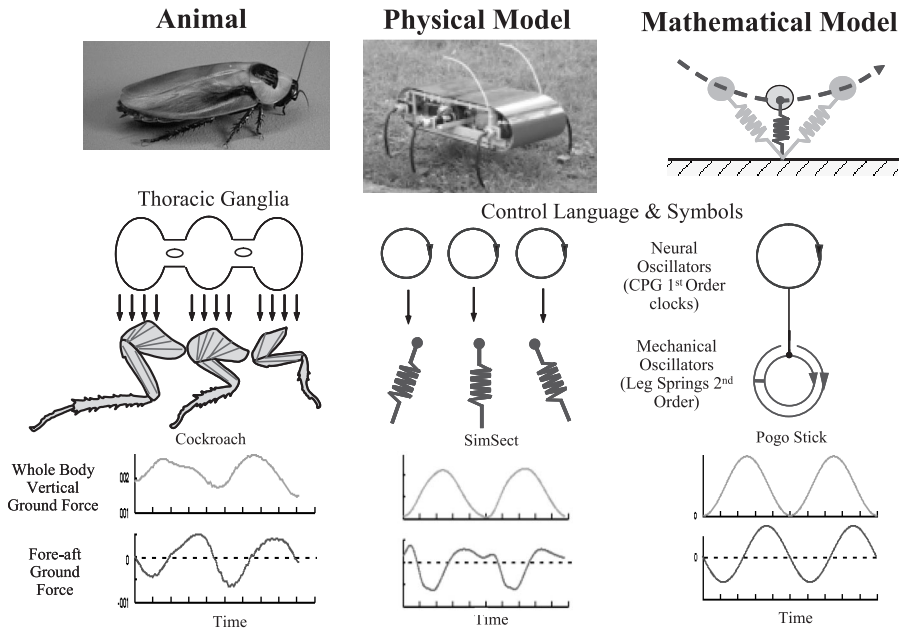

Fig. 5 *The SLIP as a model for the COM dynamics of animals and legged machines. Left panel shows the cockroach* Blaberus discoidalis *with schematic diagrams of thoracic ganglia, containing the CPG, legs, and muscles. Central panel shows the robot RHex, with motor-driven passively sprung legs, and right panel shows SLIP. Single circles denote neural oscillators or "clocks"; double circles denote mechanical oscillators. Lower panels show typical vertical and fore-aft forces experienced during rapid running by each system. Reprinted from* [208] *with permission from Elsevier.*

issues hold less sway, two complications still impede the corresponding local analysis. First, the representation of physical sensors in abstracted SLIP models does not seem to admit an obvious form, so that alternative "output maps" relative to which stabilizability might nominally be assessed are missing. Second, neither the hybrid Poincaré map nor even its Jacobian matrix (from which the local stabilizability properties are computed) can be derived in closed form. We have recently been able to show [12] that deadbeat[6] stabilization is impossible in the absence of an inertial frame sensor, but the question of sensory burden required for SLIP stabilization remains open.

Nonetheless, the SLIP is a useful model on which to build, and so we close this section by summarizing the common ground among animals, legged machines, and SLIP in Figure 5, which also introduces the symbols for neural and mechanical oscillators that we shall use again below. While the sources and mechanisms of leg movements range from CPG circuits, motoneurons, and muscles to rotary motors synchronized by proportional derivative controllers, the net behavior of the body and coordinated groups of legs in both animals and legged machines approximates a mass bouncing on a passive spring.

2.3. Neural Circuitry and CPGs. Animal locomotion is not, of course, a passive mechanical activity. Muscles supply energy lost to dissipation and foot impacts; they

[6]Deadbeat control corrects deviations from a desired trajectory in a single step, so that control objectives are met immediately.

may also remove energy, retarding and managing inertial motions (e.g., in downhill walking), or in agonist–antagonist phasic relationships, e.g., [134]. The timing of muscular contractions, driven by a CPG, shapes overall motions [17, 260, 232], but in both vertebrates [79, 313] and invertebrates [5] motor patterns arise through coordinated interaction of distributed, reconfigurable [232] neural processing units incorporating proprioceptive and environmental feedback and goal-oriented "commands."

Whereas classical physics can guide us through the landscape of mechanical locomotion models as reviewed in sections 2.1–2.2, there is no obvious recourse to first principles in neural modeling. Rather, one must choose an appropriate descriptive level and adopt a suitable formal representation, often phenomenological in nature. In this section we introduce models at two different levels that address the rhythm generation, coordination, and control behaviors to be reviewed in section 2.4 and taken up again in greater technical detail in section 5.

2.3.1. Single Neuron Models and Phase Reduction. Neurons are electrically active cells that maintain a potential difference across their membranes, modulated by the transport of charged ions through gated channels in the membrane. They fire action potentials (spikes), both spontaneously and in response to external inputs, and they communicate via chemical synapses or direct electrical contact. Neurons admit descriptions at multiple levels. They are spatially complex, with extensive dendritic trees and axonal processes. Synaptic transmission involves release of neurotransmitter molecules from the presynaptic cell, their diffusion across multiple distributed synaptic clefts, and complex receptor biochemistry within the postsynaptic cell. Texts such as [193, 95] provide extensive background on experimental and theoretical neuroscience.

These complexities pose wonderful mathematical challenges, but here they will be subsumed into the single compartment ODE description pioneered by Hodgkin and Huxley [180]. This assumes spatial homogeneity of membrane voltage within the cell and treats the distributed membrane transport processes collectively as ionic currents, determined via gating variables that describe the fraction of open channels. See [1, 200] for good introductions to such models, which take the form

$$C\dot{v} = -I_{\text{ion}}(v, w_1, \ldots, w_n, c) + I_{\text{ext}}(t), \tag{11a}$$

$$\dot{w}_i = \frac{\gamma_i}{\tau_i(v)} \left(w_{i_\infty}(v) - w_i\right), \qquad i = 1, \ldots, N. \tag{11b}$$

Equation (11a) describes the voltage dynamics, with C denoting the cell membrane capacitance, I_{ion} the multiple ionic currents, and $I_{\text{ext}}(t)$ synaptic and external inputs. Equations (11b) describe the dynamics of the gating variables w_i, each of which represents the fraction of open channels of type i, and γ_i is a positive parameter. At steady state, gating variables approach voltage-dependent limits $w_{i_\infty}(v)$, usually described by sigmoidal functions

$$w_{i_\infty}(v; k_{i_0}, v_{i_{th}}) = \frac{1}{1 + e^{-k_{i_0}(v - v_{i_{th}})}}, \tag{12}$$

where k_{i_0} determines the steepness of the transition occurring at a threshold potential $v_{i_{th}}$. Gating variables can be either *activating* ($k_{i_0} > 0$), with $w_{i_\infty} \approx 1$ for depolarized voltages $v > v_{i_{th}}$ and $w_{i_\infty} \approx 0$ for hyperpolarized levels $v < v_{i_{th}}$, or *inactivating* ($k_{i_0} < 0$), with $w_{i_\infty} \approx 1$ when hyperpolarized and $w_{i_\infty} \approx 0$ when depolarized. The timescale τ_i is generally described by a voltage-dependent function of the form

$$\tau_i(v; k_{i_0}, v_{i_{th}}) = \operatorname{sech}\left(k_{i_0}(v - v_{i_{th}})\right). \tag{13}$$

The term I_{ion} in (11a) is the sum of individual ionic currents I_α, each of which takes the form

$$I_\alpha(v, \mathbf{w}) = \bar{g}_\alpha \, w_i^a w_j^b \, (v - E_\alpha) \,, \tag{14}$$

where E_α is a (Nernstian) reversal potential, $\bar{g}_\alpha$ is the maximal conductance for all channels open, and the exponents a, b can be thought of as representing the number of subunits within a single channel necessary to open it. Hodgkin and Huxley's model [180, 200] of the giant axon of squid included a sodium current with both activating and inactivating gating variables (m, h) and a potassium current with an activating variable alone (n), and they fitted sigmoids of the form (12) to space-clamped experimental data. Many other currents, including calcium, chloride, calcium-activated potassium, etc., have since been identified and fitted, and a linear leakage current $I_{\text{L}} = \bar{g}_{\text{L}} \, (v - E_{\text{L}})$ is usually also included.

The presence of several currents, each necessitating one or two gating variables, makes models of the form (11) analytically intractable. However, often several of the gating variables have fast dynamics, i.e., $\gamma_i/\tau_i(v)$ is relatively large in the voltage range of interest: such variables can then be set at their equilibrium values $w_j = w_{j_\infty}(v)$ and their dynamical equations dropped. Likewise, functionally related variables with similar timescales may be lumped together [275]. This reduction process, pioneered in FitzHugh's polynomial reduction of the Hodgkin–Huxley model [122, 123] (cf. [281, 202, 152, 200]), may be justified via geometric singular perturbation theory [194]. We shall appeal to it in deriving a three-dimensional model for bursting neurons in section 5.4.

A deeper geometrical fact underlies this procedure and allows us to go further. Spontaneously spiking neuron models typically possess hyperbolic (exponentially) attracting limit cycles [166]. Near such a cycle, Γ_0, of period T_0, the $(N+1)$-dimensional state space of (11) locally splits into a phase variable ϕ along Γ_0 and a foliation of transverse *isochrons*: N-dimensional manifolds M_ϕ with the property that any two solutions starting on the same leaf M_{ϕ_0} are mapped by the flow to another leaf M_{ϕ_1} and hence approach Γ_0 with the same asymptotic phase [165]. Writing (11) in the form

$$\dot{\mathbf{x}} = \mathbf{f}(\mathbf{x}) + \epsilon \mathbf{g}(\mathbf{x}, \dots), \tag{15}$$

where $\mathbf{g}(\mathbf{x}, \dots)$ represents external (synaptic) inputs, choosing the phase coordinate such that $\dot{\phi} = \omega_0 = 2\pi/T_0$, and employing the chain rule, we thus obtain the scalar oscillator equation:

$$\dot{\phi} = \omega_0 + \epsilon \frac{\partial \phi}{\partial \mathbf{x}} \cdot \mathbf{g}(\mathbf{x}(\phi), \dots) \, |_{\Gamma_0(\phi)} + \mathcal{O}(\epsilon^2) \,. \tag{16}$$

Here we implicitly assume that coupling and external influences are weak ($\epsilon \ll 1$), and that Γ_0 perturbs to a nearby hyperbolic limit cycle Γ_ϵ, allowing us to compute the scalar phase equation by evaluating along Γ_0. For neural models in which inputs and coupling enter only via the first equation (11a), $\frac{\partial \phi}{\partial v} \stackrel{\text{def}}{=} z(\phi)$ is the only nonzero component in the vector $\frac{\partial \phi}{\partial \mathbf{x}}$. This *phase response curve* (PRC) $z(\phi)$ describes the sensitivity of the system to inputs as a function of phase on the cycle. It may be computed asymptotically, using normal forms, near local and global bifurcations at which periodic spiking begins; see [114, 46].

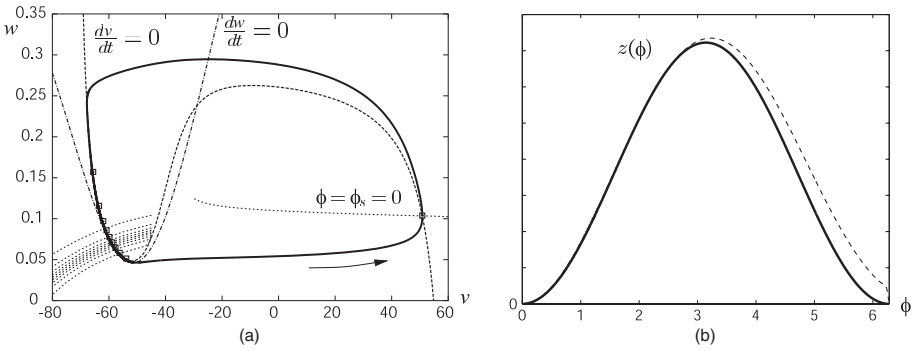

Fig. 6 (a) *Phase space structure for a repetitively spiking Rose–Hindmarsh model, showing attracting limit cycle and isochrons. The thick dashed and dash-dotted lines are nullclines for* $\dot{v} = 0$ *and* $\dot{w} = 0$*, respectively, and squares show points on the perturbed limit cycle, equally spaced in time, under a small constant input current* I_{ext}*.* (b) *PRCs for the Rose–Hindmarsh model; the asymptotic form* $z(\phi) \sim [1 - \cos\phi]$ *is shown solid, and numerical computations near the saddle node bifurcation on the limit cycle yield the dashed result. For details see* [47]*, from which these figures were adapted.*

Figure 6 shows an example of isochrons and PRCs computed for a two-dimensional reduction due to Rose and Hindmarsh [281] of a multichannel model of Connor, Walters, and McKown [88]:

$$\begin{aligned} C\dot{v} &= [I^b - g_{\mathrm{Na}} m_\infty(v)^3(-3(w - Bb_\infty(v)) + 0.85)(v - E_{\mathrm{Na}}) \\ &\quad -g_K w(v - E_{\mathrm{K}}) - g_L(v - E_{\mathrm{L}}) + I^{ext}], \\ \dot{w} &= (w_\infty(v) - w)/\tau_w(v)\,, \end{aligned} \tag{17}$$

where the functions $m_\infty(v), b_\infty(v), w_\infty(v)$, and $\tau_w(v)$ are of the forms (12)–(13). Since the gating variables have been reduced to a single scalar w by use of the timescale separation methods noted above, the isochrons are one-dimensional arcs. Note that these arcs, equally spaced in time, are bunched in the refractory region in which the nullclines almost coincide and flow is very slow. In fact, as the bias current I^b is reduced, a saddle-node bifurcation occurs on the closed orbit of (17), and use of normal form theory [166] at this bifurcation allows analytical approximation of the PRC [114], as shown in panel (b).

The phase reduction method was originally developed by Malkin [228, 229], and independently, with biological applications in mind, by Winfree [338]; also see [118, 114, 183]. It has recently been applied to study pairs of cells electrically coupled by gap junctions [225] and the response of larger populations of neurons to stimuli [46, 47]. We shall use it below, followed by the averaging theorem [166, 116, 210, 183], to simplify the CPG model developed in section 5.4.

2.3.2. Integrate-and-Fire Oscillators. We shall shortly return to phase descriptions, but first we mention another common simplification. Since action potentials are typically brief ($\sim$ 1 msec) and stereotyped, the major effect of inputs is in modulating their timing, and this occurs during the refractory period as the membrane potential v recovers from post-spike hyperpolarization and responds to synaptic inputs. Integrate-and-fire models [1, 95] neglect the details of channel dynamics and

consider the membrane potential alone, subject to the leakage current and inputs:

$$\dot{v} = \bar{g}_{\mathrm{L}}(v_\infty - v) + \sum_{i,j}(v - E_{\mathrm{syn},j})A(t - t_{i,j})\,. \tag{18}$$

Thus, v increases toward a limit v_∞, and when (and if) it crosses a preset threshold v_{thres} it is reset to 0 (another example of a hybrid system). In this model postsynaptic (external) current inputs to the cell are typically characterized by a function $A(t)$ (often of the type $t^k \exp(-k_j(t - \tau_j))$, summed over input cells j and the times $t_{i,j}$ at which they spike. This allows relatively detailed inclusion of time constants and reversal potentials $E_{\mathrm{syn},j}$ of specific neurotransmitters without modeling the spike explicitly (e.g., [74, 50]).

2.3.3. Networks of Phase Oscillators. Phase oscillators have the advantage of mathematical tractability—along with integrate-and-fire models they are common templates of mathematical neuroscience—but in the past they were rarely anchored in biophysically based models such as those of section 2.3.1. Notable exceptions occur in the work of Hansel et al. [171, 172, 173], and recently Kopell and her colleagues [195, 3] have used phase reduction and the related "spike time response" method to study network synchrony ([195] is especially relevant here, being concerned with locomotory CPGs). The PRC and averaging methodology described above provides a principled way to achieve this, and in section 5.4 we shall summarize current work on insect CPGs [147] in which it is used to derive oscillator networks from (relatively) detailed ionic current models. However, in many cases (including that of the cockroach) the precise neural circuitry of CPGs remains unknown (although there are exceptions, e.g., [65]), and phase descriptions are useful in such cases where little or incomplete information on neuron types, numbers, or connectivity is available.

In such models, each phase variable may represent the state of one cell or, more typically, a *group* of cells, including interneurons and motoneurons, constituting a quasi-independent, internally synchronous subunit of the CPG. This was the approach adopted in early work on the lamprey notocord [76, 78], in which each oscillator describes the output of a spinal cord segment, or a pair of oscillators, mutually inhibiting and thus in antiphase, describe the left and right halves of a segment. In reality, there are probably $\mathcal{O}(100)$ active neurons per segment, and the architectures of individual "oscillators" can extend over as many as four segments [80, 76]. Murray's book [251] introduces and summarizes some of this work.

Since we will return to them in section 5.4, it is worth describing phase models for networks of oscillators in more detail. They take the general form

$$\dot{\phi_i} = f_i(\phi_1, \phi_2, \ldots, \phi_N),\ i = 1, \ldots, N\,, \tag{19}$$

where the f_i are periodic in each variable; such a system defines a flow on an N-dimensional torus. In many cases a special form is assumed in which each uncoupled unit rotates at constant speed and coupling enters only in terms of phase differences $\phi_j - \phi_k$. As noted in section 2.3.1 and outlined for an insect CPG example of section 5.4, this form may be justified by assuming that each underlying "biophysical" unit has a normally hyperbolic attracting limit cycle [166] and that coupling is sufficiently weak, and by appeal to the averaging theorem; see [183, 116, 118] for more details.

In the simplest possible case of two oscillators, symmetrically coupled, we obtain ODEs whose right-hand sides contain only the phase difference $\phi_1 - \phi_2$:

$$\dot{\phi_1} = \omega_1 + f(\phi_1 - \phi_2)\,,\ \dot{\phi_2} = \omega_2 + f(\phi_2 - \phi_1)\,; \tag{20}$$

note that we allow the uncoupled frequencies ω_j to differ, but here the functions $f_i = f$ are supposed identical. Letting $\theta = \phi_1 - \phi_2$ and subtracting (20), we obtain the scalar equation

$$\dot{\theta} = (\omega_1 - \omega_2) + f(\theta) - f(-\theta)\,. \tag{21}$$

A fixed point $\bar{\theta}$ of (21) corresponds to a *phase-locked* solution of (20) with frequency

$$\bar{\omega} = \omega_1 + f(\bar{\theta}) = \omega_2 + f(-\bar{\theta})\,,$$

as may be seen by considering the differential equation for the phase sum $\phi_1 + \phi_2$. In the special case that f is an odd function and $f(-\theta) = -f(\theta)$, the resulting frequency is the average $(\omega_1 + \omega_2)/2$ of the uncoupled frequencies. For smooth functions, stability is determined by the derivative $f'(\theta) - f'(-\theta)|_{\theta=\bar{\theta}}$—negative (resp., positive) for stability (resp., instability)—and stability types alternate around the phase difference circle. Fixed points typically appear and disappear in saddle-node bifurcations [166], which occur when the value of a local maximum or minimum of $f(\theta) - f(-\theta)$ coincides with $\omega_1 - \omega_2$. The number of possible fixed points is bounded above by the number of local maxima and minima of this function, but hyperbolic fixed points must always occur in stable and unstable pairs, since they lie at neighboring simple zeros of $f(\theta) - f(-\theta)$.

Coupling typically imposes a relation between the oscillator phases, determined by inverting the fixed-point relation

$$f(\theta) - f(-\theta) = \omega_2 - \omega_1\,, \tag{22}$$

and vector equations analogous to (22) emerge in the case of a chain of N oscillators with nearest-neighbor coupling [76]. The original lamprey model of [76] took the simplest possible odd function $f(\theta) = -\alpha \sin(\theta)$ (the negative sign being chosen so that "excitatory" coupling would have a positive coefficient). In this case, a stable solution with a nonzero phase lag, corresponding to the traveling wave propagating from head to tail responsible for swimming, requires a nonzero frequency difference $\omega_i - \omega_{i+1} > 0$ from segment to segment. At the time of the original study [76], evidence from isolated sections taken from different parts of spinal cords suggested that there was indeed a frequency gradient, with rostral (head) segments oscillating faster in isolation than caudal (tail) segments. Subsequent experiments showed this not to be the case: a significant fraction of animals was found to have caudal frequencies exceeding rostral ones, and to account for the traveling wave in this case Kopell and Ermentrout [116, 210] introduced nonodd, "synaptic," coupling functions with a "built-in" phase lag. Indeed, as they pointed out, although electrotonic (gap junction) coupling leads to functions that vanish when membrane voltages are equal, the biophysics of synaptic transmission implies that nonzero phase differences typically emerge even if the cells fire simultaneously.

Other groups have studied networks of planar "lambda-omega" or van der Pol–type oscillators (cf. [166]) that have simple expressions in polar coordinates, making the PRC analyses of section 2.3.1 particularly simple. The bio-inspired CPG for robotics of [52] is a recent example that can produce various gaits with suitable coupling. But regardless of oscillator details, rather powerful general conclusions may be drawn regarding possible periodic solutions of symmetric networks of oscillators using the group-theoretic methods of bifurcation with symmetry [153, 156]. Golubitsky, Collins, and their colleagues have applied these ideas to CPG models, thereby

finding network architectures that support numerous gait types, especially those of quadrupeds [154, 155], although Collins and Stewart also have a paper specifically on insect gaits [85]. Here the symmetries are discrete, primarily the left–right bilateral body symmetry and (approximate) front–hind leg symmetries; we shall see examples in the insect CPG model of section 5.4. In sections 2.1–2.2 and sections 4–5, the continuous symmetry of planar translations and rotations with respect to the environment plays a different role in biomechanical models.

We end by briefly noting interesting work of Beer and others in which CPG networks are "evolved" using genetic algorithms [23, 72, 22, 189]. Within a basic architecture new cells and connections can be established, and connection weights changed. This method could be extended to explore multiparameter spaces of coupled neuromechanical systems

2.4. On Control and Coordination. We have seen that CPGs, including the motoneurons that generate their outputs, acting in a feedforward manner through muscles, limbs, and body, can produce motor segments that might constitute a "vocabulary" from which goal-oriented locomotory behaviors are built. As we shall suggest in sections 5.4–5.5, integrated, neuromechanical CPG–muscle–limb–body models are still largely lacking, but the analysis of simple neural and mechanical oscillators, such as the phase and SLIP models introduced above, can elucidate animal behavior [206] as well as suggest coordination strategies for robots [205]. However, assembling these motor segments, and adapting them to environmental demands, requires both reflexive feedback and supervisory control. We therefore end this section with a discussion of control issues, focusing on two specific questions, namely: How are the distributed neural processing units, referred to at the start of section 2.3, coordinated? What roles do they play in the selection, control, or modulation of the distributed excitable musculoskeletal mechanisms?

Little enough is presently known about these questions that motor science may perhaps best be advanced by developing prescriptive, refutable hypotheses. Here "prescriptive" loosely denotes a control procedure that can be shown mathematically (or perhaps empirically, in a robot) to be in a logical relationship of necessity or sufficiency with respect to a specific behavior. "Refutable" implies that the behavior admits biological testing. Before sketching our working version of these hypotheses for insect locomotion in section 3, we review parts of a vast relevant literature.

2.4.1. Mechanical Organization: Collapse of Dimension and Posture Principles. Some forty years ago, A.N. Bernstein [24, 25] identified the "degrees-of-freedom problem" in neuromuscular control, which may be exemplified as follows. Typical limb movements, such as reaching to pick up a small object from a table, require precise fingertip placement, but leave intermediate hand, arm, wrist, elbow, and shoulder joint angles and positions undetermined. Moreover, some limbs have fewer DOFs than the number of muscles actuating them (e.g., seven muscles actuate the three index-finger joints that together give it four DOFs[7] [324]). How are these (statically indeterminate) DOFs "programmed" and how are multiple muscles, possibly including co-activated extensors and flexors for the same joint, coordinated throughout such movements? Are coordination patterns unique within species?

Such patterns certainly exist. Empirical laws describing movement trajectories both in the inertial (world) frame and within the body–limb frame have been formulated and their neural correlates sought. For example, a power law inversely relating

[7]The metacarpophalangeal (top) joint rotates about two axes, the others about one.

speed to path curvature, originally derived from observations of voluntary reaching movements [220], has been proposed to describe diverse mammalian motor patterns, including walking [190]. Moreover, primate motor cortex recordings of voluntary arm movements [295] reveal a neural velocity "reference signal" that precedes and predicts observed mechanical trajectories, prescribing via variable time delay the power law of [220]. This suggests partition of a reference trajectory into modular constituents of a putative motor vocabulary and meshes with yet more prescriptive notions of optimal trajectory generation whose cost functionals can be shown to generate signals that respect such power laws [319, 271].

However, interpreting these descriptive patterns is challenging. Trajectories generated by low-frequency harmonic oscillations fit to motion-capture data in joint space *also* respect a power law as an accidental artifact of nonlinear kinematics [287]. Moreover, when these fitted oscillations grow large enough in amplitude to violate the pure power law, they do so in a punctuated manner, again apparently accidentally evoking a composed motor vocabulary. Moreover, in a critique of proposals addressing the role of neural precursors to voluntary arm motion, Todorov [318] has pointed out that motor cortex signals have been correlated in various papers with almost all possible physical task space signals: an array of correspondences that could not be simultaneously realized. In sum, power law and similar phenomenological descriptions do not seem to impose sufficient constraints on the structure of dynamical coordination mechanisms to support the refutable hypotheses that we seek.

The coordination models of central concern in this review, to be introduced later in this section, at least suffice to explain the observed mechanical patterns associated with *collapse of dimension*: the emergence of a low-dimensional attractive invariant submanifold in a much larger state space. This dynamical collapse appears to be associated with a *posture principle*: the restriction of motion to a low-dimensional subspace within a high-dimensional joint space. A kinematic posture principle has been discovered in mammalian walking [219], as demonstrated by planar covariation of limb elevation angles which persists in the face of large variations in steady state loading conditions [190]. In studying static grasping by human hands Valero-Cuevas [324, 325, 326] has shown that activation patterns of the seven muscles of the index finger when producing maximal force in five well-specified directions are subject-independent and predicted to take the finger to its performance limits, suggesting common motor strategies motivated by biomechanical constraints. Moreover, the activation patterns employed, while uniquely determined at the boundaries of feasible force-torque space, continue to be used to produce submaximal forces. This implies a solution to the DOF problem that circumvents redundancy (of three dimensions in this case) by adopting the unique solution imposed by constraints at the performance boundaries.

More directly relevant to the models to be described below, a study of kinematic posture in running cockroaches using principal components analysis [132] also reveals very low dimensional linear covariation in joint space (cf. [43]). Such biomechanical discovery of dimension collapse and posture principles complements increasing evidence in both vertebrate [55, 159, 283, 56] and invertebrate [258] neuroscience that neural activation results in precise, kinematically selective synergies of muscle activation. Posture principles have also proved useful in designing controllers for legged robots [286, 285]. In sections 5.3–5.4 we will address the collapse of more complex models to the templates introduced earlier in section 2.3 and to be described in sections 5.1–5.2.

The DOF problem has been approached theoretically by the "equilibrium-point" hypothesis in the physiological literature [30], and in the robotics literature by constructing cost functions and performance indices [253]. Both of these imply collapse of dimension. Moreover, Arimoto has recently suggested an alternative to the equilibrium-point hypothesis that is essentially task-space proportional-derivative position feedback control with linear velocity-dependent damping [15, 14]. He shows that this produces attraction to a lower-dimensional manifold under rather general assumptions and that use of physiologically realistic muscle activation functions in the "virtual springs" that define the cost function produces reaching motions similar to those of human arms.

The question arises how to render such descriptive observations more prescriptive by finding refutable hypotheses connected with them. The selection of a motor control policy may be governed by energy costs, muscle or bone stress or strain levels, stability criteria, or speed and dexterity requirements. Gait changes in quadrupeds, especially horses, have been shown to correlate with reductions in energy consumption as speeds increase [233, 184, 8, 335]. Muscle and bone strain criteria have also been suggested [120, 28]. With regard to stability, our own recent work using the LLS model of section 5 suggests that animal design and speed selection might place gaits close to stability optima [290, 133]. However, we are wary of the optimality framework, commonly employed in engineering [51], as a foundation for the prescription of natural or synthetic motion control, in part because it transfers the locus of parameter tuning from plant loop parameters to the cost function, which largely determines the quality of the resulting solution. Similarly, in biology, cost function details can significantly modify the resulting solutions, potentially shifting the phenomenology of describing the task to that of choosing the right cost function.[8]

Instead, we prefer to examine and model locomotion dynamics in regimes in which Newtonian mechanics dominates and hence constrains possible control mechanisms. Specifically, at high speeds, inertial effects render passive mechanics an essential part of the overall dynamics, and there are severe time constraints on reflex control pathways. Recent impulsive perturbation experiments on running cockroaches in [192] reveal, for example, that corrective motions are initiated within 10–15 msec, while corrective neural and muscle activity is estimated to require 25–50 msec. We also believe that the rapid running regime pushes animals close to limits of feasible neuromuscular activity and hence constrains the space of activations and dynamical forces available, much as in the case of static force production [327, 326], making it more likely that lower-dimensional behavior will emerge.

We shall therefore focus on regimes in which control target trajectories, even if selected by higher centers, must conform to mechanical constraints. We do this both to limit the scope of this review and to suggest a key principle in modeling complex behaviors: to develop and validate models in constrained (limiting) situations before attempting to "explain everything." To repeat our remark in the introduction, simple models—templates—can be invaluable in revealing basic principles: a model that leaves nothing out is not a model! However, we recognize that our focus on stereotypical high-speed gaits biases the scope of the resulting models, which will, *and should*, fail to describe the remarkable flexibility of low-speed exploratory behaviors. There are several recent reviews on reflexive-based control and coordination in this regime; see [111, 108] in particular for models and their implications for robots. While

[8] Optimization ideas can, of course, be useful in fitting model parameters if they cannot be directly measured or estimated, e.g., [93].

such studies have led to elaborate feedback control schemes [92, 93, 204] that generate realistic gait patterns, full investigations of the body–limb Newtonian dynamics of the type emphasized here remain to be done. We note, however, that analytical maps describing phase relationships between pairs of leg oscillators for such models of stick insects have been derived [63].

2.4.2. Neuromechanical Coupling: Centralized and Decentralized Coordination; Feedforward and Feedback Control. However they are formed, mechanical synergies such as templates and posture principles offer the nervous system attractive points of influence over the musculoskeletal system's interaction with its environment. Recent work on the cellular and molecular basis of sensorimotor control [59] and the use of noninvasive imaging to reveal specific brain regions active in learning and the planning and execution of movements [260, 199, 226] corroborate a growing consensus within the animal neuromotor community that control is organized in a distributed modular hierarchy [252]. In this view, complex motor functions are governed by afferent-mediated [259] networks of variably coupled [55], feedforward, pattern-generating units [162] located remotely [31] from higher (brain) centers of function. These networks supply motor program segments that may be combined in various ways at cortical command. It is tempting to think of these segments as solutions of coupled CPG–muscle–body–limb–environment dynamical systems, excited by appropriately shaped motoneuronal outputs and amplified by appropriately tuned muscles. Indeed, as we shall argue, cortical stimulation of such dynamical models can parsimoniously account for many of the observed correlations, and we offer the beginnings of a prescriptive interpretation in section 3.3.

In reading the motor coordination literature as well as in formulating the hypotheses of section 3.3 we have found it helpful to refer to the architectural "design space" depicted in Figure 7 as a two-dimensional coordination-control plane whose axes represent the degree of centralization and the influence of feedback. This viewpoint, which informed development of the hexapedal robot RHex [208], allows us to divide the studies of motor rhythms in distributed networks into three subgroups.

The first employs networks of biophysically based, ion channel neuron models of Hodgkin–Huxley [180] type, or reductions thereof [123, 179, 200], patterned closely upon the specific physiology of isolated tissues such as lamprey notocord [164], the arthropod stomatogastric ganglion [303, 150], and respiratory centers [60, 61, 96]. As noted in section 2.3.1 above, these models, and the experiments on which they are based, typically isolate the CPG by removing signals from sensory neurons and lesioning "control" inputs from higher brain centers [97, 79, 163]. Fairly detailed neural architectures and details of individual neuron types are required for their formulation; hence they are most appropriate for "small" systems. In this work the spontaneous generation and stability of rhythms are studied, perhaps in the presence of tonic excitation, but their volitional control or translation into physical motion is largely ignored.

The second group focuses on modeling the internal generation of rhythmic CPG patterns in the vertebrate spinal and supraspinal nervous systems by networks of coupled phase oscillators of the type introduced in section 2.3.3. Here the neurobiology is more complex and often less well characterized, so phenomenological models are more appropriate. The work on lamprey CPGs cited there [76, 78] and substantial extensions and generalizations of it by Kopell, Ermentrout, and others (e.g., [116, 210, 117, 211, 212, 77, 213, 197]) provide examples of this approach. As noted in section 2.3.3, in going directly to phase oscillators representing pools of neurons or

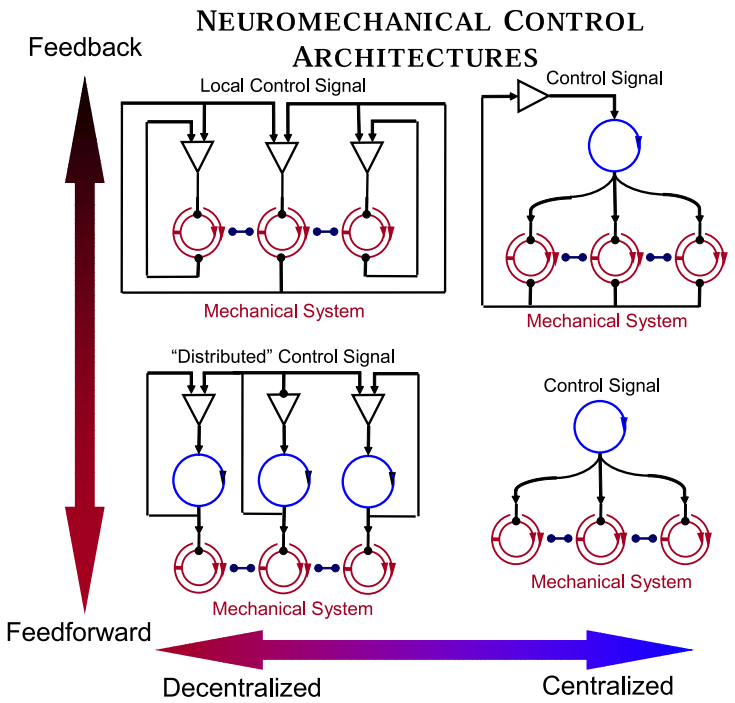

Fig. 7 *The schematic two-dimensional space of control architectures. As in Figure 5, single circles represent CPG oscillators, double circles represent mechanical oscillators such as limb components, and triangles represent neural control elements (analogous to operational amplifiers). Reprinted from* [208] *with permission from Elsevier.*

local circuits containing several neuron types, one frequently abstracts away from specific physiological identification, although useful information on coupling strengths along the cord can be derived by fitting parameters in such models [203]. These models also typically exclude muscles and mechanical aspects of the motor system and interactions with its environment, although in [212], for example, the effect of mechanical forcing of a fish's tail is modeled.

Their focus on the emergence of synchrony in distributed networks and the necessary presumption of the primacy of neural excitation in eliciting motor activity places these two classes of models on the feedforward level of Figure 7, at various points along the centralized–decentralized axis. Moreover, in both of these approaches, the generation and stability of rhythms are studied, but not their translation into physical motion. Indeed, in the absence of a mechanical model, the relative influence of mechanical feedback cannot be addressed.

Integrative neuromuscular models are beginning to appear. Simple coupled models of the nervous system and its mechanical environment have been developed by a third "ecological" school [201, 21], following the lead of the Haken–Kelso–Bunz (HKB) model of coordinated finger-tapping [168]. In these systems, (neural) phase oscillators are coupled to phenomenological (generic mechanical) oscillators representing simplified muscle–limb dynamics that may be interpreted as phase coordinate representations of the hybrid templates introduced in sections 2.1–2.2. There appear to be few comprehensive studies of specific locomotory systems, however, with the exception of

lamprey (anguilliform = eel-like) swimming, which has been modeled by Ekeberg and Grillner [110, 112] (cf. [189]) and Bowtell, Carling, and Williams [44, 45, 66]. In the former papers, bodies composed of rigid links actuated by simplified spring/damper muscle models are used and the fluid environment is represented by empirical drag and lift forces applied along the body; a recent paper on salamander locomotion considers both aquatic and terrestrial gaits [188] from a similar viewpoint. In [44, 45, 66], continuum body models coupled with the Navier–Stokes equations of incompressible hydrodynamics are solved numerically with a prescribed moving boundary representing the lamprey's body. Models of even the former (finite-dimensional) type are too complex to permit substantial analysis, although studies of linearized systems can be helpful, even for continuum models [45], so this work relies heavily on numerical simulations. Indeed, analytical treatment of coupled neuromechanical oscillators is thus far limited to very simple single DOF dynamical manipulation such as juggling [288, 312].

As Figure 7 illustrates, control architectures may also be described in terms of their reliance on sensory feedback from body mechanics and the environment. For example, proprioceptive sensing of leg forces and joint angles may directly influence CPG and motoneurons to maintain phase relationships in a decentralized, peripheral manner [257, 263, 20, 272], while visual and tactile sensing, or odor tracking, may require central processing before appropriate feedback can be applied to adjust gaits or change direction [149]. Models of feedback circuits that provide inter- and intralimb coordination based on proprioceptive sensing have their origins in D.M. Wilson's work [336, 337]; cf. [158]. They have been extensively developed for stick insect locomotion by Cruse and Büschges [20, 93, 111] and used to suggest rule-based pattern generating networks for hexapedal robots [73, 92, 108]. However, as we have noted, the substantial sensing, neural computation, and motoneuronal activation implicit in such schemes, whether centralized or decentralized, makes them unlikely candidates for overall control of high-speed running [192]. Nonetheless, cockroach antennal sensing can induce turning at high speeds with very short delays [64], suggesting that fast direct pathways to the CPG may exist. In turn CPG activity and central commands can modulate and even reverse the negative feedback typically exerted by proprioceptive sensors such as the stretch reflex [75].

More prescriptive versions of the power laws reviewed above emphasize optimal feedforward trajectory generation, although feedback is known to play an important role in both vertebrate [344] and invertebrate [109] locomotion, and the importance of feedforward reference signals is by no means generally accepted [91]. The observation that certain DOFs exhibit significantly higher variability than others can be interpreted in the framework of stochastic optimal feedback control as a hedge against noise [320]. Depending on environmental demands, the full range from pure feedback to pure feedforward control policies is probably employed in animal motion. Indeed, the suggestion, based on linear systems theory, that feedback should be preferred when internal models are uncertain or unavailable, while feedforward strategies should be more appropriate in the presence of significant sensor noise [218], seems very reasonable. The extremes of this continuum are exemplified, respectively, by "mirror laws" developed for juggling machines [53] and legged robots [286, 285], and passive stabilization based on preflexes, as exhibited by the SLIP and LLS models described in this paper. Overall, since centralized feedback circuits imply greater time delays, as running speeds increase, we expect control to emphasize decentralized modes, and increasingly to rely on feedforward strategies.

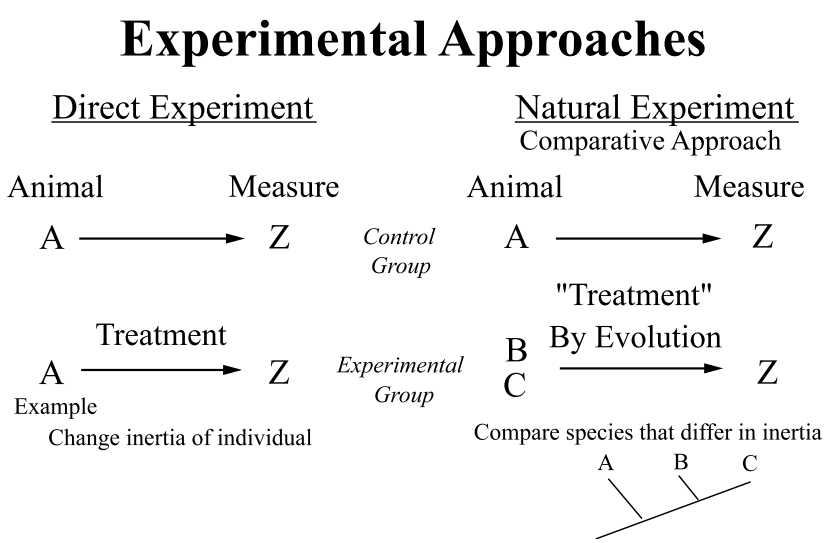

Fig. 8 *Schematic illustration of the direct and comparative experimental approaches, with an example of investigation of the effects of moment of inertia. In a direct experiment, a single parameter of interest is varied. In the comparative approach direct experimental controls are lacking, and one must use phylogenetic information to deduce how evolution may have changed multiple parameters. From Figure* 13.1 *of* [130]. *Reprinted with kind permission from Springer Science and Business Media.*

3. Experimental Evidence: Comparative Studies. Simple models of legged locomotion, such as the SLIP of section 2.2, have emerged from data collected using a powerful approach: the comparative method [130]. Direct experiments on individual animals in which a single variable is manipulated are often effective in establishing cause and effect relationships, but large parameter ranges can rarely be probed without disrupting function elsewhere in a finely integrated system. There are limits, for example, to how much an animal's mass or moments of inertia can be changed by the addition of weights, in studying their influence on its dynamics.

The comparative approach takes advantage of nature's diversity to overcome such limitations and enables the discovery of general principles as well as remarkable exceptions to the rules. We can infer function by comparing among species that differ widely in a variable of interest, rather than by direct experimental manipulation of a single species. Effectively, we observe experiments performed by nature, in which the "treatment" has been evolution, and naturally occurring variations in dependent variables permit investigation and isolation of mechanisms of interest in nearly-ideal settings of exceptional function. Figure 8 illustrates the direct and comparative methods.

The largest variations are found in comparing animals that differ greatly in size [289, 62]. Fortunately, variation in dependent variables as a result of size often shows remarkably general correlations that can be used to infer function and predict performance. For example, while the metabolic cost of legged locomotion typically varies less than tenfold when speed, stride frequency, inclines, or added loads are altered in individuals, it naturally differs by over *five orders of magnitude*, while exhibiting a single power-law relationship, when all legged animals are compared (Figure 9).

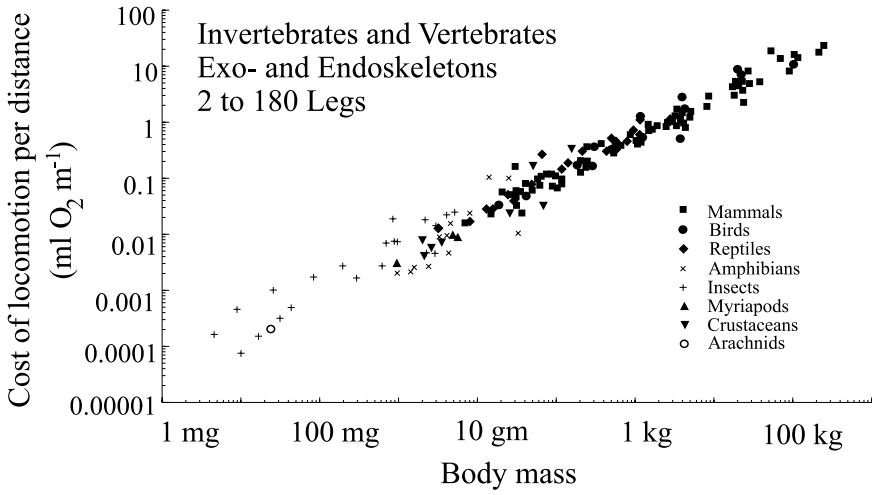

Fig. 9 *Metabolic cost of locomotion vs. body mass for a broad range of animals, showing an approximate power law relationship: cost* $\propto m^{0.68}$. *From* [126].

Equally important are those animals that demonstrate spectacular performance while deviating from the general pattern. Large, measurable differences have evolved over millions of years in diverse species having different lifestyles or operating in extreme environments. Characterization of these specialized systems can allow extrapolation to others in which the properties of interest are not as extreme, but for which functional principles are similar. For example, hopping red kangaroos can increase speed without increasing metabolic energy cost [94], and measurements of ground reaction and muscle forces reveal substantial elastic strain energy storage in the tendons of kangaroos and wallabies [10, 6, 26]. It is therefore reasonable to conclude, at least in larger vertebrates such as humans, that tendons serve a similar role, albeit to a lesser extent than in specialized, bipedal hoppers.

Natural experiments are nonetheless imperfect because they lack appropriate controls. Seldom do even closely related species under comparison differ *only* in the variable of interest. For example, two species may differ in moment of inertia and one be less stable than the other, but we cannot immediately conclude that inertia is the sole cause: the more stable animal may have more effective reflexive feedback control. However, the comparative method is strengthened by knowledge of evolutionary history or phylogeny [185, 140, 223]. Techniques in phylogenetic analysis [121, 141] can remove the effects of history or use them to hint at present function. If the process of interest has severe functional or structural constraints or nearly complete adaptation has taken place, then the potentially confounding effects of historical differences may be of little consequence. If, however, constraint and adaptation have been less than completely dominant, then the most parsimonious assumption is that the process operates as it did in the ancestor. An evolutionary, comparative approach can aid in answering mechanistic questions, but only if each species is studied in sufficient depth to elucidate the mechanism and a satisfactory phylogeny exists [18, 231]. Unfortunately, agreed-upon phylogenies are rare and in-depth studies of many species can take years.

In-depth studies are also enabled by nature's diversity. As August Krogh remarked at the 13th International Congress of Physiology in Boston in 1929, "For many problems there is an animal on which it can be most conveniently studied" [215]. The selection of "choice" or *model species* is based on its amenability to particular experimental procedures. The giant squid axon and the gastrocnemius muscle of frogs are notable, relevant examples, although results from model species that are easy to study are not necessarily generalizable. Generalization is usually most successful at the lowest levels of organization such as cellular and molecular structures and genetic and biochemical networks. In this regard, *E. coli*, nematodes, and fruit flies have proved invaluable model organisms. At the level of organs and organisms, careful selection using existing phylogeny of more basal species will more likely lead to general discoveries. The nervous system of the lamprey has been argued to be such an example [79], hence its use as a model to probe vertebrate CPG architectures, as noted in section 2.3.3. Alternatively, direct measurements of performance for a wide range of species that differ in size can be invaluable for identifying possible generality. For example, Figure 9 suggests that the metabolic cost of legged locomotion appears to be independent of leg number, leg design, skeletal type, or whether the animal is warm- or cold-blooded. Phylogenetic effects that may limit the generality of conclusions are absent from relationships such as these. It is therefore reasonable to assume that discoveries in insects, as discussed here, will lead to general principles for all legged locomotors.

3.1. Mass Center Mechanics of Legged Locomotion. Cavagna, Saibene, and Margaria [69] provided early experimental evidence for the spring-mass model of legged locomotion introduced in section 2.2. The metabolic energy cost of human running was determined by measuring oxygen consumption, and mechanical energy estimated from the fluctuations in kinetic and potential energy calculated from ground reaction forces measured with a force platform. Efficiencies, much higher than those estimated for muscle, supported the use of leg springs. Similarly, using movie film and force platforms to study jumping dogs and hopping kangaroos, Alexander [7, 10] calculated a substantial degree of elastic recoil in ankle extensor tendons. More recently, Biewener, Konieczynski, and Baudinette [27] directly measured tendon force and muscle length change in hopping wallabies and found that elastic strain energy storage in ankle extensor tendons reduces total work by 45% during hopping at the fastest speeds.

Alexander and Jayes [9] proposed that dynamically similar legged locomotors should exhibit equal ratios of inertial to gravitation forces for equivalent gaits. Their argument is based on the idea that the centrifugal force acting on the body as it rotates over a rigid supporting limb of length l must balance the ground reaction force on the limb. (For elastic legs, such as in the SLIP, spring forces also contribute, so this argument requires modification.) Animals as diverse as dogs and camels all lie near a single function when data on relative stride length is plotted as a function of this ratio, v^2/gl, which is called the Froude number[9] (Figure 10). More remarkably, mammals with different evolutionary histories change gait from a walk to a trot at Froude numbers of 0.3 to 0.5, and from a trot to a gallop between 2 and 3.

The Froude number is essentially the ratio of kinetic to potential energy and is often viewed as a dimensionless speed. Both it and its relative, the Strouhal number,

[9]In hydrodynamics, where it originated, the Froude number is defined as $v/\sqrt{gl}$ [105], but here we follow the biomechanical convention that avoids the square root [8].

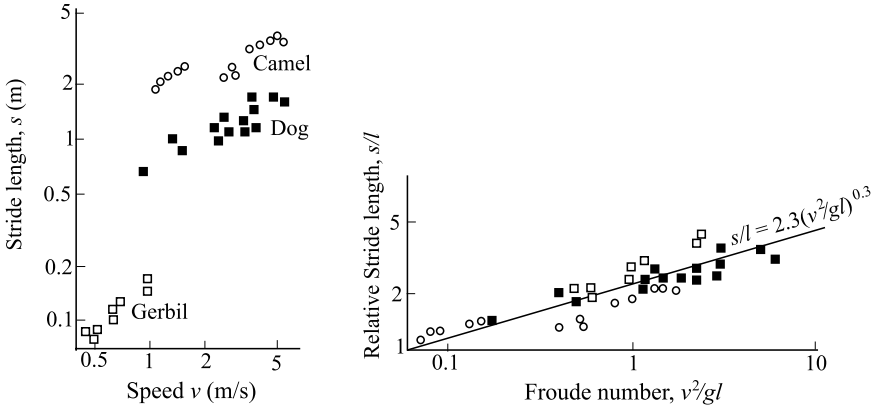

Fig. 10 *Stride length vs. speed and relative stride length vs. the Froude number for various animals. From Figure* 3 *of* [9]. *Reprinted with permission from Blackwell Publishing Ltd.*

which is appropriate for dynamic similarity in motions dominated by elastic forces [8], will play important roles in nondimensionalizing the models of section 5.1.

3.1.1. Walking and Running Data Viewed in the Sagittal Plane. In 1977 Cavagna, Heglund, and Taylor [68] collected ground reaction force data on two- and four-legged mammals in an effort to explain the general energetic relationship of Figure 9. Their data supported two basic mechanisms for minimizing energy: an inverted pendulum and a mass atop a spring. Walking was proposed to be an energy-conserving mechanism analogous to an inverted pendulum, much like an egg rolling end over end [70, 68, 175] (cf. the compass walker described by McMahon [242]). Kinetic energy and gravitational potential energy fluctuate in antiphase in such a mechanism, allowing exchange of energy as the animal's center of mass rises and falls during each step. Vaulting over a stiffened leg in humans was once argued to conserve up to 70% of the energy that must otherwise be provided by muscles and tendons [70], but recent models including a double support phase and collision losses question the extent of exchange [103].

At faster speeds, animals behave more like a mass atop a springy leg [103], in which kinetic and gravitational energy remain in phase, but fluctuate in antiphase with the elastic energy stored in the spring. Cavagna, Heglund, and Taylor [68] hypothesized that kinetic and gravitational potential energy lost during the first half of the stance phase were stored as elastic strain energy at midstance and then returned as the animal's center of mass rose and accelerated forward. As noted in section 2.2, the inverted pendulum and spring-mass mechanisms have been combined into a single model: the SLIP [296]. This two-DOF system limits on the single DOF inverted pendulum or compass walker as its leg stiffness increases; see section 4.4 below.

3.1.2. Evidence for a General SLIP Model. Blickhan and Full [33] discovered that SLIP behavior was far more general than imagined and was not restricted to upright-posture birds and mammals. Force platform data showed that eight-legged sideways-moving crabs can use a pendulum-like mechanism during walking, recovering as much as 55% of the energy otherwise supplied by muscles. At faster speeds, ghost crabs change gait from a walk to a bouncing trot. Full and Tu [135, 136] used a miniature force platform to show that the most prevalent taxon on earth, *Insecta*,

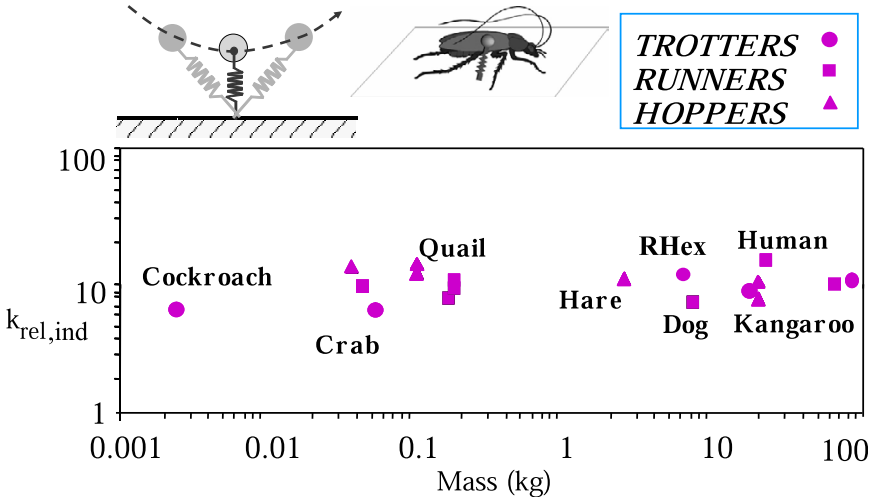

Fig. 11 *Relative individual leg stiffness vs. body mass for various animals and for the hexapedal robot RHex. Reprinted from* [208] *with permission from Elsevier.*

bounce dynamically as they run over a wide range of speeds. Indeed, the SLIP describes the COM dynamics during locomotion in animals ranging in body size from a cockroach (0.001 kg) to a horse (135 kg), a five decade range (Figure 11).

An effective SLIP spring stiffness can be estimated as the ratio of the peak ground reaction force to maximal leg compression at midstance. If F_{vert} denotes the vertical whole-body ground reaction force and Δl the compression of the whole-body leg spring, then the absolute spring stiffness is

$$k = \frac{F_{\text{vert}}}{\Delta l}\,. \tag{23}$$

Force platform data on mammals from Farley, Glasheen, and McMahon [119] show that larger animals have stiffer springs: a trotting horse has a SLIP stiffness 100-fold greater than that of a rat. Comparison of mammals over a thousandfold range of body mass m shows that the SLIP stiffness increases as $m^{\frac{2}{3}}$.

To compare leg stiffnesses of diverse animals, allowances for both size and leg number must be made [34]. A dimensionless stiffness relative to size is required to correct for body weight and length differences. Such a relative SLIP stiffness k_{rel} can be calculated by dividing the peak whole-body ground reaction force at midstance, normalized for body weight, mg, by the compression normalized by hip height, l:

$$k_{\text{rel}} = \frac{F_{\text{vert}}/mg}{\Delta l/l}\,. \tag{24}$$

The number of legs supporting the body during stance that sum to produce SLIP behavior varies from one in running bipeds to four in trotting crabs (see Figure 4 in section 2.2). For example, insects trotting in a double tripod gait compress their SLIPs by one-third relative to bipedal runners. Because the relative force is the same as in bipedal runners, the SLIP stiffness of the insect is threefold greater than for bipeds. Since the SLIP stiffness is determined by the number of legs supporting body weight, a relative individual-leg stiffness $k_{\text{rel,ind}}$ can be estimated by dividing the relative

SLIP stiffness by this number (e.g., for an insect $k_{\mathrm{rel,ind}} = k_{\mathrm{rel}}/3$, and for a trotting quadruped or a hopper such as the kangaroo $k_{\mathrm{rel,ind}} = k_{\mathrm{rel}}/2$). Relative individual-leg stiffness is surprisingly similar in trotters, runners, and hoppers using from one to four legs in stance; the data summarized in Figure 11 indicates $k_{\mathrm{rel,ind}} \approx 10$. Thus, relative individual-leg force is about tenfold greater than relative compression in six-legged trotters (cockroaches), four-legged trotters (dogs, horses), two-legged runners (humans, birds), and two-legged hoppers (kangaroos).

3.2. Dynamics of Sprawled Postures and Many Legs: Running Insects. Insects have become model organisms for the study of locomotion, as evidenced by advances in areas such as neurobiology [261, 262, 257, 263, 97, 98, 99, 91, 57, 58, 330, 331, 321, 322], muscle function [196, 134, 4], and biomechanics [135, 136]. Insects can exhibit extraordinary locomotor performance; are inexpensive, hearty, and abundant; have experimentally tractable neuromuscular systems; and often follow remarkably general relationships, encompassing both invertebrates and vertebrates (cf. Figures 9 and 11).

3.2.1. Evidence for Equivalent Gaits. Cockroaches exhibit bouncing gaits over 85% of their speed range. Even at lower speeds they do not walk like inverted pendula [135, 136], and although their energy recovery averages only 6–15%, their dynamics suggest that arthropods with exoskeletons can use springs and bounce during running much like mammals. Equivalent gaits may exist among legged runners that differ greatly in morphology. Further evidence of this equivalence comes from examining relationships between stride frequency and running speed.

In quadrupedal mammals, stride frequency increases linearly with speed during trotting [177, 176], but becomes nearly independent of speed as mammals switch to a gallop, higher speeds being obtained by increasing stride length. Similar relationships have been found in cockroaches and ghost crabs [135, 33]: as speed increases stride frequency attains a maximum. Comparison of maximum sustainable stride frequency and the speed at which it is attained in crabs and cockroaches with data from mammals [177, 176] suggests the possibility of equivalent gait transitions in two-, four-, six-, and eight-legged animals. Surprisingly, when the size effect is removed, legged animals attain a similar maximum sustainable stride frequency at a similar speed [124, 125]. For example, a crab and a mouse of the same mass change gait at the same stride frequency (9 Hz) and speed (0.9 m sec^{-1}) [33]. Proposed causes for the trot-to-gallop transition include a decrease in metabolic energy cost [184, 8] and a reduction in musculoskeletal strain [120]. Blickhan, Full, and Ting [35] placed strain gauges on ghost crab legs and found an abrupt change at the trot-gallop transition, but strain *increased* fivefold rather than decreased. Until the recent modeling efforts reported in section 5.3 (see Figure 32 below), no explanation was available for the gait change in cockroaches.

3.2.2. Individual Leg Function. Trotting quadrupedal mammals, such as dogs, produce nearly the same ground reaction force pattern with each leg [68, 191], much like SLIP ground reaction forces. In fact, successful trotting quadrupedal robots have been designed that produce similar forces on each leg, differing only in relative phase [269]. However, individual leg ground reaction forces, measured using a miniature force platform [129] and photoelastic gelatin [137], show that hexapedal runners do *not* behave like quadrupeds with an added set of legs. At constant average running speed, each contralateral leg pair of the cockroach is characterized by a unique ground reaction force pattern, as indicated in the left column of Figure 12. The front leg decelerates the COM in the fore-aft direction throughout a step, the hind leg accelerates

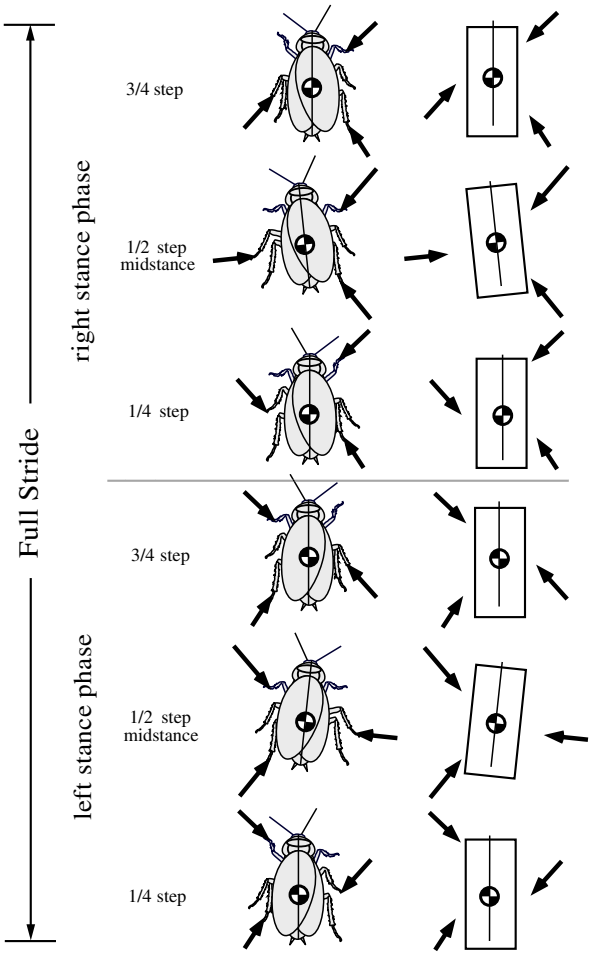

Fig. 12 *Left column: the double tripod gait of insects, showing typical individual foot force vectors near beginning, at middle, and near end of each stance phase. Right column: the rigid body prescribed force model of Kubow and Full. Adapted from* [216].

it, and the middle leg does both, initial deceleration being followed by acceleration, much like legs of bipedal runners and quadrupedal trotters. Peak vertical ground reaction forces for each leg are approximately equal in magnitude, and significant lateral ground reaction forces are directed toward the body. Nonetheless, the differing individual leg forces in insects combine to produce net forces on the body COM in the sagittal plane similar to those of the single leg of a bipedal runner.

One important consequence of the large lateral and opposing leg ground reaction forces involves muscle force production. In the cockroach, peak ground reaction forces are oriented toward the coxal joints (analogous to hips in a biped) that articulate with the body. This tends to minimize joint moments and muscle forces [129]. Legs of animals do not generate vertically directed ground reaction forces that result in large torques about the "hip" as do some legged robots, nor do they operate under the horizontal, zero-foot force criterion used in some robot designs [328]. Insect legs push against one another, but force vectors are aligned approximately along the legs

and directed largely toward joint centers of rotation, much as in upright-posture birds and mammals. Hence, sprawled posture locomotion of arthropods, amphibians, and reptiles does not necessarily result in large joint moments or muscle forces. This appears consistent with data showing that the minimum metabolic costs of locomotion in species that differ in posture can be similar [125]; cf. Figure 9.

To discover if individual insect legs can function as springs, Dudek and Full [342, 106] oscillated legs dynamically with a computer-controlled lever. Cockroach legs, in particular, have the potential to function as passive exoskeletal springs in the sagittal plane because their joint axes are oriented approximately vertically. Stiffness, damping, and resilience[10] were measured during vertical oscillations orthogonal to the plane of joint rotations [106, 107]. Leg resilience was found to be high, ranging from 65–85%, and independent of oscillation frequency. A damping ratio was estimated using the stiffness and damping coefficients from a Voigt model, assuming the body rests on a support tripod of legs during stance phases in running [106, 107]. The results suggest that the tripod of legs used by running cockroaches is underdamped, permitting partial energy storage and recovery.

3.2.3. Static and Dynamic Stability. The springy legs of insects radiating from their mass centers almost certainly provide performance advantages beyond energy storage and return. A sprawled posture bestows a wide base of support and low center of mass, both of which reduce overturning moments. Additionally, most insects use an alternating tripod gait over a broad range of speeds (Figure 12); indeed, Hughes [186] stated that six legs are the "end-product of evolution," because the animal can always be statically stable.

However, while Ting, Blickham, and Full [317] found that running death-head cockroaches *Blaberus discoidalis* do keep their COMs within a tripod of support over a wide range of speeds, these insects are *statically unstable* at their fastest speeds. Their percent stability margin (the shortest distance from COM to the boundaries of support normalized by the maximum possible stability margin) was found to decrease with increasing speed from 60% at 10 cm s^{-1} to negative values at speeds faster than 50 cm s^{-1}, implying static instability. Certainly, the fastest gait of the American cockroach *Periplaneta americana* cannot be statically stable, for at 1.5 m sec^{-1}—nearly 50 body lengths per second—this species runs bipedally [136]. Nonetheless, in both animals, dynamic stability is maintained throughout.

Discoveries of spring-mass behavior, static instability in a fast tripod gait, and dynamically stable bipedal running such as those summarized above suggest that energy use in insects might not be minimized, but rather *managed*, to ensure dynamic stability. Moreover, preliminary studies on cockroaches also show that preferred speed is maintained during rapid running over rough terrain [128]. A fractal arrangement of blocks reaching up to three times higher than the COM offers little resistance: animals do not step carefully over it or cause their legs to adopt a follow-the-leader gait like those of some legged robots, but continue to use the same alternating tripod gait observed on flat terrain. Simple feedforward motor output appears to be effective in the negotiation of such rough terrains when used in concert with a mechanical system tuned to stabilize passively.

Overall, these observations lead to the hypothesis that dynamic stability and a conservative motor program allow many-legged, sprawled-posture animals to misstep

[10] Resilience is the ratio of work done in extending or bending a material minus the work recovered when released, to the work done in extension or bending.

and collide with obstacles, but suffer little loss in performance. Rapid disturbance rejection appears to be an emergent property of the musculoskeletal mechanical system.

3.2.4. Self-Stabilization in the Horizontal Plane. To develop a more precise hypothesis on the mechanical system's role in stabilizing running, Kubow and Full [216] created a feedforward, three-DOF dynamic model of a hexapod, representing a sprawled-posture insect in the horizontal plane, as pictured in the right-hand column of Figure 12. Vertical motions and gravity were excluded, yaw and translation instabilities being assumed to be more critical than the insect flipping over or falling and striking its abdomen. The model, a rigid body with six massless legs, was formulated with direct biomechanical data taken from death-head cockroaches, including body mass and inertia, individual leg ground reaction forces, and foot positions relative to the body [135, 129, 34, 317, 137, 214]. Stereotyped periodic force inputs were prescribed at foot positions fixed in inertial space throughout each step, but force vector directions were allowed to rotate with the body as it yawed during each stance phase. The model was driven by this feedforward signal with no equivalent of neural feedback among any of the components.

The resulting forward, lateral, and rotational velocities were similar to those measured in the animal at its preferred velocity. More surprisingly, the model self-stabilized on a biologically relevant timescale following instantaneous velocity perturbations acting on its COM. The rate of recovery depended on the orientation of the perturbation. Recovery from lateral perturbations took multiple strides, whereas recovery from rotational perturbations occurred within one step. Recovery to 63% from fore-aft perturbations was very slow, taking almost 50 strides. Heading (i.e., the compass direction of COM) never recovered from lateral velocity perturbations. Recovery was dynamically coupled such that perturbations in one velocity component necessarily changed the others. Perturbed COM positions and body angles relative to the fixed feet provided mechanical feedback by altering leg moment arms. This anchored model inspired the LLS templates that we discuss in section 5, and both it and they motivated the following experiments.

Jindrich and Full [192] perturbed rapidly running insects to experimentally test the self-stabilization hypothesis. An apparatus was mounted onto the thorax of a cockroach and positioned to propel a projectile laterally, delivering a specific impulse in linear momentum near the animal's COM. Chemical propellants were used to accelerate a small metal ball, producing impulsive reaction forces less than 10 ms in duration, but yielding an almost tenfold increase in lateral velocity relative to maxima observed during normal running. Lateral velocity began to recover within 13 ms after initiation of the perturbation. This recovery duration is comparable to all but the fastest reflex responses measured in insects [182] and is likely shorter than a neurally mediated correction when the delays of the musculoskeletal system response are allowed for. Cockroaches recovered completely in 27 ms and did not require step transitions to recover from imposed lateral perturbations. The animal's COM response exhibited viscoelastic behavior in the lateral direction with leg spring stiffnesses similar to those estimated for unperturbed running. This rapid onset of recovery from lateral perturbations supports the hypothesis that mechanical preflexes augment or even dominate neural stabilization by reflexes during high-speed running.

The models to be described in section 5 allow us to take this question up again and, as noted in section 5.1.4, also suggest an explanation for the fact noted in section 3.2.3 that insects can negotiate rough terrain without departing from their preferred speed and normal gait. Indeed, for the LLS model, we find that stability is *greatest* at preferred speed, in the sense that recovery times are minimized precisely in this range.

3.3. Toward a Theoretical Framework for Animal Experiments in Locomotion. We are now approaching the midpoint of this article. We have summarized a voluminous literature on animal locomotion, generated from several disciplinary viewpoints, emphasizing in each case the general implications for mathematical modeling, and addressing the manner in which these diverse collections of facts might inform the sort of mathematical models that will be described in sections 4–5. Before moving to that more technical discussion, we conclude our literature review by describing four biological hypotheses that motivate and that will (we hope) justify the exercise. Although short of listing concrete experiments, these propositions nonetheless suggest how a unified framework can give rise to new ways of asking questions about the structure, organization, and function of locomotion. The first three hypotheses were presented and discussed in the context of legged robot design in [208].

3.3.1. Hypothesis H_1: Stable Dynamical System. We hypothesize that the primary requirement of an animal's locomotive control strategy is to stabilize its body around steady-state gaits whose patterns emerge from the dynamical system formed by mutual coupling of the neural and musculoskeletal systems to the environment. The body and limbs follow paths dictated by (Newtonian) mechanics of the musculoskeletal system, prompted by feedforward input from the CNS and CPG, and modified by reflexive feedback. This hypothesis contrasts with reference trajectory planning, described in section 2.4 above, in which neural controllers command limbs to follow prescribed paths and sensory feedback activates muscles to maintain them. Reference trajectory planning leads to markedly different predictions of response to acute position and velocity perturbations from our dynamical system hypothesis.

Dynamical systems theory predicts that perturbations in different directions in phase space will recover at rates and along paths locally determined by the equations of motion, and hence by the neuromechanical properties of the animal. For example, eigenvalues and eigenvectors of the Poincaré maps linearized about steady gaits, as described below, predict the nature of local coupling among state variables. Presuming a biological apparatus with sufficiently low noise floor to probe the neighborhood governed by the linearized dynamics, and sufficient repeatability to gather enough observations within that neighborhood, the absence of the predicted patterns is immediate grounds to reject such models. In contrast, perturbation recovery in reference trajectory planning depends upon gains in the feedback control loops. Thus, while not necessitated by theory, other considerations being equal, one expects a greater uniformity in perturbation response time and coupling for reference trajectory control.

For periodic gaits, reference trackers seek to maintain a fixed phase relation of animal position with respect to the reference trajectory. Thus, perturbations from steady state are countered not merely by convergence to a limit cycle, but also to a preferred time parametrization along it. Phase resetting [338] would therefore immediately refute the trajectory tracking hypothesis. In contrast, the general framework of Figure 7 suggests nontrivial phase response in reaction to perturbation. Since the clock "hears back" from the mechanism, its dynamics depends on the paired state, and perturbations can move it from one isochron to another in the coupled state space (cf. section 2.3.1). An exception to this occurs in the specialized (but important) feedforward decentralized setting (bottom left of Figure 7) in which the feedforward nature of the clock signal may lend it something of the character of a classical reference signal. In this case, the internally generated rhythm would persist despite external perturbation, and convergence may occur to a fixed reference phase.

These two examples illustrate both the advantages and limitations of what we have termed "prescriptive" mathematical models for guiding experiments. One can

typically develop experimentally viable tests that are mathematically necessary (e.g., the predicted local transients are necessary to validate a proposed template) and some that are sufficient (e.g., the observation of phase resetting is sufficient to refute trajectory tracking). However, it is most unusual to find empirically accessible conditions that are both necessary and sufficient for the same hypothesis. Directionally uniform responses to perturbations suggest but do not necessitate trajectory tracking—there might be reasons unrelated to the structure of the linearized Poincaré map for preferential dissipation of tracking errors in some directions. Similarly, absence of phase resetting suggests but does not prove that control is dominated by trajectory tracking, since the system could be operating in a localized feedforward mode.

3.3.2. Hypothesis H_2: Collapse of Dimension. We noted in section 1 (Figure 1) the challenge of explaining how simple templates such as the SLIP apparently emerge from complex models (anchors) that include body segments, legs, muscles, and neural circuitry. Templates can resolve the redundancy of multiple legs, joints, and muscles by a "posture principle" that imposes symmetries and exploits synergies (section 2.4.1). In section 3.1 we reviewed a growing body of evidence establishing that diverse species differing in leg number and posture run stably like the SLIP in the sagittal plane. The remainder of this paper will focus on the closely related LLS model as a template for horizontal plane running and will summarize our attempts to discover how this template might arise within insects.

Explaining how simple templates emerge within complex bodies undertaking agile maneuvers has stimulated new models, as we shall show in section 5. The effort to find control mechanisms that effectively collapse dimension must address details of morphology and command and impose specific expectations about the role of multiple legs, the joint torques that actuate them, muscle recruitments that produce those torques, and neural circuits that activate the ensemble. Unfortunately, the present lack of prescriptive hypotheses limits our ability to draw specific conclusions on how postures might anchor templates. While robot postures can be shown to be sufficient for anchoring templates with copious feedback and computationally intensive control [53, 279, 254, 334, 285], they are not necessary, and their reliance upon high control authority may be biologically implausible, as remarked in section 2.2. Moreover, whereas preflexive (sensorless) postures are empirically observed to anchor the SLIP template in RHex [13], a mathematical basis for this observation is still lacking.

In spite of this, the success of the SLIP and (as we shall show) LLS templates in modeling many-legged, sprawled-posture animals suggests that a passively self-stabilized, feedforward, tuned mechanical system can reject rapid perturbations and thus simplify control. Specifically, in running, we hypothesize that preflex- and reflex-mediated joint dynamics leads to spring-mass template motions. Existing mathematical insight dictates that sets of neurons, muscles, and joints must act synergistically, and the resulting preferred postures enable animals to reduce the number of control signals required throughout a stride. Limb motions tracking a reference trajectory would require many more signals, since each DOF would require a separate reference with its own feedback channel.

In the next subsection we introduce a hypothesis that presumes this notion of template reduction and uses a phase variable as the single state to be internally coordinated. However, any periodic behavior, interpreted as a normally hyperbolic attracting limit cycle of a dynamical system, induces a scalar phase via the theory of isochrons (section 2.3.1), so from a purely mathematical viewpoint, the generality of phase allows the direct participation of the complete anchor in limb coordination. Why, then, would templates be needed?

We believe that the communication and computational burdens implied by high-dimensional state exchange across an entire limb and the subsequent identification of isochrons "on the fly" would largely negate the virtues of phase variables for interlimb coordination, *unless* intralimb components, and the CPG and muscle complexes activating them, are stereotypically coordinated during high-speed running. If such a low-dimensional neuromechanical limb template exists, however, then its further reduction to a phase oscillator (section 2.3.3) would be simple and would effectively summarize the *only* state variable that needs to be communicated to other limbs to ensure coordination. Thus, if we can show that detailed CPG, muscle, and limb models can be reduced to phase oscillators under suitable conditions, and interlimb coordination described by these alone, we shall have gone some way toward our goal. In section 5.4 we show that CPG and motoneuron models, at least, can be so reduced in a purely feedforward setting.

3.3.3. Hypothesis H_3: Tunable Coordination Control Architecture. Figure 7 illustrates two key trade-offs that arise during the evolution of a locomotor control system: between feedback vs. feedforward control, and between centralized vs. decentralized coordination. Numerical simulations [206] and empirical work [333] suggest that these trade-offs largely determine the efficacy of a particular machine gait in a particular environment, and there is a voluminous neuroethology literature devoted to tracing their impact on animal locomotion, reviewed in section 2.4.2. But how does the articulation of this control space sharpen our ability to make predictions about locomotion?

First, we hypothesize that when an animal runs fast, has noisy sensors, or is able to appropriately tune its musculoskeletal system to its environment, it will operate primarily in a feedforward, decentralized fashion, attaining stability via preflexes and coordination by mechanical coupling of springy legs. In contrast, when moving slowly, with accurate sensors or in uncertain environments, animals will function in a predominantly feedback, centralized fashion via neural reflexes and synchronized oscillators. The models described in section 5 (especially section 5.4), and the physical robots that have accompanied them [11, 333], explicitly couple neural control to the mechanical system, thus providing parameterizations that are analytically and empirically accessible on robots and, hence, may serve as guides to the forms that these connections take in animals.

Second, we hypothesize that diverse behavioral repertoires require animals to move within their control architecture space by tuning controls to adapt locomotion to different environments and to different operating regimes within a given environment. However, linear systems theory, with its clear design prescriptions, cannot directly address the strongly nonlinear, coupled neuromechanical systems of interest, and characterizations of environmental properties that demand different operating points are even less well developed. Substantially more modeling, and analytical progress, will be required before this hypothesis can be tested more than qualitatively, for example, by examining simulated, physical robot, and biological behaviors that fail in specific environments with inappropriate operating points.

Whether set correctly or not, the question of how to determine an "operating point" at all raises interesting methodological problems. In a physical or numerical model, the wiring diagram of Figure 7 is explicitly parametrized [205] and the operating point is designated by the user. In contrast, one requires a more abstract information-theoretic framework of a kind only recently emerging from computational neuroscience [314] within which to develop relationships between such diagrams and parametrizations to experimental outcomes with neural circuitry. Within such a

framework, absent knowledge of the source code or even the details of physiological connections, the operating point on our architectural plane can be at least partly surmised by assessing the bit rate of measured neural signal flow [315]. Under any circumstances, the strength of the coupling gains is limited by the channel capacity of the network that supports them. As the time constants of external task demands become shorter, the internal synchronization gains would exceed channel capacity constraints, forcing a decrease in the degree of centralization and a concomitant increase in distributed sensing.

Within this framework, our hypotheses can be used to make specific predictions about how animals' coordination capabilities will change or even fail as internal noise (decrements in the available neural channel capacity) or external bandwidth requirements (increments in the speed and/or precision of the required mechanical coordination) are varied. In the face of the highest bandwidth performance tasks, the neural communications channels may be too noisy to permit high enough feedback or synchronization gains, and the animal may be forced to operate in a decentralized and feedforward manner, in which coordination is achieved through mechanical coupling and stability obtained by preflexes. As the bandwidth requirements of the task decrease, higher reflex and synchronization loop gains could be tolerated, increasing the efficacy of feedback and central authority.

3.3.4. Hypothesis H_4: Task Level Control and Its Identification. In foraging, mating, exploring, and fleeing, animals are capable of impressive feats of navigation. We hypothesize that to accomplish these, they function as if "directing" a simple, self-stabilizing spring-mass template. Such systems require few tunable parameters to steer (e.g., velocity and COM height at mid-flight), and these act as control affordances in support of a goal (e.g., the body should track a nearby wall). This in turn defines a "higher" task-level description (e.g., stride-to-stride relation of the mass center to the wall as a function of parameters). We suppose that environmental sensing loops are closed with respect to such dynamical tasks, thus generating new attractors for the overall neuromechanical system that achieve desired trajectories: e.g., sensory signals from antennae contacting the wall may shape spring-mass parameters from stride to stride, creating a virtual stability basin two centimeters from the wall.

We hypothesize that these virtual task basins are "emergent properties" of control loop architectures that animals "follow" in a natural manner, much as they follow attractors emerging from their mechanical characteristics within higher-speed preflexive regimes. This differs significantly from the conventional notion of servo-controlled matching to predefined trajectories within a "sense-plan-act" scheme. We believe that it is now possible to seek and empirically characterize these virtual task basins. Data collection and analysis methods arising from the information-theoretic view of the animal nervous system, along the lines described in the previous subsection, should be capable of supporting or refuting these hypotheses. But since the variety of volitional tasks must exceed their basic behavioral constituents, a more open-ended approach to discovering new behavioral patterns is needed. We refer to this strategy as "dynamical data mining."

4. Hybrid Dynamical Systems. The models of legged locomotion considered in this paper are more complicated than classical (smooth) mechanical systems. Due to impacts, ground reaction forces, and changing stance patterns, the governing equations define *hybrid* systems in which the continuous-time vector fields describing evolution change at discrete times or *events*. Indeed, since the constraints that define these vector fields depend on the number and identity of legs in contact with the

ground, even the dimension of the governing vector field may change at an event, and different coordinate systems may be called for. While various definitions have been proposed for hybrid systems, we shall follow one similar to that introduced by Back, Guckenheimer, and Myers [19]. Their approach is predicated upon four requirements: (1) existence of solutions in a general setting, (2) straightforward implementation of simulations, (3) inclusion of systems drawn from a wide range of applications, and (4) amenability to analysis using tools from singularity theory and smooth dynamical systems. From a computational perspective, however, there are some differences between the present situation and that of [19] in that, due to the piecewise-holonomic constraints noted in section 2.1, the equations of motion are typically *differential-algebraic equations* (DAEs) rather than purely differential equations.

4.1. Introductory Examples. There are several mathematical and computational obstacles to formulating a fully satisfactory definition of hybrid systems. The basic idea of following a vector field until an event occurs, then "jumping" to a new initial condition for a new vector field and continuing to flow from there is clear, but it seems impossible to fully maintain the basic properties of existence and continuous dependence of solutions of ODEs on initial data. We illustrate this with a pair of two-dimensional examples.

Consider first a piecewise constant vector field $\mathbf{f}$ defined by $\mathbf{f}(x, y) = (1, -1)$ if $y \geq 0$ and $\mathbf{f}(x, y) = (1, 1)$ if $y \leq 0$, assigning different discrete states to the upper and lower half-planes. When a trajectory arrives at the x-axis, the event changes its discrete state but leaves its location unchanged. It is evident that there is no solution of the system with initial condition on the x-axis. Trajectories in the upper half-plane point into the lower half-plane and those in the lower half-plane point into the upper half-plane. The state is stuck on the attracting line $y = 0$, on which the vector field is multivalued, perhaps "wanting" to switch back and forth between the two discrete states infinitely often. This *chattering* conundrum is well known in engineering, and two strategies have been developed to address it. The "thermostat" strategy derives from the desire to turn heat on when temperature is below a set point T_0 and off when it exceeds T_0. Indeterminacy at T_0 is overcome by overlapping the regions in which the heat is on and off. An offset δ is defined and switches from on to off are made at $T_0 + \delta$ and from off to on at $T_0 - \delta$, producing hysteretic cycling, whose rate can be adjusted by changing δ.[11]

The second strategy for dealing with chattering is to try to constrain the system to lie along the boundary between the two states. This is not feasible for the thermostat, but in mechanical devices we often wish to maintain such a constraint. The theory of *sliding modes*, based upon differential inequalities, achieves this [323]. In the context of motor control, imagine a situation in which two muscles with nearby insertion points can be contracted to achieve motion of a limb. Since forces from the two muscles add, a suitable linear combination of contraction can be applied to enforce the desired constraint. Both of these strategies are clearly relevant and appropriate to biomechanical systems. In terms of hybrid systems theory, we regard sliding modes as distinct discrete states in their own right, with DAEs defining the vector field which maintains a constraint.

A second example shows that conflicting choices between "target" states seem unavoidable in hybrid systems. Consider a two-dimensional vector field describing

[11] A second approach to the thermostat problem is to define a minimum time that the heat remains off or on. Theoretically, we regard this approach as undesirable for two reasons: it introduces "delays" into the system that complicate the theory, and the choice of off/on state at temperature T_0 is not really resolved: two different trajectories are allowed from the same initial point.

discrete state 1 of a system. When a trajectory in the first quadrant reaches the x-axis, we assume that there is a transition to discrete state 2, and when a trajectory reaches the y-axis, there is a transition to a distinct discrete state 3. When a trajectory reaches the origin, a decision must be made between transitions to states 2 and 3, or the origin must be regarded as a further discrete state. Whichever choice is made, we lose continuous dependence of solutions on initial data. Whether this is reasonable in the example depends on the underlying "physics." The situation is reminiscent of what happens in a locomotion model when two feet make simultaneous ground contact. In the analogous problem of *triple* collisions in the three body problem [241], it is known that no "regularization" is possible and that solutions do not depend continuously on initial conditions (in contrast, double collisions are regularizable).

Issues such as these leave us in a quandary regarding formal definitions of hybrid systems. More restrictive definitions yield stronger results on existence, uniqueness, and continuous dependence on initial data, while less restrictive ones encompass a larger set of examples. We adopt the principle that computational simulation of models is a priority: without simulation, it is difficult to extract useful information about model behaviors. Consequently, we choose definitions that ease the implementation of simulations. With this in mind, we turn to the definition proposed by Back, Guckenheimer, and Myers [19].

4.2. Formal Definitions. The state space of a hybrid system is a union

$$V = \bigcup_{\alpha \in I} V_\alpha \,,$$

where I is a finite index set and each V_α is a connected open set in $\mathbb{R}^{n_\alpha}$. The V_α are called *charts*. Note that the dimension of the charts may depend upon α. A state of the system consists of an index α together with a point in the chart V_α. We assume that a continuous time dynamical system is defined on each chart. If these systems are defined by DAEs rather than ODEs, we regard the chart as the set of points satisfying the algebraic constraints and suppose that the system is (uniquely) solvable at each point of the chart. Inside each chart V_α, we assume that there is a *patch* U_α, an open set whose closure $\bar{U}_\alpha \subset V_\alpha$ lies in the chart. We assume that the boundary of the patch is a finite union of level sets of smooth *boundary functions* $h_{\alpha,i} : V_\alpha \to \mathbb{R}$. We further assume that there are *transition maps* $T_\alpha : \partial U_\alpha \to V \times I$ that apply a change of states to points of the patch boundaries. Depending upon context, we may wish to leave the transition maps undefined on (small) subsets of the patch boundaries where the evolution of the system is not determined by underlying physics. We assume that the images of the transition maps lie at states that are initial points for a continuous time trajectory inside the closure of a patch. Intersection of a continuous time trajectory with a patch boundary is called an *event*.

Global evolution of the system consists of concatenation of flows along continuous time trajectories to events, followed by applications of the transition map at the event point. More precisely, a *trajectory* defined on the time interval $[t_0, t_n]$ with events at times $t_1 < \cdots < t_{n-1}$ consists of discrete states $\alpha_0, \ldots, \alpha_{n-1}$ and smooth curves $\gamma_i : [t_i, t_{i+1}] \to V_{\alpha_i}$ with the properties that

- γ_i is a trajectory of the continuous time dynamical system on V_{α_i}, and
- $T_{\alpha_i}(\gamma_i(t_{i+1})) = \gamma_{i+1}(t_{i+1})$.

We call the time intervals $[t_i, t_{i+1}]$ *epochs*.

Steady gaits in locomotion are represented by periodic orbits, and their stability properties are clearly of great importance. To determine stability, a Jacobian for the

Poincaré return map linearized on a periodic orbit of a generic hybrid system can be constructed as the composition of derivatives of the flow maps during each epoch, interleaved with derivatives of the transition maps between the epochs. Since flow maps along the epochs lead to variable event times, determined by when trajectories hit patch boundaries, this computation is somewhat subtle. The derivative of the map along the flow to the event surface is not simply the derivative of the flow map at a prespecified time, but must be computed as follows.

Let $\dot{\mathbf{x}} = \mathbf{f}(\mathbf{x}, t)$ be an n-dimensional vector field with flow $\Phi(\mathbf{x}, t) : \mathbb{R}^n \times \mathbb{R} \to \mathbb{R}^n$, and let $g : \mathbb{R}^n \to \mathbb{R}$ be a smooth function whose level set $g = c$ defines the patch boundary hit by trajectories with initial conditions near $\mathbf{x}_0$. We assume that the level set of g is transverse to the vector field, $\mathbf{D}g \cdot \mathbf{f} \neq 0$, at the point where the event occurs. We denote the time of an event along the trajectory with initial condition $\mathbf{x}$ by $\tau(\mathbf{x})$, a function determined implicitly by $g(\Phi(\mathbf{x}, \tau(\mathbf{x}))) = c$. We define $\Psi : \mathbb{R}^n \to \mathbb{R}^n$ to be the map that sends $\mathbf{x}$ to the intersection of its trajectory with the surface $g = c$; i.e., $\Psi(\mathbf{x}) = \Phi(\mathbf{x}, \tau(\mathbf{x}))$. Thus $g \circ \Psi$ is constant, Ψ is singular, and

$$\mathbf{D}_{\mathbf{x}}\Psi(\mathbf{x}) = \mathbf{D}_{\mathbf{x}}\Phi + D_t\Phi \cdot \mathbf{D}_{\mathbf{x}}\tau \,. \tag{25}$$

Differentiating the equation $g(\Phi(\mathbf{x}, \tau(\mathbf{x}))) = c$ gives

$$\mathbf{D}_{\mathbf{x}}g \cdot (\mathbf{D}_{\mathbf{x}}\Phi + D_t\Phi \cdot \mathbf{D}_{\mathbf{x}}\tau) = 0 \,. \tag{26}$$

Now $D_t\Phi = \mathbf{f}(\mathbf{x}, \tau)$ by the flow property and $\mathbf{D}_{\mathbf{x}}g \cdot \mathbf{f} \neq 0$, so (26) implies that $\mathbf{D}_{\mathbf{x}}\tau = -(\mathbf{D}_{\mathbf{x}}g \cdot \mathbf{f})^{-1} \cdot \mathbf{D}_{\mathbf{x}}g \cdot \mathbf{D}_{\mathbf{x}}\Phi$. Using this, we compute the following from (25):

$$\mathbf{D}_{\mathbf{x}}\Psi = \mathbf{D}_{\mathbf{x}}\Phi - (\mathbf{D}_{\mathbf{x}}g \cdot \mathbf{f})^{-1} \cdot \mathbf{f} \cdot \mathbf{D}_{\mathbf{x}}g \cdot \mathbf{D}_{\mathbf{x}}\Phi \,. \tag{27}$$

These formulae are used in the numerical computations of periodic orbits and their eigenvalues, to be described next.

4.3. Numerical Methods. Models of legged locomotion are hybrid dynamical systems in which the continuous time vector fields are constrained Lagrangian mechanical systems. These differ from generic ODEs in two substantive ways, both of which must be addressed to achieve accurate simulation.

- Events encountered by trajectories must be detected and computed accurately.
- The DAEs have index 3.

With regard to the second point, a DAE has differential index k if k differentiations of the original system are required to obtain a system of *ordinary* differential equations whose trajectories coincide with solutions of the DAE [169]. Mechanical systems with time-dependent holonomic constraints can be written in the form

$$\begin{aligned} \dot{\mathbf{q}} &= \mathbf{u} \,, \\ \mathbf{M}(\mathbf{q},\, t)\dot{\mathbf{u}} &= \mathbf{f}(\mathbf{q}\,, \mathbf{u},\, t) - \mathbf{G}^T(\mathbf{q},\, t)\lambda \,, \\ \mathbf{g}(\mathbf{q},\, t) &= \mathbf{0} \,, \end{aligned}$$

where $\mathbf{M}$ is a positive-definite mass matrix, $\mathbf{g}$ specifies the constraint functions, $\mathbf{G}(\mathbf{q},\, t) = \mathbf{D}_{\mathbf{q}}\mathbf{g}$, and λ is a vector of Lagrange multipliers. Since λ does not appear in the third (constraint) equation, this cannot be solved algebraically to eliminate λ, but by differentiating it twice with respect to time we obtain the DAE system

$$\begin{bmatrix} \mathbf{M} & \mathbf{G}^T \\ \mathbf{G} & \mathbf{0} \end{bmatrix} \begin{pmatrix} \dot{\mathbf{u}} \\ \lambda \end{pmatrix} = \begin{pmatrix} \mathbf{f} \\ -(\mathbf{u}^T\, \mathbf{D}_{\mathbf{qq}}\mathbf{g}\, \mathbf{u} + \mathbf{D}_{\mathbf{q}t}\mathbf{g}\, \mathbf{u} + \mathbf{D}_{tt}\mathbf{g}) \end{pmatrix},$$

in which the matrix is generically nonsingular. Differentiating once more yields a regular ODE for λ. This makes three differentiations in all. See [265, Chapter 2] for more details.

Before addressing numerical issues per se, one must first express the equations of motion in consistent forms amenable to the solution methods to be used. For multibody mechanical systems, doing this by hand is tedious and error-prone. In this section, we describe new methods from E. Phipps' thesis [265] that have the potential to significantly outperform existing methods in accuracy and ease of problem formulation.

Newton's laws of motion for a constrained multibody system state that the time-derivatives of its linear and angular momenta are given by the forces and moments acting on the bodies. Application of these laws requires a minimal set of coordinates that specify the state of the system. As even the simpler examples of section 5 below indicate, expressions for velocities and accelerations in these coordinates can be lengthy, making it cumbersome to derive Newton's equations in this "direct" manner. While automated systems have been developed to aid in these derivations, Lagrangian formulations give a more concise approach, their main advantage being that the system's kinetic and potential energies can be described in terms of redundant coordinates so long as these are subjected to the relevant constraints. The price paid for doing this is that the resulting Euler–Lagrange equations of motion are DAEs rather than ODEs. Moreover, even in the Lagrangian formulation, the differentiations that produce the Euler–Lagrange differential equations yield lengthy expressions for systems of modest size. It is therefore desirable to simulate a system automatically from inputs that consist *only* of the Lagrangian and the constraints. Phipps [265] designed and implemented codes to do just this.

Phipps computes Taylor series expansions of trajectories, as functions of time, directly from the Lagrangian and the constraints. He allows constraint functions that are smooth in positions and linear in velocities. In principle, this is a straightforward process involving substitution of expansions with undetermined coefficients into the Euler–Lagrange and constraint equations and solving for the coefficients. In practice, one needs methods that handle data structures for the Taylor series expansions and the lengthy algebra involved in solving the equations. Such methods have been developed as part of a collection of techniques known as *automatic differentiation* or *computational differentiation* [160, 161]. A code that evaluates a function expressed in terms of elementary functions contains the information needed to compute its derivatives. Automatic differentiation codes carry out the process by applying differentiation rules for elementary functions and binary operations in a step-by-step fashion. Many intermediate results are generated in automatic differentiation; these need not be explicitly displayed, but the methods are memory intensive. Indeed, the Euler–Lagrange equations themselves can be hidden from the user. One of the advantages of automatic differentiation over approximation of derivatives by finite differences is that there are no truncation errors: accuracy is limited only by round-off errors in applying differentiation rules.[12]

The result of applying automatic differentiation to a Lagrangian with constraints is a large system of equations for the coefficients of the degree-d Taylor polynomial

[12]Since the Euler–Lagrange equations contain derivatives of the Lagrangian, automatic differentiation codes must be capable of recursive application: if F is defined by applying automatic differentiation to a function f, then we want to be able to apply automatic differentiation to the function F. Making extensive use of C++ templates, Phipps developed an automatic differentiation code with this capability.

of a trajectory. Here d is an algorithmic parameter that determines the asymptotic order of accuracy of the algorithm. In the case of ODEs, the system of equations is triangular and readily solved. Equations derived from DAEs are not triangular, so it is necessary to address their regularity and efficient methods for their solution. Phipps states hypotheses that the constraints must satisfy for regularity to hold, implying that the DAE reduces to an ODE on a submanifold of the state space. (These are satisfied for many locomotion models; indeed, a minimal set of generalized coordinates explicitly defines the vector field on such a submanifold.) He then gives procedures for evaluating this vector field and computing its Taylor series expansion.

The problem of computing events accurately is easy to solve with Taylor series methods. The representation of trajectories as a concatenation of segments defined by Taylor polynomials is *dense*: its order of accuracy is maintained at all points of the segment. Therefore, intersections of the curves defined by the Taylor polynomials with patch boundaries locate the events to the same order of accuracy employed in the numerical integration. This property is manifestly *not* true for many numerical integration methods in which the order of accuracy is attained only at the endpoints of an integration step. Here, the computation of events reduces to a one-dimensional root-finding problem along curves defined by the Taylor polynomials.

The simplest method for seeking periodic orbits (steady gaits) is to follow trajectories for a long time, hoping that they converge to the desired periodic orbit. This strategy works best when the periodic orbit is asymptotically stable with return map having eigenvalues well inside the unit circle. In these circumstances, the orbit has a neighborhood that is attracted to it at an exponential rate determined by the eigenvalues. However, as the examples of section 2.1 and those to come indicate, the periodic orbits of interest here come in continuous families and there are directions which may be unstable, neutrally stable, or only weakly stable. Thus, algorithms that compute periodic orbits directly are a valuable tool for the analysis of locomotion models. We briefly describe methods that can be built "on top" of the Taylor series integrator described above.

Direct computation of a periodic orbit is a boundary value problem. If Φ is the flow of an n-dimensional dynamical system, we seek solutions of the equation $\Phi(\mathbf{x}, t) = \mathbf{x}$. Boundary value methods solve discretized versions of this equation. The most widely used method for computing periodic orbits directly is a *collocation* method implemented in the program AUTO [102], but this has not yet been adapted to hybrid systems. In contrast, *shooting* algorithms assume that Φ and its Jacobian can be computed via a numerical integration method and used directly to solve the equation. In *simple shooting*, one tries to solve the equation $\Phi(\mathbf{x}, t) = \mathbf{x}$. One technical problem that must be addressed is that the system is underdetermined: there are n equations but $n + 1$ variables $(\mathbf{x}, t)$. To obtain a unique solution, one adds another equation (called a *phase condition*), which is satisfied by isolated points of the periodic orbit. Simple shooting algorithms are indeed simple to implement; the Jacobian of Φ is easy to obtain automatically with the Taylor series methods described above. If the return map has no unit eigenvalues and the phase condition defines a surface transverse to the periodic orbit, then the Jacobian of the augmented simple shooting system of equations will be regular and Newton's method will converge quadratically to the solution from nearby starting values.

Simple shooting methods are hopelessly ill-conditioned on many problems. Multiple shooting methods alleviate this difficulty by breaking up the periodic orbit into segments, solving a system of equations $\Phi(\mathbf{x}_i, t_i) = \mathbf{x}_{i+1}$ for points $\mathbf{x}_0, \mathbf{x}_1, \ldots, \mathbf{x}_N$ and times $t_0, \ldots, t_N$ with $\mathbf{x}_{N+1} = \mathbf{x}_0$. This seems to complicate the problem, creating

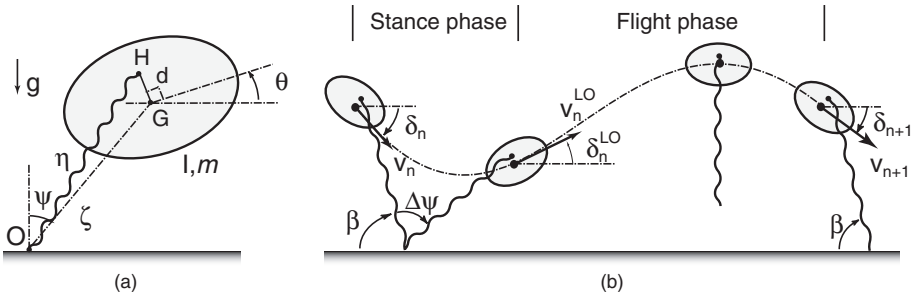

Fig. 13 *The SLIP including pitching.* (a) *The stance coordinate system;* (b) *the stance and flight phases comprising a full stride. Adapted from* [145].

a larger system of equations to solve and making the system even more underdetermined. The payoff is that a much broader class of problems can be solved, and extension to hybrid systems is straightforward. Specifically, transition maps are included in the discretization $(\mathbf{x}_i, t_i)$ of the periodic orbit by regarding the boundary functions defining events as phase conditions for the boundary value solver. The transition maps are applied at events and their Jacobians are inserted in the computation of Jacobians for the periodic orbit. Guckenheimer and Meloon [167] describe implementations of multiple shooting methods using the Taylor series integration described above. Phipps [265] extends these multiple shooting methods to hybrid systems.

4.4. A Piecewise Holonomic Example: The SLIP. The discrete Chaplygin sled of section 2.1.2 shows that (partial) asymptotic stability is possible in some hybrid systems, even if the continuous time vector fields defining each epoch are Hamiltonian. We now return to a more complex and realistic locomotion model that also exhibits asymptotic stability, the SLIP. However, before describing it we note that other hybrid systems have return maps whose natural canonical structures preclude asymptotic stability. One set of such examples is that of "billiards" problems involving rigid bodies bouncing elastically at collisions with each other or with prescribed boundaries [29, 310]. A particularly simple case—a single elastic ball bouncing on a sinusoidally vibrating table—may be simplified as the area-preserving standard map [166, section 2.4].

In order to relate to horizontal plane (LLS) models in which yawing motions play an essential role, we describe a generalized SLIP, endowed with rotational inertia (Figure 13; cf. Figure 4), although here we shall analyze only the nonrotating or point mass case. A massless, axially sprung leg of unstressed length l is attached to an extended body of mass m and moment of inertia I at a hip joint, H, a distance d from the COM, G. The system's configuration is determined by the pitch angle θ and COM position $(x_{\mathrm{G}}, y_{\mathrm{G}})$ referred to an inertial frame, although during stance it is convenient to replace the Cartesian coordinates $(x_{\mathrm{G}}, y_{\mathrm{G}})$ by polar coordinates: the angle ψ between the line joining foothold O to G and the vertical (gravity) axis, and the distance ζ from foothold to COM (Figure 13(a)). (Note that ψ increases clockwise, while θ increases counterclockwise.) The (compressed) spring length is

$$\eta = \sqrt{d^2 + \zeta^2 + 2d\zeta \cos(\psi + \theta)}\,. \tag{28}$$

For simplicity, we take frictionless joints at O and H. Cartesian coordinates provide the simplest description during flight. The body is assumed to remain in the sagittal

plane throughout. As we have noted, more complex running models with elastic legs that include leg masses and hip springs have also been studied [268, 236].

A full stride divides into a stance phase with foothold O fixed, the leg under compression, and the body swinging forwards (ψ increasing); and a flight phase in which the body describes a ballistic trajectory under the sole influence of gravity. Stance ends when the spring unloads at leg length l and the foot reaction force drops to zero; flight then begins, continuing until touchdown, which occurs when the landing leg, uncompressed and set at a predetermined angle β relative to horizontal, contacts the ground (Figure 13(b)). Control is applied only to reorient the leg during flight, prior to touchdown. The touchdown and liftoff events are, respectively, determined by COM height y_{G} first reaching $l\sin\beta - d\cos\theta$ from above and leg length η first reaching l from below, and COM positions and velocities are unchanged by either event. Thus, relative to the stance phase coordinate origin O of Figure 13, at liftoff $(x_{\mathrm{G}}^{LO}, y_{\mathrm{G}}^{LO}) = (\zeta^{LO}\sin\psi^{LO}, \zeta^{LO}\cos\psi^{LO})$. A similar transition map from Cartesian to polar coordinates applies at touchdown.

Using the coordinate system of Figure 13, the kinetic and potential energies of the body may be written as

$$T = \frac{1}{2}m\left(\dot{\zeta}^2 + \zeta^2\dot{\psi}^2\right) + \frac{1}{2}I\dot{\theta}^2\,, \tag{29}$$

$$V_{tot} = mg\zeta\cos\psi + V\left(\eta\left(\zeta,\psi,\theta\right)\right)\,, \tag{30}$$

where V denotes the spring potential. Forming the Lagrangian $L = T - V_{tot}$ and writing $\partial V/\partial\eta = V_\eta$, we obtain the equations of motion for the stance phase:

$$\ddot{\zeta} = \zeta\dot{\psi}^2 - g\cos\psi - \frac{V_\eta\left(\eta\right)}{m\eta}\left(\zeta + d\cos\left(\psi+\theta\right)\right)\,, \tag{31a}$$

$$\zeta\ddot{\psi} = -2\dot{\zeta}\dot{\psi} + g\sin\psi + d\frac{V_\eta\left(\eta\right)}{m\eta}\left(\sin\left(\psi+\theta\right)\right)\,, \tag{31b}$$

$$\ddot{\theta} = d\zeta\frac{V_\eta(\eta)}{I\eta}\sin\left(\psi+\theta\right). \tag{31c}$$

The flight phase dynamics are determined by the ballistic COM translation and torque-free rotation equations, which may be integrated in Cartesian coordinates to yield

$$x_{\mathrm{G}}(t) = x_{\mathrm{G}}^{LO} + \dot{x}_{\mathrm{G}}^{LO}t\,,\ y_{\mathrm{G}}(t) = y_{\mathrm{G}}^{LO} + \dot{y}_{\mathrm{G}}^{LO}t - \frac{1}{2}gt^2\,,\ \theta\left(t\right) = \theta^{LO} + \dot{\theta}^{LO}t\,, \tag{32}$$

where the superscripts LO refer to the system state at liftoff.

Equations (31) are in general nonintegrable [16, 166, 181] and the stance trajectory must be obtained numerically, even in the special case $d = 0$ in which the rotation (θ) variable decouples and the system reduces to the two-DOF point mass SLIP of [32, 34]. However, if $d = 0$ and we additionally assume that the spring is sufficiently strong, elastic energy dominates the gravitational potential during most of the stance phase and we may neglect the gravitational force and moment entering (31a)–(31b). In this case the COM dynamics becomes a central force problem with cyclic angular variables [151] that vanish from the right-hand sides of these equations, so the moment of linear momentum of the COM about the foot, $m\dot{\psi}\zeta^2$, is also conserved and (31a) may be integrated precisely as in the $d = 0$ and truly gravity-free LLS analyzed in section 5.1.1. This approximation is assessed and discussed in detail in [298].

Geyer, Seyfarth, and Blickhan [143] employ a different approximation, retaining gravitational forces but linearizing about the midstance compressed state. Their approximation is effective for small angles and weak springs, and reveals the interaction between elastic and gravitational forces. Ghigliazza et al. [145] conduct parameter studies of SLIPs with both linear and nonlinear spring laws (the latter corresponding to pneumatic devices used in some hopping robots [268]) in terms of a nondimensional parameter $\gamma = kl/mg$. This parameter is the product of Strouhal (kl^2/mv^2) and Froude (v^2/gl) numbers and expresses the relative importance of elasticity and gravitation.

Composition of the stance and flight phase dynamics yields the approximate touchdown-to-touchdown Poincaré map

$$P : \begin{bmatrix} v_{n+1} \\ \cos(\delta_{n+1}) \end{bmatrix} = \begin{bmatrix} v_n \\ \sqrt{1 - \frac{2gl}{v_n^2}(\sin(\beta + \Delta\psi) - \sin\beta)}\cos(\delta_n + \pi - \Delta\psi - 2\beta) \end{bmatrix}, \tag{33}$$

in which the system's state at the nth touchdown is described by the COM velocity magnitude v_n and direction δ_n with respect to a horizontal datum (Figure 13(b)). In (33) the angle $\Delta\psi$ swept by the leg is given by the quadrature

$$\Delta\psi(v_n, \delta_n) = 2\int_{\zeta_b}^{l} \frac{d\zeta}{\zeta\sqrt{\frac{[mv_n^2 - 2V(\zeta)]\zeta^2}{mv_n^2 l^2 \sin^2(\beta - \delta_n)} - 1}}, \tag{34}$$

where ζ_b is the leg length at midstride. In reducing this two-DOF system to a two-dimensional rather than three-dimensional return map, we are using the fact that the prescribed leg touchdown angle fixes the COM position relative to the stance coordinate origin: $(x_{\mathrm{G}}^{TD}, y_{\mathrm{G}}^{TD}) = (-l\cos\beta, l\sin\beta)$. If pitching motions were allowed, two further state variables, θ_n and $\dot{\theta}_n$, would be required, and the map would be four-dimensional, as for the LLS and other models of section 5.

Note that, due to energy conservation and the "constant height" touchdown protocol for $d = 0$, the COM speed v_n is the same at each touchdown. This is true even when gravity is included during stance. The dynamics is therefore captured by the one-dimensional map formed from the second component of (33) with speed $v_n = \bar{v}$ viewed as a parameter. Figure 14 shows an example for a linear spring $V = k(\eta - l)^2/2$. The gap in the domain of definition for higher speeds is caused by liftoff conditions for which the COM fails to reach the necessary touchdown height during flight and "stumbling" ensues [145]. The maps shown here indicate that, for speeds $\bar{v}$ above a critical lower limit $\bar{v}_{SN}$ at which a saddle-node bifurcation [166] occurs, a stable fixed point exists, although its domain of attraction shrinks dramatically as $\bar{v}$ increases. For other parameter choices and spring laws, period doubling and even chaos may occur [145]. For $\bar{v} < \bar{v}_{SN}$, the forward velocity at touchdown is too low to overcome the potential energy barrier due to the forward-oriented spring leg, and the mass (eventually) bounces backward; hence no periodic gaits exist.

Although the quadrature of (34) can be evaluated, in the case of a quadratic potential, in terms of Jacobian elliptic functions [291], the expressions are difficult to use and the return maps of Figure 14 were computed by direct (fourth-order Runge–Kutta) integration of (31a)–(31b) for $d = g = 0$.

We have also computed analogous maps including gravitational effects (but still for $d = 0$) using the Taylor series methods described in section 4.3. Rather than reducing to a two- or one-dimensional map, here one finds polynomial approximations to trajectories of this two-DOF hybrid system in the full four-dimensional phase

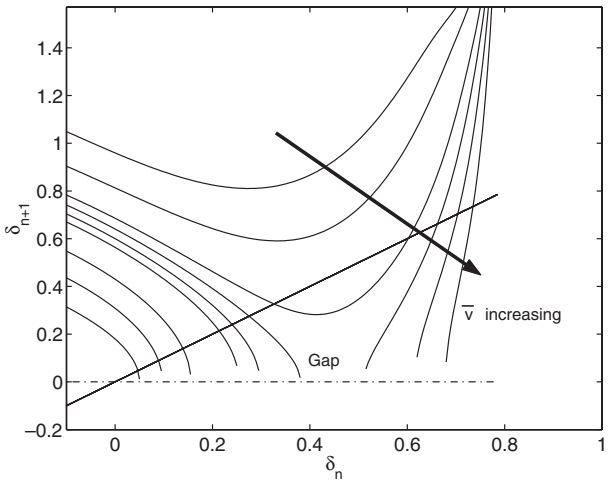

Fig. 14 *A family of approximate one-dimensional Poincaré maps for a linear spring SLIP with* $k = 10, m = 1, l = 1.5, \beta = \pi/4$ *and speeds* $\bar{v}$ *ranging from* 3.2 *to* 8. *The fixed points appear in a saddle-node bifurcation, and a gap then opens as* $\bar{v}$ *increases. When a pair of fixed points exists, the one at larger* δ *is unstable; the lower* δ *one may be stable or unstable, and for very high speeds only the latter exists. From* [145].

space. Applying Newton's method to the resulting return map and computing its Jacobian, we find, for example, that the stable fixed point has eigenvalues $0, 1, 1$, and approximately -0.146 at $\bar{v} = 5.12$. The (generalized) eigenspace of 1 is tangent to the plane spanned by the vector field (i.e., the direction along the orbit) and the family of periodic orbits obtained by varying $\bar{v}$, and the zero eigenvalue is due to the singularity of the transition map at touchdown. The final eigenvalue is that of the reduced one-dimensional map. Figure 15 shows results for a range of speeds (total energies); this figure should be compared with Figure 14. Note the qualitative agreement and quantitative differences.

It seems a natural generalization to leave the saggital plane and consider fully three-dimensional SLIP models, at first as three-DOF point masses bouncing on passive springs, and subsequently as six-DOF rigid bodies. However, aside from simulation studies such as those referred to in section 2.3, there appear to have been few analyses. The thesis of Carver [67], in which control strategies for steering and foot placement were developed, is a notable exception, and it has also recently been shown, neglecting gravity during stance as above, that the point mass monopod SLIP is always unstable to a mode that involves toppling out of the saggital plane, but that it can be easily stabilized by suitable, step-to-step feedback adjustments of leg angle at touchdown [301, 299]. See section 5.1.5 for more information.

The partial asymptotic stability of the saggital SLIP, and of the horizontal plane LLS models to be studied in section 5 below, prompts the following question.

Question. What are the characteristics of the events and transition maps needed to obtain asymptotically stable periodic orbits in a (conservative) piecewise holonomic system? In systems with symmetries, what is needed to obtain partially asymptotically stable periodic orbits? See Altendorfer, Koditschek, and Holmes [12] for a relevant, albeit far from complete, discussion.

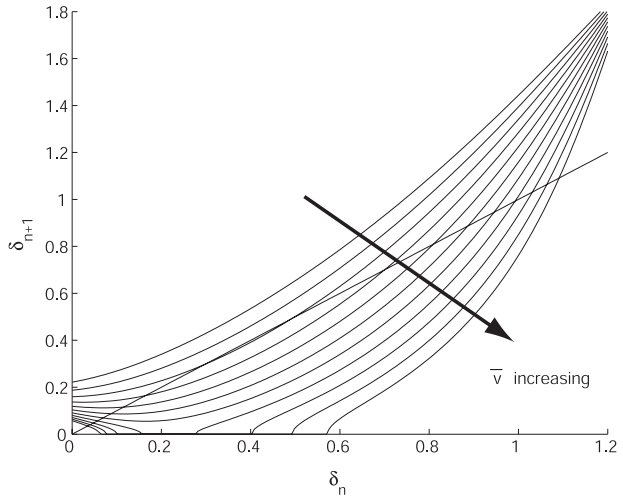

Fig. 15 *A family of one-dimensional Poincaré maps computed by Phipps' method. Gravity was included during stance. Fixed parameters are* $m = 1$ *and* $l = 1.5$ *with the gravitational constant normalized to be* 1. *The touchdown speed* $\bar{v}$ *is varied from* 3.2 *to* 8 *in steps of* 0.48, *to match the speeds used for Figure* 14. *Newton's method was used to precisely compute the stable periodic orbit with* $\bar{v} = 5.12$. *The nontrivial eigenvalue of its monodromy map is* -0.146.

At this point it is worth noting an important distinction between *inertial* and *body frame* coordinate systems. Newton's laws must be formulated in an inertial (nonaccelerating) frame [151], while limb positions and forces generated in muscles, or collectively by limbs, are usually most conveniently represented in body coordinates. Proprioceptive sensing and preflex or reflex control also take place in the body frame. In formulating (31)–(32) we use only inertial frames, but in the models of section 5 we pass back and forth between inertial and body frames using rotation matrices.

The point mass SLIP with the fixed touchdown protocol described above is simple enough to be amenable to (almost) complete analysis, although little is known about coupled pitching motions (in case $d \neq 0$), or other touchdown protocols. Here we have assumed the simplest such, requiring a minimum of feedback: mere knowledge of the inertial horizontal datum during flight. Given this, leg placement is effected by feedforward control. More complex procedures have been proposed, including ones in which the leg is retracted so that either it begins its back swing prior to touchdown [304, 305, 307, 12], or, as in the hexapedal robot RHex [284, 285], after liftoff it continues to rotate in the same direction, passing "over the shoulder." These effectively enlarge the domain of attraction of stable gaits, partly by allowing the SLIP to recover from stumbling.

5. Mathematical Models for Horizontal Plane Dynamics. We now move from a general survey of biomechanics and neuromuscular control of locomotion to an account of a range of models that we have developed ourselves. We offer these as examples, starting with a simple biomechanical template—the LLS—and culminating in work in progress to integrate CPG, muscles, body, and limbs in a more detailed model anchored in biology. To make the main ideas clear, we give a fairly detailed description of the simplest model and then successively curtail our accounts as we move to more complex models, referring the reader to relevant literature.

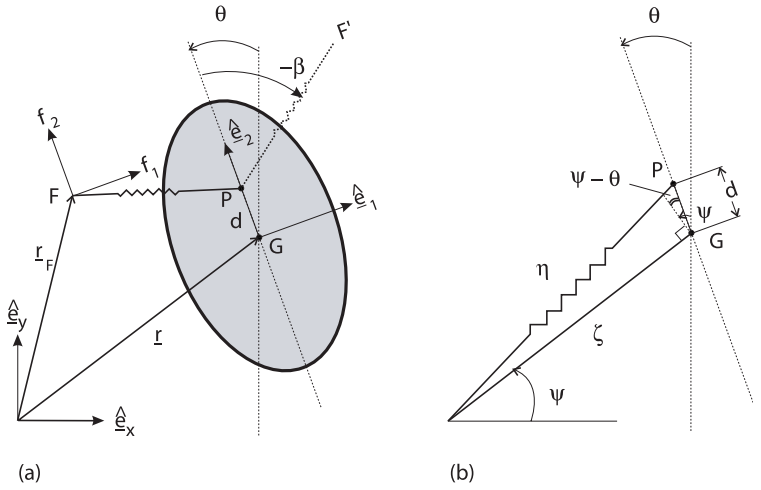

Fig. 16 *The LLS model:* (a) *the general setup;* (b) *the* (ζ, ψ, θ) *polar coordinate system used during left stance phase. Here leg length is* η *and* $\pm\beta$ *denote leg touchdown angles. From Figure* 2 *of* [291]. *Reprinted with kind permission from Springer Science and Business Media.*

As we have described, legged dynamics in the sagittal plane is often modeled by an inverted elastic pendulum or SLIP (e.g., [68, 242, 32, 244, 34]). Since the typical splayed insect leg posture implies sagittal static stability for the majority of stance positions [317], in [291, 292] we introduced a similar model (without gravity) to explore motions in the horizontal plane: the lateral leg spring (LLS) system. Our hope is that, at least in near-steady gaits, sagittal and horizontal plane dynamics might be only weakly coupled, so that independent analyses will help us build toward an understanding of the full six-DOF body motions (see section 5.1.5 below). Moreover, since in many insects leg masses are a small fraction of body mass, we neglected limb masses. (In *Blaberus*, for example, if we include the coxa joint, which does not move appreciably, with the body, total leg mass is $\approx 5\%$ of body mass [214, Table 1].) For additional simplicity, and to capitalize on conservation of angular momentum in central force problems, we at first restrict our analysis to bipedal models with a 50% duty cycle, so that precisely one "effective foot," representing three legs of a tripod acting as one, is in ground contact at any time. If foot contact is assumed torque-free, for such models angular momentum is conserved about the stance foot, as it is about the peg in the model of section 2.1.2.

5.1. The Simplest Passive Model. The basic LLS model is shown in Figure 16(a). A rigid body of mass m and moment of inertia I moves freely in the plane under forces generated by two massless, laterally rigid, axially elastic legs, pivoted at a point P (generally displaced forward or backward a distance d from the COM G), and intermittently contacting the ground at feet F, F' with a 50% duty cycle. F, F', and P are pin joints (no torques). In considering multilegged animals, we appeal to the stereotyped use of a double-tripod gait in hexapods [136] and a double-quadruped gait in crabs [33], and represent each support set in stance by a single effective or *virtual* leg. Errors induced by collapsing leg groups linked in such stance phases to a single virtual leg are discussed below, and in section 5.3 we shall describe a hexapedal model that overcomes this problem.

A full stride begins at left touchdown at time $t = t_n$ with the left leg spring relaxed at angle $+\beta$ relative to body orientation; the left stance phase ends at t_{n+1} when the spring is again relaxed, the body having "run past its foot." The left leg then begins its swing phase and the right leg simultaneously touches down at angle $-\beta$; its stance phase, and the stride, ends with spring relaxation at right liftoff/left touchdown t_{n+2}. We use the convention that n even (resp., odd) refers to left (resp., right) stance. Balance of linear and angular momentum results in three scalar equations of motion for COM translation $\mathbf{r}(t) = (x(t), y(t))$ and body orientation $\theta(t)$ during stance:

$$m\ddot{\mathbf{r}} = \mathbf{R}(\theta(t))\,\mathbf{f}\ , \quad I\ddot{\theta} = (\mathbf{r}_{\mathrm{F}}(t_n) - \mathbf{r}) \times \mathbf{R}(\theta(t))\,\mathbf{f}, \tag{35}$$

where $\mathbf{R}(\theta)$ is the rotation matrix, needed to transform leg forces $\mathbf{f}$, usually specified relative to the body, to the inertial frame; $\mathbf{r}_{\mathrm{F}}(t_n)$ denotes touchdown foot position, expressed via d, l, β, and body angle $\theta(t_n)$ at touchdown, and $\times$ denotes the vector cross-product. The "hip-pivot" P may be fixed or may move in a prescribed manner (perhaps dependent on leg angle ϕ relative to body); the specific (linear) rule

$$d = d_0 + d_1(\psi - \theta) \tag{36}$$

exemplifies both cases ($d_1 = 0$: fixed; $d_1 \neq 0$: moving). We shall initially suppose that d is fixed.

Global conservation of total energy and conservation of angular momentum $L_F = I\dot{\theta} + (\mathbf{r} - \mathbf{r}_F) \times m\dot{\mathbf{r}}$ about the foot in each stance phase assist in integration of (35), which is most easily done in a polar coordinate system centered on the foot: Figure 16(b). We summarize the results, a complete account of which appears in [291]. In terms of the polar coordinates (ζ, ψ) and θ, the kinetic and potential energies and the total angular momentum about the (left) stance foot take the forms

$$T = \frac{1}{2}m(\dot{\zeta}^2 + \zeta^2\dot{\psi}^2) + \frac{1}{2}I\dot{\theta}^2\,, \tag{37}$$

$$V = V(\eta) \quad \text{with} \quad \eta = \sqrt{\zeta^2 + d^2 + 2\zeta d\sin(\psi - \theta)}, \tag{38}$$

$$L_F = m\zeta^2\dot{\psi} + I\dot{\theta} \stackrel{\mathrm{def}}{=} p_\psi + p_\theta\ (= \text{const.}), \tag{39}$$

and Lagrange's equations are

$$m\ddot{\zeta} = m\zeta\dot{\psi}^2 - \frac{V_\eta}{\eta}[\zeta + d\sin(\psi - \theta)], \tag{40a}$$

$$m(2\zeta\dot{\zeta}\dot{\psi} + \zeta^2\ddot{\psi}) = -d\frac{V_\eta}{\eta}\zeta\cos(\psi - \theta), \tag{40b}$$

$$I\ddot{\theta} = d\frac{V_\eta}{\eta}\zeta\cos(\psi - \theta). \tag{40c}$$

Reflecting about $\theta = 0$, which takes $\theta \mapsto -\theta$, we obtain an analogous description for right foot stance; thus, appeal to our n even-left odd-right convention and replacement of θ by $(-1)^n\theta$ in (40) supplies the two vector fields that, alternately applied, define the hybrid dynamical system. This formulation allows a general spring potential V, but the explicit examples that follow assume a linear spring $V = k(\eta - l)^2/2$. Note that (40) is a gravity-free version of the full SLIP model (31) in its stance phase (with a different definition of leg angle ψ).

Assuming that one stiffness parameter suffices to describe the spring, as in the linear case, the entire model is characterized by six physical parameters: leg stiffness

k, relaxed length l, and pivot position relative to COM d, along with m, I, and β. Normalizing lengths with respect to l and nondimensionalizing time $\tilde{t}$, these may be reduced to four nondimensional groups:

$$\tilde{k} = \frac{kl^2}{mv^2}\ , \quad \tilde{I} = \frac{I}{ml^2}\ , \quad \tilde{d} = \frac{d}{l}\ , \quad \text{and } \beta; \quad \text{with } \tilde{t} = \frac{vt}{l}. \tag{41}$$

Here v is a representative speed (e.g., COM velocity magnitude at touchdown, or average forward speed $\langle v \rangle$) and $\sqrt{\tilde{k}}$ is a Strouhal number characterizing the ratio of storable potential to kinetic energy. Dynamically similar periodic motions have the same Strouhal number [8]. Indeed, for fixed $\tilde{k}, \tilde{I}, \tilde{d}$, and β, solutions of (35) describe *identical* paths in $(\mathbf{r}, \theta)$-space, scaled by l, at rates determined by $\tilde{t}$. This formulation is useful for parameter studies [293], but here we shall retain dimensional quantities to permit direct comparisons with experimental data.

For most of the examples to follow, parameters characteristic of the death-head cockroach *Blaberus discoidalis* were selected [135, 317, 214]: $m = 0.0025$ kg, $I = 2.04 \times 10^{-7}$ kg m^2, $l = 0.01$ m, $d = -0.0025$ m, $k = 2.25 - 3.5$ N m^{-1}, $\beta = 1$ radian (57.3°). I and m may be directly measured, and choices of l and β are constrained by the requirement that stride length $L_s = 4 \cos\beta \approx 0.022$ m at the animal's preferred speed of ≈ 0.25 m s^{-1}. Stiffnesses were chosen to give a reasonable average forward speed range for steady gaits (above $\langle v \rangle \approx 0.15$ m s^{-1}) and to ensure that leg compressions at midstride were not excessive. We shall refer to these choices as the "standard" parameter set.

The three DOFs of (35) or (40) demand specification of six initial conditions; however, as for the sleds of section 2.1, the system is invariant under SE(2) in the sense that only the COM position relative to foothold $(\mathbf{r} - \mathbf{r}_F(t_n))$ and body angle θ relative to inertial frame appear in the governing equations. We find it convenient to define a reduced set of four variables that describe the body's "internal dynamics" at touchdown. As in the SLIP of Figure 13 these are the COM velocity magnitude $v(t_n) = |\dot{\mathbf{r}}_n(t)|$, COM velocity direction or "heading" $\delta(t_n)$ relative to body axis, along with body orientation $\theta(t_n)$ relative to the inertial reference frame, and body angular velocity $\omega(t_n) = \dot{\theta}(t_n)$; see Figure 17(a). Here we retain the "mechanical" terminology of [291, 292]. In traditional biological usage, heading denotes the COM velocity with respect to compass direction, that is, the quantity $\delta + \theta$, and body orientation denotes the angle the body makes with the velocity vector (δ). Note that δ is positive *toward* the leg that is touching down, and $\delta \in [\beta - \pi/2, \beta]$.

Given the total (kinetic) energy at touchdown,

$$E = T_0 = \frac{p_\zeta^2}{2m} + \frac{p_\psi^2}{2m\zeta_0^2} + \frac{p_\theta^2}{2I}\,, \tag{42}$$

where

$$\zeta_0 = \frac{l \sin(\pi - \beta)}{\sin\alpha} \quad \text{and} \quad d \sin\alpha = l \sin(\beta - \alpha) \tag{43}$$

are determined by touchdown geometry, and noting that

$$\dot{\zeta} = v \cos(\beta - \delta) \quad \text{and} \quad \dot{\psi} = \frac{v}{\zeta_0} \sin(\beta - \delta) \tag{44}$$

at touchdown, all six initial values necessary for integration of (40) may be found from $(v, \delta, \theta, \omega)$ and the touchdown parameters l, β. Integration yields left and right

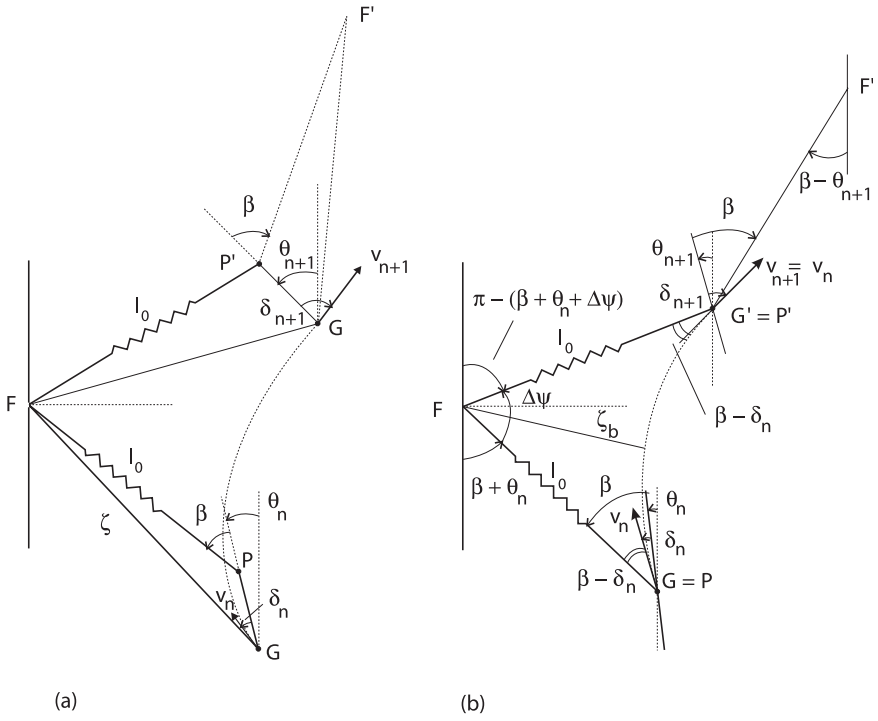

Fig. 17 *Defining a Poincaré map for the LLS model:* (a) *the general case;* (b) *the case* $d = 0$. *From Figure* 3 *of* [291]. *Reprinted with kind permission from Springer Science and Business Media.*

single stance maps $\mathbf{F}_{\mathrm{L}}$ and $\mathbf{F}_{\mathrm{R}}$ specifying these variables at each touchdown instant t_{n+1} in terms of their values at the preceding touchdown t_n, and composition yields the "full L-R stride" Poincaré map $\mathbf{P} = \mathbf{F}_{\mathrm{R}} \circ \mathbf{F}_{\mathrm{L}}$:

$$(v_{n+2}, \delta_{n+2}, \theta_{n+2}, \omega_{n+2}) = \mathbf{P}(v_n, \delta_n, \theta_n, \omega_n), \tag{45}$$

where $v_n = v(t_n)$, etc. Note that the "full stride" includes left and right stance phases, unlike the stance-flight SLIP map of section 2.2, and might more properly be called double stride.

Four-dimensional Poincaré maps of the form (45) suffice to describe *all* the models treated in this section. No matter how many or complex their legs, muscles, or neural architectures, the feet in stance ultimately supply forces and moments to the body via equations of the general form (35), leading to incrementation of the dynamical variables $(v, \delta, \theta, \omega)$ from stride to stride. Thus, the locomotive behaviors of both the LLS template and the more complex and anchored hexapedal and neuromechanical models of sections 5.3–5.4 are summarized by the four-dimensional maps. Of course, this does not mean that the maps are simple to compute in *any* of the examples, but solutions of some special cases may be found in closed form or approximated perturbatively. To these we now turn.

5.1.1. An Integrable Limit: $d = 0$. Using (39), equations (40) can be reduced to two DOFs, but in general no further constant of motion, excepting the total energy, exists. However, if the legs are attached at the COM ($d \equiv 0$), the rotational DOF

θ trivially uncouples and each component p_ψ and p_θ of L_F is individually conserved (cf. (40b), (40c): both ψ and θ are cyclic coordinates). The system is therefore completely integrable and may be reduced to a quadrature using conservation of energy [151, 16]:

$$E = \frac{m\dot{\zeta}^2}{2} + \frac{p_\psi^2}{2m\zeta_0^2} + \frac{p_\theta^2}{2I} + V(\zeta) = E_0\,. \tag{46}$$

Specifically, since $\zeta \equiv \eta$, symmetry of the phase portraits about midstance implies that the angle $(\beta-\delta)$ between the mass center velocity direction and the leg is equal at liftoff to its value at touchdown. As may be seen from Figure 16(b), this implies that the angle δ_{n+1} at right touchdown may be computed from v_n, δ_n at left touchdown as

$$\delta_{n+1} = \delta_n + \pi - (\Delta\psi_n + 2\beta) + (\theta_{n+1} - \theta_n), \tag{47}$$

where $\Delta\psi_n = \Delta\psi(v_n, \delta_n)$ is the net angle the leg turns through during the stance phase. This leads to the single stance maps (n even-left, odd-right)

$$\begin{aligned} v_{n+1} &= v_n, \\ \delta_{n+1} &= \delta_n + \pi - (\Delta\psi(v_n, \delta_n) + 2\beta) + (-1)^n \omega\tau(v_n, \delta_n), \\ \theta_{n+1} &= \theta_n + \omega_n\tau(v_n, \delta_n), \\ \omega_{n+1} &= \omega_n, \end{aligned} \tag{48}$$

where $\tau(v_n, \delta_n)$ denotes the stance phase duration.

Using (44) with $\zeta_0 = l$ and the conserved mass center kinetic plus potential energy, from (40) with $d = 0$ we compute the quadratures

$$\tau(v, \delta) = 2\int_{\zeta_b}^{l} \frac{\sqrt{m}\zeta\; d\zeta}{\sqrt{[mv^2 - 2V(\zeta)]\zeta^2 - mv^2 l^2 \sin^2(\beta - \delta)}}\,, \tag{49}$$

$$\Delta\psi(v, \delta) = 2\int_{\zeta_b}^{l} \frac{d\zeta}{\zeta\sqrt{\frac{[mv^2 - 2V(\zeta)]\zeta^2}{mv^2 l^2 \sin^2(\beta-\delta)} - 1}}\,, \tag{50}$$

where ζ_b is the (minimal) spring length at midstride ($\dot{\zeta} = 0$: Figure 17(b)), given by

$$[mv^2 - 2V(\zeta_b)]\zeta_b^2 = mv^2 l^2 \sin^2(\beta - \delta)\,. \tag{51}$$

Explicit formulae for the cases of quadratic and inverse square potentials, corresponding to a linear spring and a model for an "air spring" [268], are given in [291], but the former are in terms of Jacobi elliptic functions and awkward to use. Schwind and Koditschek [298] provide useful approximations in terms of elementary functions. An upper bound for $\Delta\psi$ is easily found by considering the limit $\bar{v} \to \infty$, in which potential energy may be neglected and the COM travels in a straight line [291]:

$$\Delta\psi(v, \delta) \le \pi - 2(\beta - \delta)\,. \tag{52}$$

Figure 18 shows graphs of the resulting one-dimensional single stance return map (the second row of (48)) for a linear spring and parameters characteristic of *Blaberus discoidalis* over a range of touchdown velocities. When $\Delta\psi$ has a unique maximum and its slope is always less than 2 (for which (52) is necessary but not sufficient, but which holds for linear and air springs [291, 293]), then this map is unimodal [166] and has at most one stable fixed point, an unstable fixed point, and no other invariant sets. Moreover, there is no gap in its domain of definition. (Compare Figure 18 with the SLIP Poincaré maps shown in Figures 14–15 of section 4.4.)

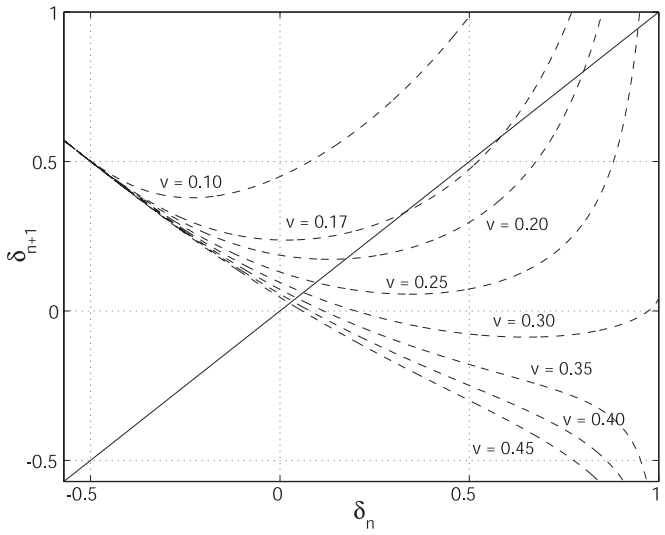

Fig. 18 *The single-stance return map for mass center touchdown velocities* $\bar{v} = 0.1 - 0.45\,\mathrm{m\,sec}^{-1}$ *in the case of a linear spring with* $m = .0025$, $l = .01$, $k = 2.25$, *and* $\beta = 1$. *Reprinted from* [293] *with permission from Elsevier.*

Question. An open question which may appeal to analysts is how to classify those potential energy functions $V(\eta - l)$ that, via (50)–(51), yield return maps possessing at most a unique stable fixed point, or, more generally, a single attractor. The latter would follow if it could be proved that $\delta - \Delta\psi$ has negative Schwarzian derivative [311, 166]. Direct computation of derivatives of $\Delta\psi$ yield indeterminate forms that appear difficult to deal with, and the Schwarzian involves derivatives up to order 3.

Fixed points of (48) correspond to symmetric gaits in which left and right stance phases are mutual reflections and the COM oscillates about a straight path: $(\bar{v}, \bar{\delta}, \bar{\theta}, 0)$, with $\bar{\delta}$ implicitly determined in terms of $\bar{v}$ by

$$\Delta\psi(\bar{v}, \bar{\delta}) = \pi - 2\beta\,. \tag{53}$$

The eigenvalues of the linearized map $\mathbf{DP}(\bar{v}, \bar{\delta}, \bar{\theta}, 0)$ are $\lambda_{1-3} = 1$, with eigenvectors $(0, 0, 1, 0)^T$, $(\partial\Delta\psi/\partial\delta, -\partial\Delta\psi/\partial v, 0, 0)^T$, and a generalized eigenvector; and $\lambda_4 = 1 - \partial\Delta\psi/\partial\delta|_{(\bar{v},\bar{\delta})}$, with eigenvector $(0, 1, 0, 0)^T$. The first of these is associated with rotational invariance and the second with conservation of energy; the third is special to this uncoupled case; as we shall see, for $d \neq 0$ it perturbs away from 1. Note that, as $\bar{v}$ increases, fixed points appear at a critical speed $\bar{v}_c$ in a saddle-node bifurcation when (53) is satisfied and simultaneously $\partial\Delta\psi(\bar{v}, \bar{\delta})/\partial\delta = 1$. For $\bar{v} < \bar{v}_c$ kinetic energy at touchdown is insufficient to overcome the spring potential and the body bounces back. Bifurcation diagrams illustrating branches of steady gaits arising in a similar saddle-node are shown below for $d \neq 0$.

5.1.2. Fixed COP: $d \neq 0$. For $d \neq 0$ (40) is no longer integrable, so we resort to numerical solutions to construct the full stride map $\mathbf{P}$. Details of the methods adopted, including finite difference methods to approximate the Jacobian $\mathbf{DP}$, are given in [291]. For small d a perturbative calculation, using power series approximations for the state variables (η, ψ, θ) on the periodic gait, confirms these results [293].

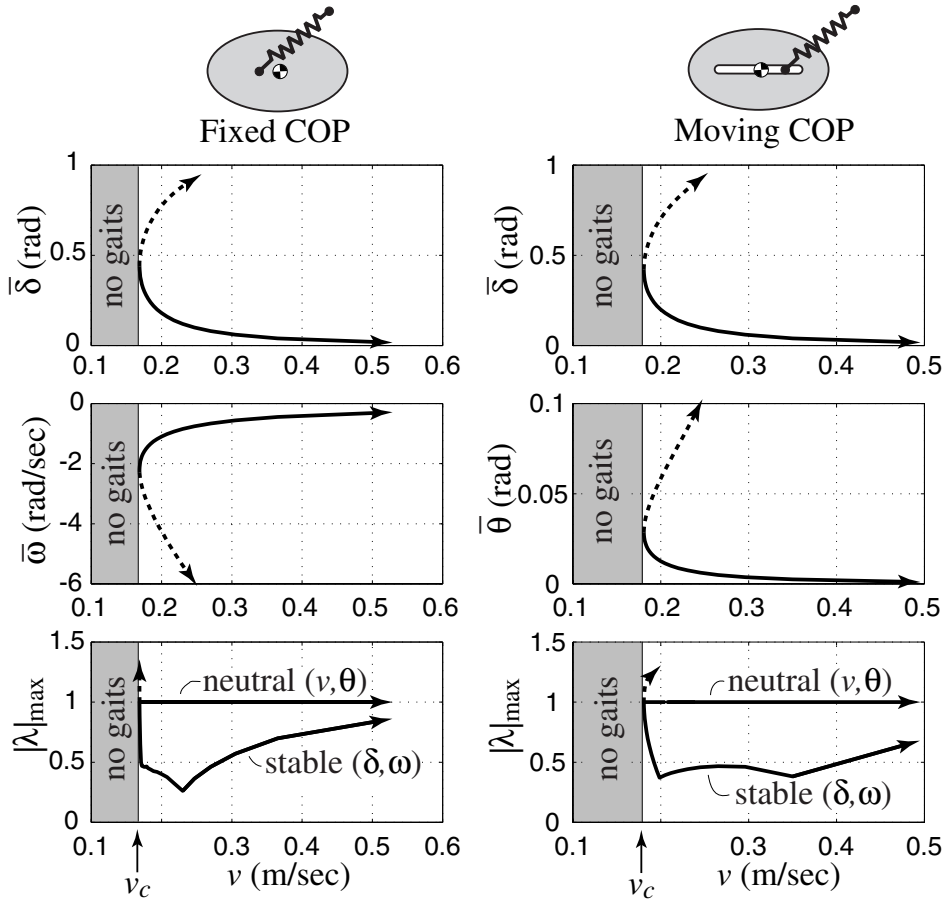

Fig. 19 *Families of periodic gaits for the fixed and moving COP models with "standard" parameters characteristic of* Blaberus discoidalis. *From top to bottom the panels show COM velocity vector direction δ, body angular velocity $\omega \equiv \dot{\theta}$, or body orientation θ at touchdown, and eigenvalue magnitudes $|\lambda|$. (For fixed COP θ = const. at touchdown; for moving COP $\omega = 0$ at touchdown; hence our display of ω and θ, respectively.) Stable branches shown solid, unstable branches dashed (only the neutral and least stable eigenvalues are shown here). Note the saddle-node bifurcations at $\bar{v}_c$, below which periodic gaits do not occur. From Figure* 3 *of* [290]. *Reprinted with kind permission from Springer Science and Business Media.*

We find that the branches of fixed points persist, as shown in Figure 19 (left), and that one of the multiple eigenvalues breaks away from 1, moving inside the unit circle for $d < 0$ and outside for $d > 0$ (Figure 20). Thus, for hip behind COM, rotational coupling leads to bounded yawing oscillations and the body still moves along a straight path. Figure 21 illustrates the effect of an impulsive body angle perturbation applied at touchdown on the third stance phase. After one to two further steps, the body recovers a straight path, having suffered a net heading change due to the angular impulse. The manner in which the touchdown states recover is also shown. Further examples are given in [292].

The fixed COP model, with appropriate geometry, exhibits partially asymptotically stable motions; indeed, since it is a conservative, rotationally invariant system,

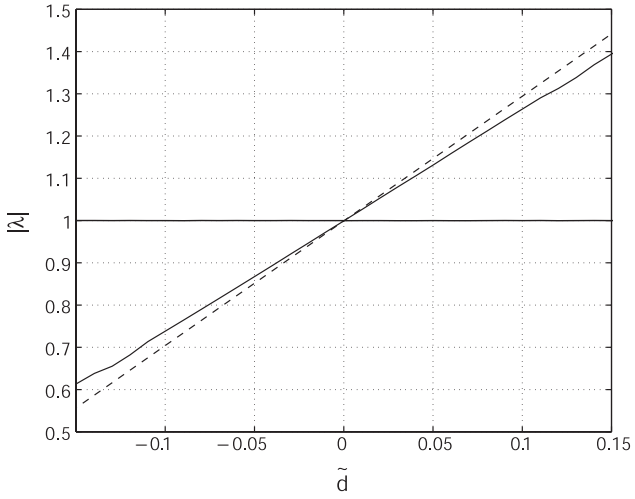

Fig. 20 *Numerically (solid) and analytically (dashed) computed eigenvalues v. nondimensional hip offset* $\tilde{d} = d/l$ *for the standard (*Blaberus*) parameter set. Reprinted from* [293] *with permission from Elsevier.*

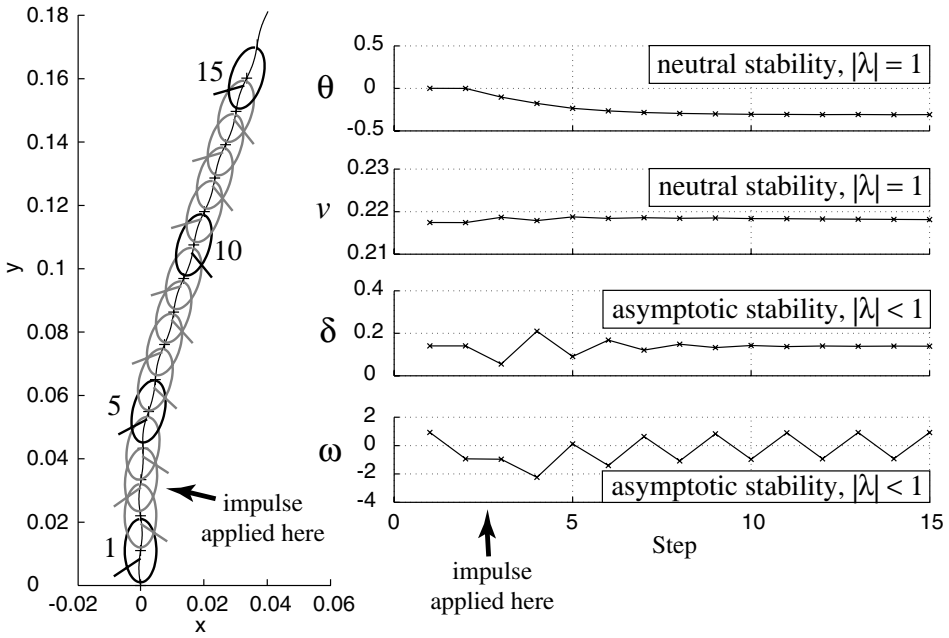

Fig. 21 *Partial asymptotic stability. The fixed COP LLS model recovers from an impulsive angular perturbation applied at arrow in* (a)*; evolution of variables at touchdown is shown in* (b)*. The model is neutrally stable in* θ *and* v *(corresponding eigenvalues* $|\lambda_{1,2}|$ *of unit magnitude) and asymptotically stable in* ω $(\equiv \dot{\theta})$ *and* δ*. From Figure* 2 *of* [290]*. Reprinted with kind permission from Springer Science and Business Media.*

two of the four eigenvalues strictly less than 1 in magnitude are the best we can do. But how well does the gait dynamics compare with experimental data? Figure 22 shows forces, moments, and velocities during a full left–right stride. Comparing forward and

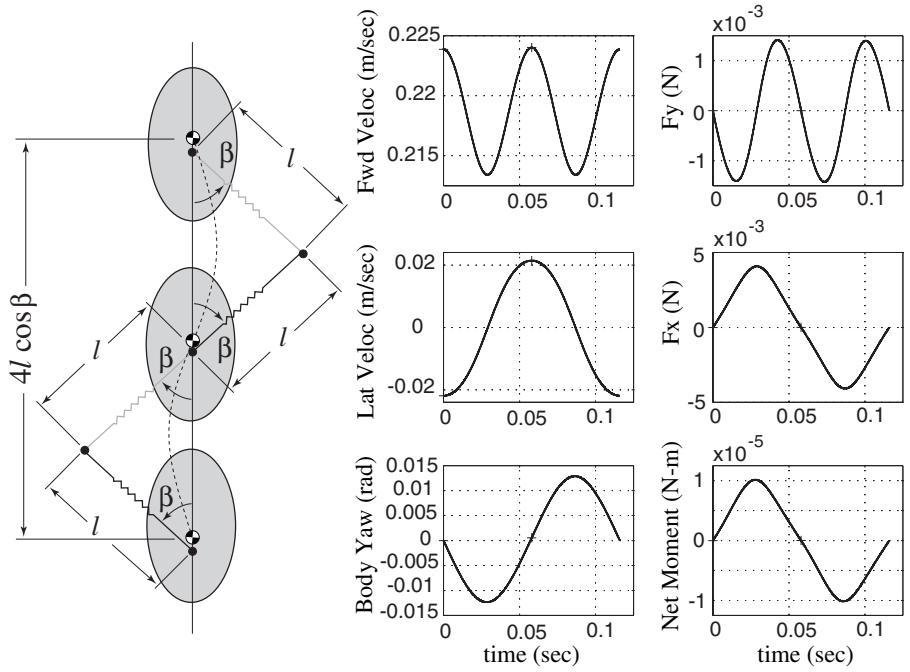

Fig. 22 *COM path, velocity, yaw, and leg force and body moment variations for steady gait of the fixed COP model with standard parameters running at preferred speed* 0.22 m s^{-1}. *From Figure* 4 *of* [290]. *Reprinted with kind permission from Springer Science and Business Media.*

lateral velocities during the stride to those reported in [135, 214] and reproduced in the model of [216] reveals that they match reasonably closely those observed for the cockroach. Forces generated at the foot (or equivalently, at P) also compare fairly well to net leg tripod forces in both orders of magnitude and time histories, although the peak fore-aft forces (± 0.0014 N) and lateral forces (± 0.0041 N) have magnitudes "reversed" from ± 0.004 N and ± 0.0032 N taken to represent typical data in [216]. However, the yawing θ variation for the model differs markedly from observations: it approximates a negative *sinusoid* (central bottom panel of Figure 22(b)). This is due to the torque, which is positive during L-stance and negative during R-stance, since $d < 0$ is fixed during stance (third panel of Figure 22(c)). Experimental studies ([214], and see Figure 24 below) reveal that θ behaves more like a positive *cosinusoid*, with $\dot{\theta} \approx 0$ at touchdown and liftoff.

Question. While explicit quadratures can be evaluated for specific spring laws [291], the resulting expressions are often difficult to use. Taylor series approximations of orbit segments about midstride were developed in [293, 294], but these are lengthy. For SLIP [298] proposed iterative approximations and [143] linearized for small compressions and leg angles close to vertical. For which species are particular approximations most suitable? Can more elegant, accurate, or general approximations be found?

5.1.3. Moving COP. We have noted that the fixed COP model (Figure 22) produces yaw oscillations of sinusoidal rather than the observed cosinusoidal form, due to body torques incurred by the fixed "hip" P. This may be remedied by allowing

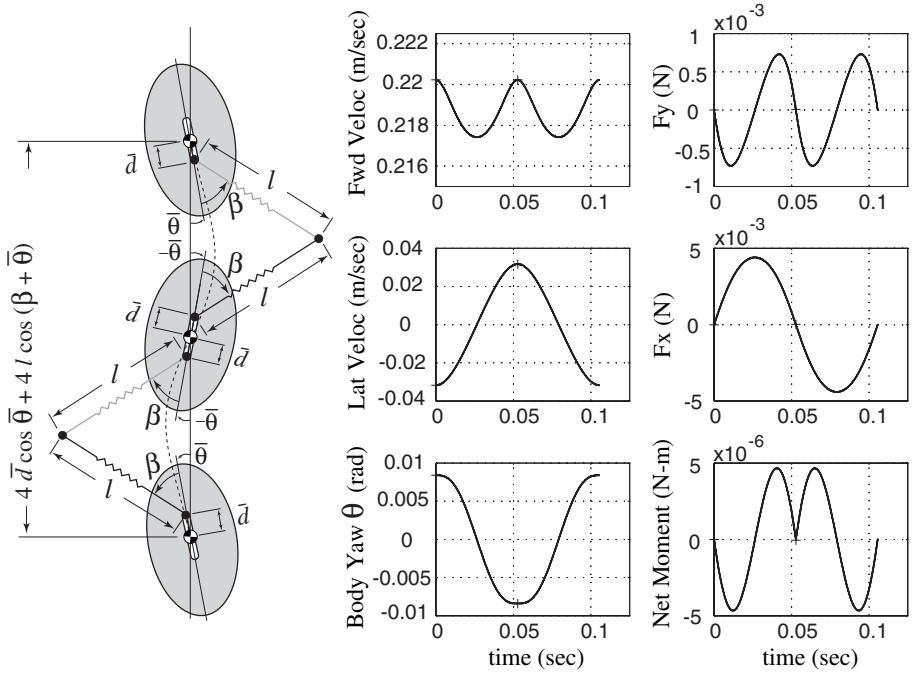

Fig. 23 *COM path, velocity, yaw, and leg force and body moment variations for steady gait of the moving COP model with standard parameters running at preferred speed* 0.22 m s^{-1}. *The stridelength formula assumes that* $d(t)$ *varies symmetrically between* $\bar{d}$ *and* $-\bar{d}$, *respectively;* $\bar{\theta}$ *is the value of* θ *at leg touchdown. From Figure* 5 *of* [290]. *Reprinted with kind permission from Springer Science and Business Media.*

a moving COP, as in Figure 23, for which d was specified by (36) with $d_0 = 0$ and $d_1 = -0.0035$ m, resulting in variation of $d = \pm 0.002$ m, with $d \approx 0$ at midstance; compare the bottom panels of Figures 22 and 23. For these computations, we took $l = 0.008$ m and $k = 3.52$ N m^{-1}; again l and β are constrained by the stride geometry; see Figure 23. Branches of gaits exist for speeds above critical much as in the fixed COP case (Figure 19 (right)).

Quantitative comparisons of lateral force and velocity magnitudes remain reasonable, model values being $\approx 30\%$ higher than experimental values. However, fore-aft magnitudes differ more appreciably, being lower than in the fixed COP model, and lower than experimental values by factors of 2–10 when compared over a large data set [135, 129, 214]. (There is significant variation among trials of individual animals, and among animals, even after scaling to the mass value ($m = 0.0025$ kg) used in the model.) The data shown as solid curves in Figure 24 were reconstructed for a typical run of one animal as in unpublished work of Garcia, Full, Kram, and Wong (2000), from trials of [129] and [214]. These data were selected for their clean phase relationships, although the fore-aft values are unusually high, and we include fore-aft data (dashed) from [135] for a second animal, closer to the mean values adopted in [216], to illustrate the variability.

We also note that the LLS model describes only horizontal plane dynamics, while Figure 24 is derived from three-dimensional motions. This may partially account for the underestimate of fore-aft forces and velocity variations by our models. More

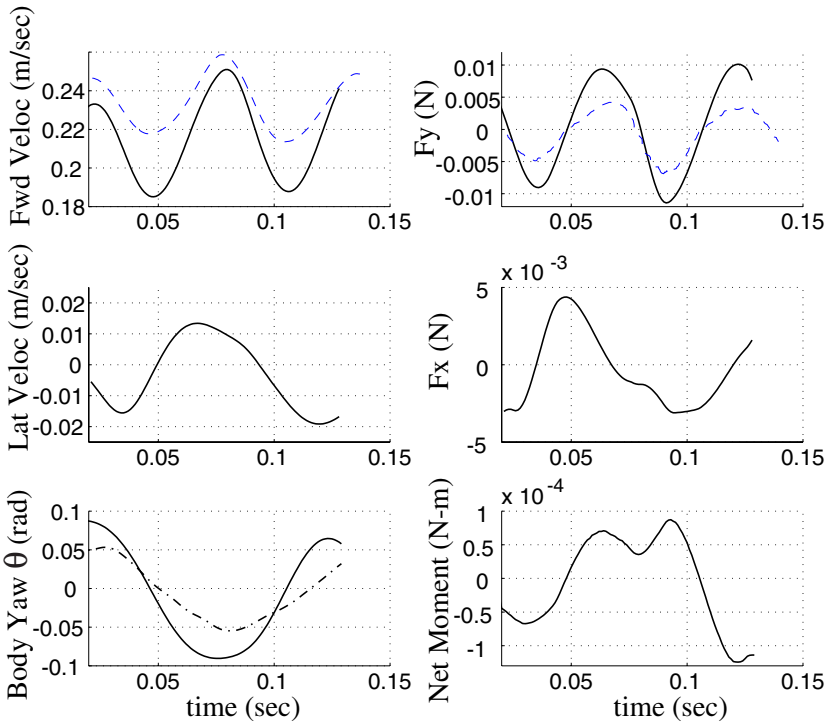

Fig. 24 *Experimentally measured COM velocity, yaw, leg force, and moment variations over a stride for* Blaberus discoidalis *moving at* 0.22 m s^{-1}. *The sign convention is the same as for the models. Data for all components from a single trial* [129, 214] *are shown solid, with yaw angle computed from net moments; the direct kinematic yaw measurement is dash-dotted. The top panels also show as dashed curves fore-aft force and velocity data from a different trial* [135]*, to illustrate variation in magnitudes and average speed (stride durations adjusted to match). Since lateral forces were not simultaneously measured in* [135]*, moments could not be computed, but they exhibit less variability. From Figure* 6 *of* [290]. *Reprinted with kind permission from Springer Science and Business Media.*

strikingly, moments and yaw angles are significantly lower than observed (by factors of 10–20). We ascribe this primarily to the collapse of the leg support tripod to a single virtual leg; for further details see [290]. In section 5.3 we show that a hexapedal model can rectify these quantitative mismatches.

5.1.4. On Similarity, Scaling, and Optimality. The LLS model was developed with insects in mind, cockroaches in particular. However, it may have relevance for other sprawled posture animals, of differing sizes, through similarity relations. For geometrically similar animals, $l \propto m^{1/3}$ and $I \sim ml^2 \propto m^{5/3}$. Stiffnesses are often assumed to scale according to elastic similarity: $k \propto m^{2/3}$ [243], and as noted in section 3.1 animal gaits are usually compared at equal Froude numbers, $Fr = v^2/gl$, as in the SLIP model [32], or equal Strouhal numbers fl/v, where f is a characteristic frequency, as in studies of flight and swimming [8]. The relaxed leg length l defined for the LLS model is the horizontal projection of a full leg length, and thus we may still appeal to Froude number similarity, leading to the relation $v \propto l^{1/2} \propto m^{1/6}$. (We also obtain this directly from Strouhal number similarity.) Hence the nondimensional parameters $\tilde{k}$, $\tilde{I}$, and $\tilde{d}$ of (41) all remain constant for geometrically

and dynamically similar animals, and the model predicts that such animals should possess the same gait characteristics and stabilities, merely scaled in size and time (frequency). For nongeometrically similar species, the scaling relationships developed in [293] also permit prediction of gait families from a single, "standard" parameter set.

By studying behaviors over ranges of parameter values beyond those for which the LLS model was developed, it is also possible to investigate questions of optimality. In [290], for example, we study eigenvalue dependence on average speed and moment of inertia. We find that the cockroach's shape and preferred speed put it close to optimality; specifically, the stride map's maximum (stable) eigenvalue magnitudes are smallest for nondimensional inertia $\tilde{I}$, hip parameter $\tilde{d}$, and forward speed $\bar{v}$ characteristic of normal operation. For example, note that the (larger of the) two stable eigenvalues shown in each of the bottom panels of Figure 19 are close to their minimum values in the preferred speed range 0.2–0.3 m s^{-1}. See [290, Figures 8 and 11], and for more general discussions of the use of simple models, see [133].

5.1.5. On Three-Dimensional Motions. At the beginning of this section we observed that studies of the LLS and SLIP models for horizontal and sagittal plane dynamics are predicated on the assumption that coupling between these motions is relatively weak, and hence that existence and stability results for gaits in those planes should help build toward fully coupled three-dimensional models. We now describe recent work in this direction. Seipel and Holmes [301, 299] have studied a point mass bipedal SLIP model with stereotypical touchdown leg placement defined by two (spherical coordinate) angles β_1, β_2 relative to a fixed inertial frame (β_1 is a splay angle analogous to the LLS leg touchdown angle; β_2 is the leg angle in a saggital plane). This three-DOF model has single leg (L and R) stance phases separated by flight phases, as in the SLIP discussed in section 4.4, and it limits on SLIP (when the touchdown velocity and leg vectors lie in a saggital plane) and LLS (when both vectors lie in the horizontal plane) at either end of a range of β_2 angles. See Figure 25(a).

Using both the approximation of neglect of gravity during stance, which reduces stance phase dynamics to a single DOF system and quadrature similar to that employed above, and numerical integrations of the full system, we find families of gaits parameterized by these angles and touchdown COM speed. The COM paths, projected onto the saggital and horizontal planes, are similar to those of pure SLIP and LLS motions (the flight phases collapse to zero as β_2 approaches the LLS limit of 0). However, all solutions with $\beta_2 \in (0, \pi/2]$ are *unstable* to a "lateral toppling" mode. This is perhaps easiest to appreciate for saggital plane gaits, in which the leg is placed in the plane containing the gait path and any perturbation out of this plane is analogous to tipping an inverted pendulum, but $\beta_1 \neq 0$ motions with legs alternately splayed to left and right in successive stance phases are also unstable.

It is easy to stabilize near-sagittal motions by a simple feedback controller that splays the touchdown leg in the direction of the perturbed touchdown COM velocity vector, thus providing a corrective lateral spring force [299]. A similar leg placement control strategy was devised by Kuo for a rigid leg passive walking model, which is also unstable to a lateral roll–type mode [217]. Carver [67] describes more elaborate leg-placement controls and addresses questions of optimality for specific maneuvers of a three-DOF SLIP. He considers SLIP motions under conditions in which leg stiffness and touchdown angle can be set in response to body position and velocity during flight, and shows that single-step deadbeat control is possible for some tasks, in contrast to asymptotic stability of an open-loop control strategy in which the COM approaches

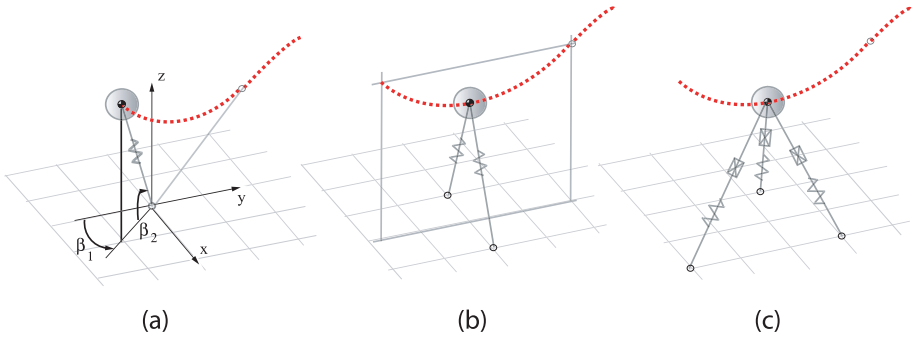

Fig. 25 *Monopedal, kangaroo-type bipedal, and tripod-supported three-dimensional point mass SLIPs. Only partial flight phases are shown. The monopod requires feedback at touchdown for stability; the biped and tripod are passively stable. Adapted from* [300].

steady behavior over many steps (cf. the maps of Figures 14–15). In cases for which deadbeat control fails, he shows that a "two-step" strategy suffices to correct deviations from the desired motion. For example, while hopping with uniform steps in a straight line, correcting a single out-of-line step and returning to the same line requires two steps.

In the context of investigating advantages of multilegged "designs," we may also ask if the use of multiple support legs during stance can provide stability without feedback. This is indeed the case: Seipel has shown that saggital plane COM motions in a bipedal, kangaroo-like hopper, which uses a pair of elastic legs in stance splayed equally to left and right, are asymptotically stable, since the legs passively generate corrective forces due to the differential displacements induced by out-of-plane perturbations [300]. Similar preflexive stability results hold for actuated tripod legs similar to those to be considered in the hexapedal horizontal plane model of section 5.3. See Figures 25(b), (c).

5.2. Muscles as Activated Springs. In [294] we augmented the passive bipedal LLS models by adding rudimentary models of muscles in the form of actuated linear springs, whose unstressed (zero force–generating) lengths change according to fixed or feedback protocols. Specifically, the second class of models adopted in that paper assume the form illustrated in Figure 26. An actuated (variable-length) spring pushes or pulls on an extension of the effective leg beyond the pivot, producing forces and moments similar to those of the musculo-apodeme complexes of [127]. For simplicity, we assume that the single effective leg is pivoted at the COM and, in place of the elastic knee and two-element limb of [127], we retain the passive axial leg spring of section 5.1 [291, 293], adding a linear viscous damper to represent losses due to muscles and flexure of the exoskeleton [139].

The nominal actuated hip spring length l_h either may be determined as a function of time alone or may depend on time and the configuration variables, for example, $l_h(\psi, \theta, t)$, the explicit time dependence representing stereotyped CPG (motoneuron) outputs. The kinetic and potential energies of the LLS with passive linear leg and active hip springs are then

$$T = \frac{m(\dot{\zeta}^2 + \zeta^2\dot{\psi}^2)}{2} + \frac{I\dot{\theta}^2}{2},$$

$$V = \frac{k_h}{2}(-h\sin(\psi - (-1)^n\theta) - l_h(\psi, \theta, t))^2 + \frac{k}{2}(\zeta - l)^2. \tag{54}$$

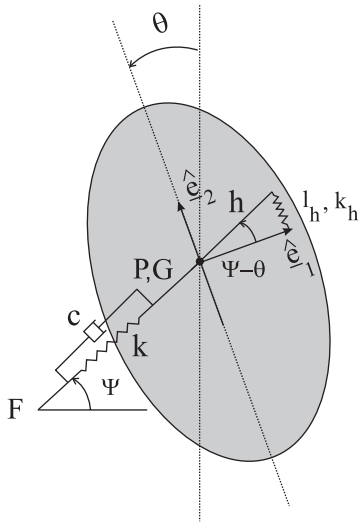

Fig. 26 *A compliant leg bipedal model with an actuated linear hip spring. From Figure* 5 *of* [294]. *Reprinted with kind permission from Springer Science and Business Media.*

In this formulation, it is assumed that the hip spring is always aligned parallel to the body centerline, so that its actual length, measured from stance center where the leg is at 90° to the body axis, is $-h\sin(\psi-(-1)^n\theta)$.

The functional form for the actuated spring length is chosen to produce a qualitatively correct moment history for the left (resp., right) stance phase: that is, negative (resp., positive) moment about the COM during the first half of each stance phase, followed by a positive (resp., negative) moment during the second half (cf. Figure 24, lower right panel). This requires that l_h be approximately odd in θ about midstride and approximately equal to its actual length at both the start and end of the stride. We therefore suppose that l_h depends on leg angle as well as time, specifically setting

$$l_h(\psi,\theta,t) = -h\sin(\psi-(-1)^n\theta)\left(\frac{2t}{t_s}-1\right)^2, \tag{55}$$

where t_s is the desired stance period duration. This guarantees that l_h is approximately odd about midstride, as evidenced by its dependence on the leg angle relative to the body, and zero at the start of the stride and approximately zero near the end, provided the actual stance duration is close to t_s—the stance duration "programmed" by the CPG.

The formulation (55) implies a feedback law in which the current leg angle $\psi-(-1)^n\theta$ is sensed and the CPG's "autonomous" signals to the muscles are modulated thereby. The resulting Lagrangian computed from (54), with generalized damping in the first variable, yields the following equations of motion:

$$\begin{aligned} m\ddot{\zeta} &= m\zeta\dot{\psi}^2 - k(\zeta-l) - c\dot{\zeta}, \\ m(2\zeta\dot{\zeta}\dot{\psi}+\zeta^2\ddot{\psi}) &= -\frac{1}{2}k_h h^2\sin(2(\psi-(-1)^n\theta))\left(1-\left(\frac{2t}{t_s}-1\right)^2\right)^2, \\ I\ddot{\theta} &= \frac{(-1)^n}{2}k_h h^2\sin(2(\psi-(-1)^n\theta))\left(1-\left(\frac{2t}{t_s}-1\right)^2\right)^2. \end{aligned} \tag{56}$$

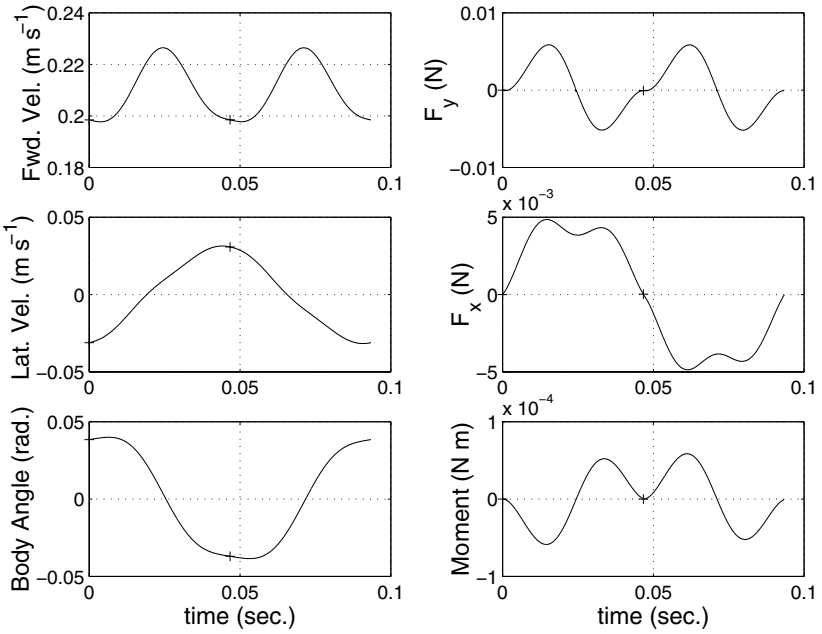

Fig. 27 *COM path, velocity, yaw, and leg force and body moment variations for steady gait of the actuated compliant leg model with a "strong" actuated linear hip spring and dissipation in the passive leg spring:* $c = 0.01$, $k_h = 300$, $h = 0.001$, $t_s = 0.0475$. *Other parameters were set to values typical of the cockroach* Blaberus discoidalis, *as described in section* 5.1. *From Figure* 11 *of* [294]. *Reprinted with kind permission from Springer Science and Business Media.*

A typical stride, with a relatively strong muscle spring constant k_h and dissipation c included, is illustrated in Figure 27. The hip torques produced by the actuated spring now match experimental moments about the COM reasonably well (compare the bottom panels of Figure 27 with those of Figure 24), but the reaction forces induced at the foot have *reversed* the phasing of the fore-aft force patterns, so that forces are positive in the first half of stance and negative in the second, *opposite* to those observed; compare the top panels of Figure 27 with those of Figure 24. Weaker muscle spring constants restore the appropriate fore-aft force patterns, but suffer the same low magnitudes as the passive LLS model (cf. [294, Figure 10]). Similar behavior occurs in a simpler model, also treated in [294], in which hip torques are directly imposed. The lateral forces and velocity variations remain approximately correct.

The observation that higher torques imposed by actuation can correct yawing motions only at the expense of producing incorrect fore-aft translational dynamics underlines the need for a hexapedal model, in which additional actuation DOFs are available due to the multiple legs active in stance.

As in the passive models of section 5.1, a family of gaits may be produced by varying the desired stance period, t_s. A typical example is illustrated in Figure 28. The energy balance induced by the actuated spring now brings a third eigenvalue, corresponding to COM speed variations, into the unit circle, leaving only the single (rotational) eigenvalue at 1. This behavior is not dependent upon the presence of dissipation; even if $c = 0$, the stride duration imposed by t_s and the balance of positive and negative work done by the actuated spring suffice to determine a stable speed.

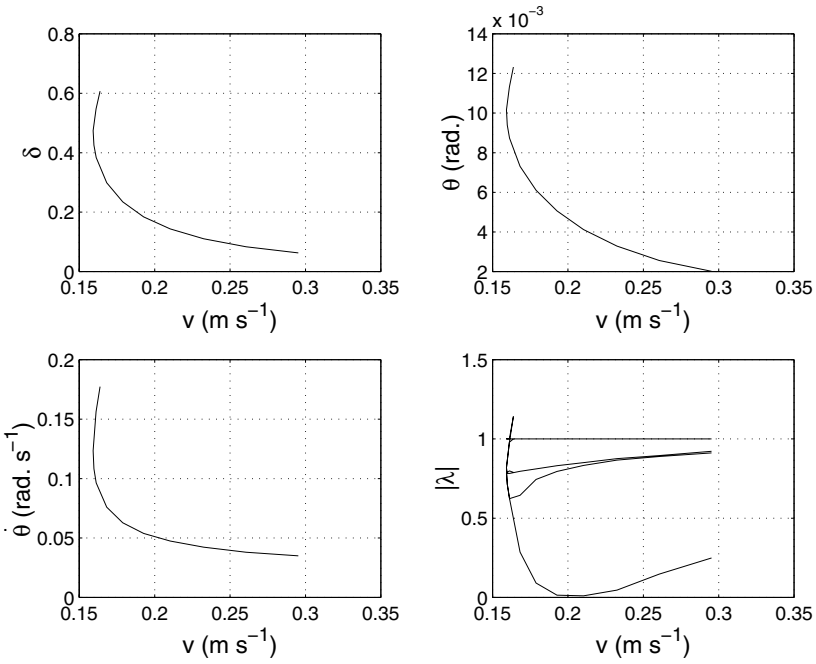

Fig. 28 *A periodic gait family for the compliant leg system with an actuated hip spring. Gaits were computed by varying t_s between $0.035 - 0.078$, with $k_h = 30$, $h = 0.1l$, and $c = 0.001$. Other values were held constant at values typical of the cockroach* Blaberus discoidalis*, as described in section* 5.1. *From Figure* 12 *of* [294]. *Reprinted with kind permission from Springer Science and Business Media.*

It is not immediately obvious that actuation or prescription of leg forces should preserve the inherent stability of the passive LLS models. Kubow and Full [216] showed, via numerical simulations of equations of the form (35) with alternating tripods summing to produce forces $\mathbf{f}(t)$ given as sinusoidal functions of time in the body frame, that purely prescribed forces could produce stable motions and select a preferred speed. In contrast, in [293] it was shown analytically (and hence proved) that bipedal LLS models with prescribed sinusoidal forces that do *not* rotate with the body (essentially, setting $\mathbf{R}(\theta(t)) \equiv \mathbf{Id}$ in (35)) are *always* unstable: their (unique) periodic gaits have at least one eigenvalue outside the unit circle. These observations, and the model described above, suggest that a subtle combination of actuation and mechanical feedback, involving either (or both) rotational coupling and passive springs, may be required for stability. Our next model incorporates these effects.

5.3. A Hexapedal Model with Activated Spring Legs. We describe a simple hexapedal model that was proposed, and is described in greater detail, in [302]. The basis of the model is the actuated, telescopic spring leg illustrated in Figure 29(a), in which a rudimentary analog of neurally activated muscle complexes is provided by the "programmable" length $l(t)$ and hip position $d(t)$. Each of these *inputs* may be independently prescribed, endowing the leg with two control variables and permitting one to match the horizontal plane components of observed single leg forces. However, unlike the purely prescribed model of [216], $l(t)$ sets only the relaxed (force-free)

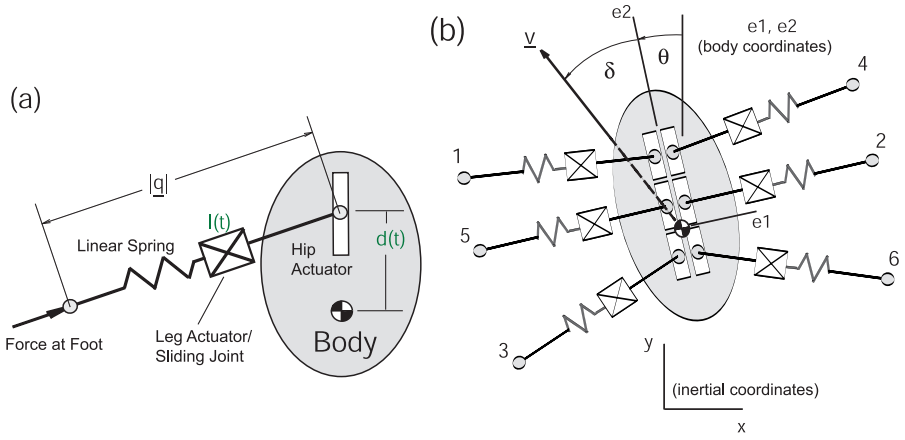

Fig. 29 *The mechanical model for an actuated telescopic leg* (a)*, and coordinate systems and leg numbering scheme for the hexapedal model* (b)*. Legs* 1*,* 2*, and* 3 *form the left tripod, and* 4*,* 5*, and* 6 *the right tripod. From Figures* 3 *and* 4 *of* [302]*. Reprinted with kind permission from Springer Science and Business Media.*

length; actual leg forces depend upon relative foot–hip displacements, and thus forces can respond to perturbations in a more natural manner. Six such units are assembled as indicated in Figure 29(b), although for simplicity we assume that the hips all move on the body centerline.

We derive the six inputs $l_j(t), d_j(t)$ for each leg tripod by requiring that the forces generated at the feet match those of the idealized model of [216], F_{jx}, F_{jy}, which were, in turn, derived from single leg force measurements in [129]. These forces are sinusoids of the forms

$$F_{jx} = A_{jx} \sin \Omega t \quad \text{(lateral forces, all feet)}, \tag{57a}$$

$$F_{jy} = A_{jy} \sin \Omega t \,, j = 1, 3 \quad \text{(fore-aft forces, front and hind feet)}, \tag{57b}$$

$$F_{2y} = A_{2y} \sin 2\Omega t \quad \text{(fore-aft forces, middle foot)}. \tag{57c}$$

Parameter values are given in [302].

We compute the COM path through a half stride: only one tripod need be considered, the left here, since bilateral symmetry supplies the inputs for the other stance phase. Neglecting body rotation, this follows simply from integration of the first equation of (35) with $\mathbf{R}(t) = \mathbf{Id}$, using the net idealized forces $\sum_{j=1}^{3} F_{jx}, \sum_{j=1}^{3} F_{jy}$:

$$(x(t), y(t)) = \left(-A_{3x}(m\Omega^2)^{-1} \sin\, \Omega t, -A_{2y}(4m\Omega^2)^{-1} \sin\, 2\Omega t + V_{des} t\right), \tag{58}$$

where we use the fact that certain force components cancel ($A_{2x} = -A_{1x}$; $A_{3y} = -A_{1y}$). The average forward speed, denoted by V_{des}, is a constant of integration that may be adjusted, but initially we set it at the preferred speed 0.25 m s^{-1} and choose the leg cycle frequency $f = \Omega/2\pi = 10$ Hz for which the idealized leg forces and touchdown foot positions were derived. These and other physical parameters are given in [216] and [302].

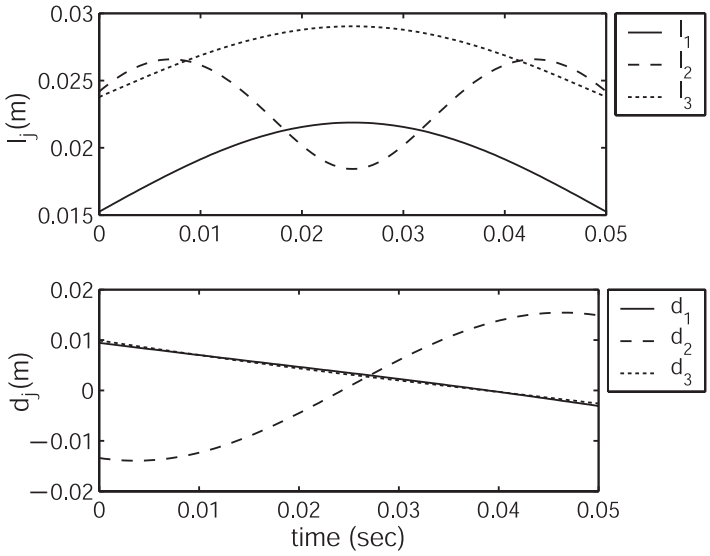

Fig. 30 *The prescribed inputs, $d_i(t)$ and $l_i(t)$, for $i = 1, 2, 3$; $V_{des} = 0.25$ m s^{-1}, $\Omega = 20\pi$ rad s^{-1}, and $k = 1$ N m. From Figure 6 of* [302]. *Reprinted with kind permission from Springer Science and Business Media.*

We assume linear springs, so that, letting $\mathbf{q}_i$ denote the vector from the ith foot to hip, force consistency requires

$$F_{jx} = F_{jx,des} \Rightarrow k_j(l_j(t) - |\mathbf{q}_j|)\frac{q_{jx}}{|\mathbf{q}_j|} = A_{jx} \sin \Omega t\,, \tag{59}$$

$$F_{jy} = F_{jy,des} \Rightarrow k_j(l_j(t) - |\mathbf{q}_j|)\frac{q_{jy}}{|\mathbf{q}_j|} = A_{jy} \sin C_j \Omega t\,. \tag{60}$$

Here q_{jx} and q_{jy} are the inertial frame components of q_j, and A_{jx} and A_{jy} are the force component magnitudes of equations (57) (note $C_j = 2$ for $j = 2$, but $C_j = 1$ otherwise). The kinematics inherent in Figure 29 allows us to express $\mathbf{q}_j$ in terms of the COM path of (58), the touchdown foot position, and the hip position $d_j(t)$. Then $d_j(t)$ may be derived by dividing the equations (60) to eliminate the common term $k_j(l_j(t) - |\mathbf{q}_j|)/|\mathbf{q}_j|$, and $l_j(t)$ found by inverting the linear force relationship. In order to obtain closed-form expressions, we neglect yawing throughout, incurring errors of up to $\approx 8\,\%$ in approximating the rotation matrix by the identity. Details are given in [302], and the resulting input functions are shown in Figure 30.

The unstressed lengths on average obey $l_1 < l_2 < l_3$, echoing leg lengths in the insect. Also, the front and back (ipsilateral) hips move backwards relative to the body during stance, while the middle (contralateral) hip moves forwards. Although the latter varies by over 3 cm, a greater distance than the insect's body length, the net movement is backwards, as in the bipedal moving COP protocol of section 5.1.3. Since moving COPs imply torques at the leg joints, this model suggests that the insect generates relatively large middle leg torques.

Equipped with the inputs as explicit functions of time, we may now integrate the fully coupled equations of motion to obtain gaits. The body coordinate system and state variables used in defining Poincaré maps remain the same as for the bipedal

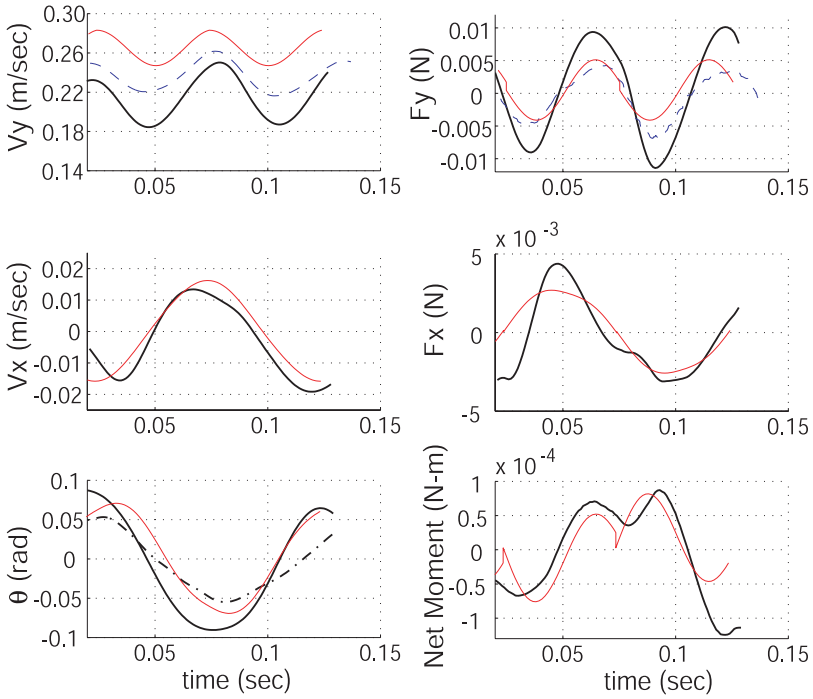

Fig. 31 *Comparison of the experimental insect COM velocity, yaw, force, and moment data of Figure* 24 *with solutions of the LLS hexapod model. Model data are shown as a red solid line. From Figure* 8 *of* [302]. *Reprinted with kind permission from Springer Science and Business Media.*

models above (cf. Figure 29(b)). We first confirm that, even permitting yawing, inputs derived from the idealized preferred speed data of [216] do produce gaits with force and velocity variations quantitatively similar to those of the animal. Figure 31 reproduces the data of Figure 24 and also shows model results: the match is remarkably good, although the actual average forward speed (≈ 0.26 m s^{-1}) is slightly higher than the desired (or design) speed V_{des} used to compute the inputs.

These gaits are stable. Indeed, we may produce branches of gaits over a range of speeds, by recomputing inputs for appropriately adjusted desired speeds, leg frequencies, and touchdown positions. As mentioned in section 3.2.1, although the insect uses a double-tripod pattern throughout the range 0.05–0.6 m sec^{-1}, it exhibits a gait transition around 0.3 m sec^{-1}. Below this, speed is regulated by leg cycle frequency, and above it, by stride length. Varying V_{des} and Ω in a piecewise-linear manner to approximate the data of [317, Figure 2], and additionally changing foot touchdown positions from those of [216] by further extending the legs at speeds above 0.25 m s^{-1}, we obtain the branch of stable gaits illustrated in Figure 32.

As in Figure 28, since the actuated springs supply and extract energy via $l_j(t)$ and $d_j(t)$, along this branch speed is also stabilized, and three of the eigenvalues lie within the unit circle, with only the "rotational" eigenvalue $\lambda_1 = 1$. Moreover the stability boundaries shown in Figure 32 provide a rationale for the gait change, since constant frequency or constant stride length protocols would enter unstable regions at either low or high speeds.

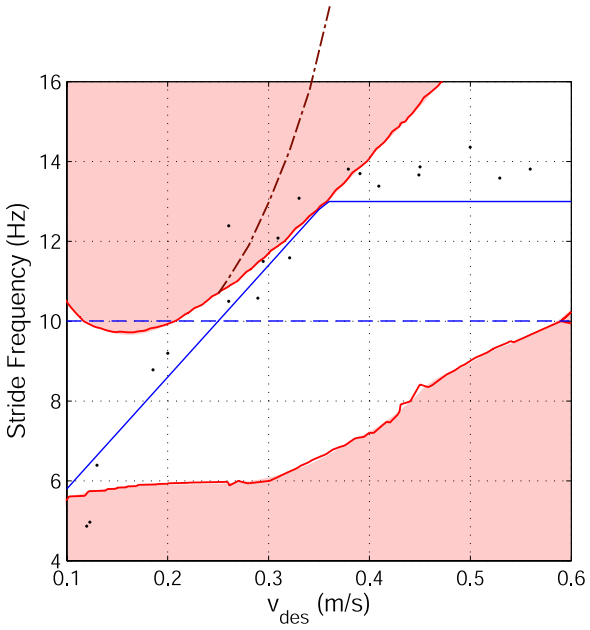

Fig. 32 *Bifurcation set for the hexapedal model in design speed-leg cycle frequency space, showing boundaries of the region in which stable gaits exist, and the speed-frequency protocol adopted. Unstable regions are shaded. The fixed frequency protocol (dashed) encounters instability at low and/or high V_{des}, while the piecewise-linear protocol (solid) remains in the stable region, albeit grazing the stability boundary at its break-point. Stability is further improved by adjusting foot placements above $V_{des} = 0.25$, as shown by modified dash-dotted upper boundary. From Figure* 14 *of* [302], *with experimental data of* [317, Figure 2] *indicated by dots. Reprinted with kind permission from Springer Science and Business Media.*

In [302] the moments generated at the COM by individual legs are also studied, and it is shown that they sum almost without cancellation to give the net COM moment pattern shown in the lower right panel of Figure 31, while individual joint moments remain within reasonable bounds. Hence this model also shows that the legs of the stance tripod work together in a relatively efficient manner to produce feedforward force and moment patterns that result in stable running.

Question. Can the net COM forces and moments due to a stance tripod of the hexapedal model be represented by a single telescopic leg with actuator $l(t)$, pivot position $d(t)$, and fixed stance foot? In short, can the hexapod model be reduced to a bipedal LLS template? If not, how well can it be approximated by one?

5.4. Toward a Neuromechanical Model. Thus far we have considered rather simple mechanical models, *templates* in the terminology introduced in section 1 [131], although we have seen that their behaviors are not always easy to derive analytically. Drawing on the material summarized in section 2.4, we now sketch the elements of a true neuromechanical model, an *anchor* that includes CPG circuitry, motoneurons, muscles, six legs, and body. This work is still in progress; the first part of it is described in [146, 147, 148], from which the following outline is adapted.

5.4.1. The CPG and Motoneurons. The CPG model is based on the work of Pearson and Iles [261, 262, 257, 263] and Ritzmann et al. [330, 331, 321, 322], who

studied motoneuron, bursting interneuron, and muscle activity in cockroach locomotion. Pearson and Iles, working with the American cockroach *Periplaneta americana*, suggest a simplified architecture for the CPG and depressor and levator motoneurons. (Here, since we do not explicitly model the swing phase when the leg is lifted, we shall be concerned only with depressor motoneurons and associated muscles.) Both slow and fast motoneurons, characterized by differing spiking patterns, are involved. The former, with their low-level, high-frequency spikes, are active during muscle contraction at all speeds, and the latter, with typically one to six larger spikes per stride, become increasingly active at high speeds. The motoneuron records presented in [134] are from fast cells, while the electromyographs (EMGs) of [330, 331, 321, 322], taken from *Blaberus discoidalis*, primarily reflect slow motoneuron activity, with spikes from fast motoneurons appearing in [322].

Examination of EMGs and both slow and fast motoneuron outputs reveals that they may essentially be described by three parameters: the bursting cycle duration or its inverse, the *bursting frequency*, which coincides with the animal's overall stride frequency (ranging from 2–14 Hz; cf. Figure 32); the *spiking frequency* or *number of action potentials* (APs) within bursts; and the *duty cycle*, the fraction of the bursting cycle occupied by spiking. The latter two modulate the power produced by muscles in a graded fashion, greater spike rates and longer bursts producing greater muscle forces. Fast motoneurons may produce from one to six spikes per cycle, and none at low speeds, while slow motoneurons exhibit significantly faster spike rates, from 100–400 Hz [257, 263, 321, 322].

In the absence of detailed information regarding ionic currents in cockroach neurons, we choose to model both fast and slow depressor motoneurons by a "generic" three-variable ODE of the following form, in which fast gating variables have been removed by assuming instantaneous equilibration, as outlined in section 2.3.1:

$$\begin{aligned} C\dot{v} &= -[I_{\mathrm{Ca}} + I_{\mathrm{K}} + I_{\mathrm{KS}} + \bar{g}_{\mathrm{L}}(v - E_{\mathrm{K}})] + I_{\mathrm{ext}}, \\ \dot{m} &= \frac{\epsilon}{\tau_m(v)}\left[m_\infty(v) - m\right], \\ \dot{c} &= \frac{\delta}{\tau_c(v)}\left[c_\infty(v) - c\right]. \end{aligned} \tag{61}$$

Here $\delta \ll \epsilon \ll 1/C$, and the fast, relatively slow, and very slow currents, respectively, are given by

$$I_{\mathrm{Ca}} = \bar{g}_{\mathrm{Ca}} n_\infty(v)(v - E_{\mathrm{Ca}}), \quad I_{\mathrm{K}} = \bar{g}_{\mathrm{K}} m \cdot (v - E_{\mathrm{K}}), \quad I_{\mathrm{KS}} = \bar{g}_{\mathrm{KS}} c \cdot (v - E_{\mathrm{KS}}), \tag{62}$$

where the subscripts Ca and K denote calcium and potassium ions, I_{KS} is a slowly modulated potassium current, and I_{ext} represents external synaptic and other input currents. As in section 2.3.1 the functions $m_\infty(v), n_\infty(v)$, and $c_\infty(v)$ are sigmoids of the forms

$$m_\infty(v) = \frac{1}{1 + \exp\left[-k_m(v - v_m)\right]}, \tag{63}$$

and the "timescale" functions are hyperbolic secants:

$$\tau_m(v) = \operatorname{sech}(k_m(v - v_m)). \tag{64}$$

Specific parameter values appropriate for fast and slow cockroach motoneurons, as well as CPG (inter)neurons, may be found in [147].

The fast (v, m) subsystem of (61) is that of the Morris–Lécar equations [250], which was developed to model barnacle muscle, hence the calcium spike mechanism. We believe that analogous results could be obtained with a persistent sodium current, as in Butera, Rinzel, and Smith [60]; cf. [147]. (As noted above, specific data for cockroach CPG neurons is lacking, so we cannot identify a specific current responsible for fast spikes.)

This model, in common with others studied by Rinzel and Lee [274, 276, 277], has a "recovery" variable c, usually identified with a calcium-dependent potassium current, which acts on the fast (v, m)-subsystem as a slowly varying parameter that modulates the current I_{KS}. The fast subsystem, which incorporates the membrane voltage v and a collective relatively slow channel variable m, has three branches of equilibria, the upper of which (w.r.t. v) undergoes a supercritical Hopf bifurcation as c increases, producing a branch of periodic orbits. These represent depolarized spiking, and they coexist with a lower branch of stable (hyperpolarized) fixed points. The periodic orbit branch terminates in a homoclinic connection to a middle branch of saddle points [166], beyond which only the lower v (hyperpolarized) equilibria are stable. The slow variable c increases, moving toward the homoclinic bifurcation point as long as spiking occurs and membrane voltages are relatively high, but returning toward the Hopf bifurcation point in the absence of spiking, when membrane voltages are lower. At a threshold corresponding to a saddle-node bifurcation in the fast system, the stable hyperpolarized rest point vanishes and the fast subsystem resumes spiking. See [200, Chapter 6] for an introduction to such two-timescale bursting models in neurobiology.

The underlying timescales are set by the parameters C, ϵ, and δ, and the behavior is modulated by conductances such as $\bar{g}_{\mathrm{KS}}$ and the input current I_{ext}. Following Pearson [257], we suppose that I_{ext} and $\bar{g}_{\mathrm{KS}}$ are influenced by external inputs from higher brain centers (a tonic excitation level, primarily a speed control) and inhibited by CPG outputs so that the depressor muscle activity is shut off during the swing phase.

Pearson [257, 263] also found evidence of bursting interneurons that constitute part of (or are driven by) the CPG, and it is thought that bistability and plateau potentials, on which spikes can ride, are crucial for bursting [17, 170]. Absent detailed knowledge of the neural architecture, we shall therefore also represent each of the six subunits of the CPG by a single bursting neuron of the form (61), with parameters chosen appropriately. We couple each ipsilateral triplet, and each contralateral pair, by nearest neighbor inhibitory synapses, in the manner characterized in Figure 33(a). The same overall architecture has been proposed for the stick-insect pattern generator [20, Figure 4]. Following [95, p. 180], we model synaptic behavior by the first-order dynamics

$$\dot{s} = \frac{s_\infty(v)(1-s) - s}{\tau_{\mathrm{syn}}}, \quad \text{with} \quad s_\infty = \frac{1}{1 + e^{-k_{\mathrm{syn}}(v - E_{\mathrm{syn}}^{\mathrm{pre}})}}, \tag{65}$$

in which v denotes the potential of the presynaptic neuron and τ_{syn} sets the timescale of the postsynaptic potential. The nondimensional synaptic variable s enters the postsynaptic cell in the first of equations (61) as

$$C\dot{v} = -[I_{\mathrm{Ca}} + \cdots] - \bar{g}_{\mathrm{syn}}\, s \cdot (v - E_{\mathrm{syn}}^{\mathrm{post}}), \tag{66}$$

where $\bar{g}_{\mathrm{syn}}$ denotes synaptic strength and the current $I_{\mathrm{syn}} = \bar{g}_{\mathrm{syn}}\, s \cdot (v - E_{\mathrm{syn}}^{\mathrm{post}})$ induced in the postsynaptic cell is typically positive (negative) for excitatory (inhibitory) synapses [193].

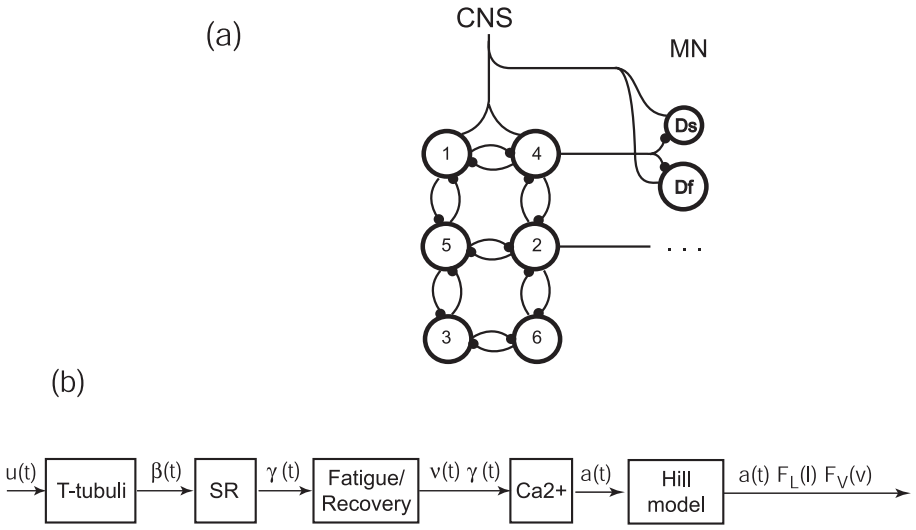

Fig. 33 (a) *The overall CPG, motoneuron, and muscle model structure: fast* (D_f) *and slow* (D_s) *depressor motoneurons are inhibited by the CPG outputs. From* [147]. (b) *Elements in the muscle fiber transduction model described in section* 5.4.3.

The CPG circuit of Figure 33(a) produces the requisite 180° antiphase difference between the tripods, as illustrated in Figure 34, which shows simulations of ipsilateral CPG outputs along the left side, and contralateral CPG and fast and slow motoneuron outputs for the front legs. Moreover, unidirectional inhibitory coupling to the motoneurons entrains them to the CPG, provided that the fast motoneurons have higher bursting frequencies than the CPG bursters driving them [147]. The slow motoneurons are set in a spiking regime, which periodic inhibition from the CPG shuts off during the swing phase.

In [146] it is shown that the "behavioral" parameters—bursting frequency, duty cycle, spiking frequency of slow motoneurons, and numbers of APs delivered in a fast motoneuron burst—can be set as follows. The parameters C, ϵ, and δ of (61) determine the timescales of fast spikes, approximate number of APs per burst, and the baseline bursting frequency, respectively, so they can be fixed to match experimental observations at preferred running speeds. Depending on the number of APs per burst, two régimes can then be identified: high (~ 15 APs) or low (~ 4 APs). In the former, bursting frequency is modulated by I_{ext}; in the latter, I_{ext} influences both bursting frequency and number of APs per burst. In the high régime, g_{KS} primarily affects the duty cycle; in the low régime, it affects both duty cycle and number of APs per burst.

Based on this, a combined single-component and network strategy for locomotive control via changes in biophysically relevant parameters is proposed in [147]. Stepping frequency and duty cycle can be adjusted by the external current I_{ext} to the CPG interneurons and by their conductances $\bar{g}_{\text{KS}}$, respectively. Provided that the intrinsic bursting frequencies are sufficiently close, motoneurons are entrained to the CPG bursting frequency and slow motoneuron spike rates may then be tuned by their external currents, and AP numbers delivered by fast motoneurons by their external currents and $\bar{g}_{\text{KS}}$ conductances. While I_{ext} is not independently tunable *in vivo*,

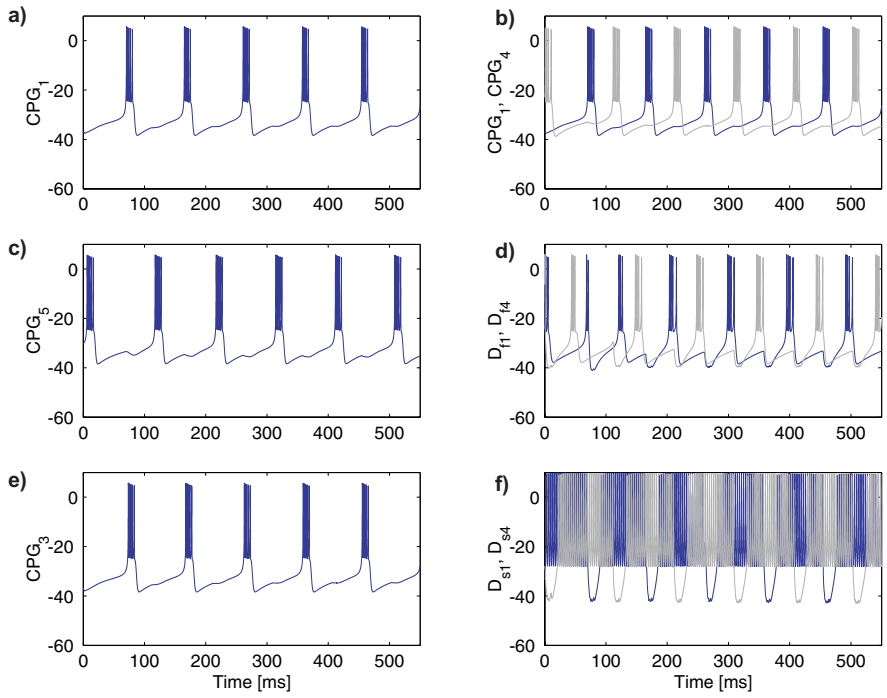

Fig. 34 *Membrane voltages from a network of six mutually inhibiting bursting neuron models driving slow and fast bursting motoneurons. Left column shows ipsilateral CPG neurons; right column shows contralateral CPG neurons and fast ($D_{\mathrm{f}\,1,4}$) and slow ($D_{\mathrm{s}\,1,4}$) motoneurons for units* 1 *and* 4. *Units* 1, 2, *and* 3, *and* 4, 5, *and* 6, *constituting the left and right tripods, respectively, rapidly fall into the appropriate antiphase relationships. From* [147].

synapses from CNS and proprioceptive neurons can effectively adjust both input currents and conductances of CPG interneurons and motoneurons, and so these control parameters seem plausible.

In Figure 35 we show that suitable variations in CPG I_{ext} and $\bar{g}_{\mathrm{KS}}$ and additional tuning of fast and slow motoneuron conductances can accurately bracket the data measured by Pearson [257]. The motoneuron outputs will be used to innervate Hill-type muscle models, but before we consider this we show that the CPG-motoneuron model anchor can be reduced to a phase oscillator template of the type given in (19).

5.4.2. Reduction to Phase Oscillators. While substantial analyses can be performed on singularly perturbed systems such as (61), in the synaptically coupled network of Figure 33(a) there are sixty ODEs, three each for the six CPG neurons and twelve motoneurons and a further six for the CPG synaptic variables (the coupling to motoneurons is one way, so motoneuron synaptic variables do not appear). This is a formidable system, but for weak coupling, and assuming identical neurons, the six-burster CPG circuit can be reduced, via phase response curve and averaging methods, to ODEs in the relative phases ψ_j of each "leg unit."

As in section 2.3.1 we write the ODEs (61) and (65) for a single burster and its synaptic variable as

$$\dot{\mathbf{x}}_i = \mathbf{f}(\mathbf{x}_i) + \sum_j \bar{g}_{\mathrm{syn},ji}\, \mathbf{g}_{ji}(\mathbf{x}_i, \mathbf{x}_j)\,;\ \mathbf{x}_i = (v_i, m_i, c_i, s_i)\,, \tag{67}$$

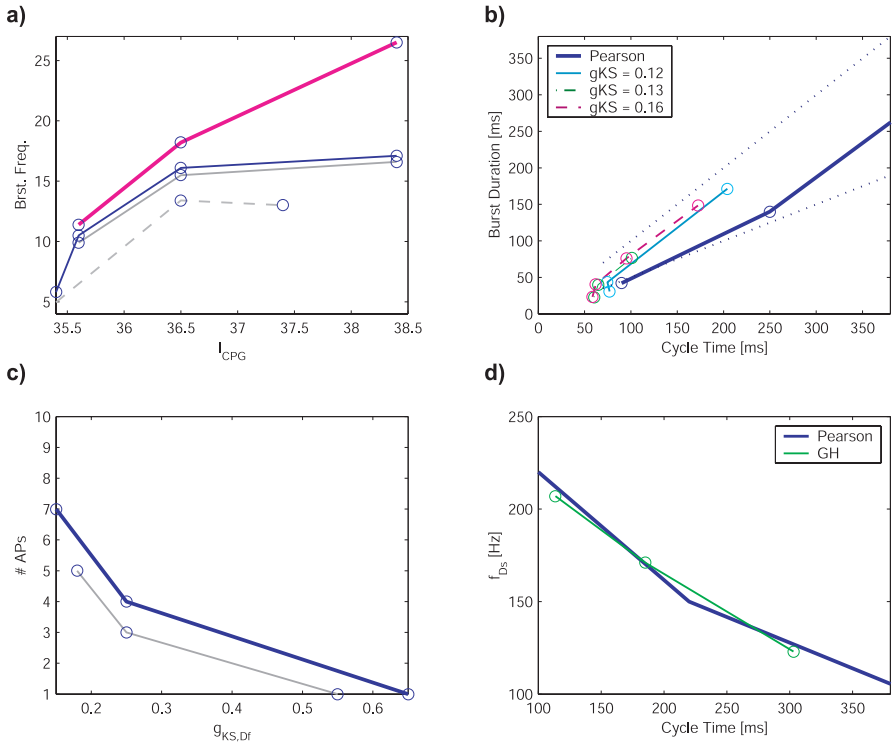

Fig. 35 *Variation of input currents and conductances for CPG bursters and motoneurons can span the range of variation found in the cockroach. Panels* (a) *and* (b) *show bursting frequency and duty cycle as I_{ext} varies for fixed $\bar{g}_{KS}$ values shown inset in* (b)*; dotted lines in* (b) *correspond to* 50% *and* 100% *duty cycle. Panels* (c) *and* (d) *show AP numbers and spike rates for fast and slow motoneurons; simulations for two different currents I_{ext} are given in* (c)*. Data from Pearson* [257] *shown bold in* (b) *and* (d)*. From* [147].

where $\mathbf{g}_{ji}$ denotes the coupling function (of strength $\bar{g}_{\mathrm{syn},ji}$) from presynaptic cell j to postsynaptic cell i, and the sum is over all cells in the network that synapse onto i. Assuming that (67) has an attracting hyperbolic limit cycle Γ_0 with frequency $\omega_0 = \frac{2\pi}{T_0}$ for $\bar{g}_{\mathrm{syn},ji} = 0$, and extending the analysis of section 2.3.1 in the obvious way, we may define a scalar phase variable $\phi(\mathbf{x}_i) \in [0, 2\pi)$ for each unit and derive a coupled set of phase equations of the form

$$\dot{\phi}_i = \omega_0 + \sum_j \bar{g}_{\mathrm{syn},ji}\mathbf{Z}(\phi_i)\cdot\mathbf{g}_{ji}(\phi_i,\phi_j) + o(\bar{g}_{\mathrm{syn},ji})\,;\ \mathbf{Z}(\phi_i(\mathbf{x}_i)) = \frac{\partial\phi_i}{\partial\mathbf{x}_i}\,|_{\Gamma_0(\phi)}\,. \tag{68}$$

In deriving (68) we are projecting solutions along *isochronic manifolds* onto the product of the unperturbed limit cycles: for N units, an N-dimensional torus [338, 165].

As noted in section 2.3.1 synaptic dynamics only enters via the variables s_j and v_i in the coupling defined by (65)–(66), so only the first component of $\mathbf{Z}(\phi_i)$ survives in the dot product of (68). This PRC can be approximated numerically by approaching the limit

$$Z_1(\phi_i) = \lim_{\substack{\Delta v_i \to 0 \\ t\to\infty}} \frac{\Delta\phi_i}{\Delta v_i} \tag{69}$$

or calculated by use of adjoint theory [183], as implemented, for example, in the software XPP [115]. Defining the relative phases $\psi_i = \phi_i - \omega_0 t$ and using the fact that the absolute phases ϕ_i evolve faster than $\psi_i(t)$, we may then average (68) to obtain

$$\dot{\psi}_i = \sum_{j \neq i}^{N} \bar{g}_{\mathrm{syn},ji} H_{ji}(\psi_i - \psi_j), \tag{70}$$

where

$$H_{ji}(\psi_i - \psi_j) = \frac{1}{T_0} \int_0^{T_0} Z_1(\phi_i)\, s_j(\Gamma_0(\phi_j))\, [v_i(\Gamma_0(\phi_i)) - E^{\mathrm{post}}_{\mathrm{syn},i}]\, dt\,, \tag{71}$$

and it is understood that $\phi_i = \psi_i + \omega_0 t$ in the integrand (cf. [166, Chapter 4] and [183, Chapter 9]). As noted in section 2.3, pairwise phase differences alone appear in the averaged coupling functions H_{ji} due to periodicity of the integrand in (71).

For mutual coupling between two identical bursters we have $\bar{g}_{\mathrm{syn},ji} H_{ji} = \bar{g}_{\mathrm{syn},ij} H_{ij}$, and the reduced phase equations (70) are

$$\dot{\psi}_1 = \bar{g}_{\mathrm{syn}} H(\psi_1 - \psi_2) \quad \text{and} \quad \dot{\psi}_2 = \bar{g}_{\mathrm{syn}} H(\psi_2 - \psi_1)\,; \tag{72}$$

we may subtract these as in section 2.3.3 to further reduce to a single scalar ODE for the phase difference $\theta = \psi_1 - \psi_2$:

$$\dot{\theta} = \bar{g}_{\mathrm{syn}}[H(\theta) - H(-\theta)] \stackrel{\mathrm{def}}{=} \bar{g}_{\mathrm{syn}} G(\theta)\,. \tag{73}$$

Now, since H is 2π-periodic, we have $G(\pi) = H(\pi) - H(-\pi) = H(\pi) - H(\pi) = 0$ and $G(0) = 0$, implying that, *regardless of the form of* H, in-phase and antiphase solutions *always* exist. For the present burster model and the specific parameters selected in [147], these are in fact the *only* fixed points; see Figure 36. Note that, unless $H(0) = H(\pi) = 0$, we have $\dot{\psi}_1 = \dot{\psi}_2 = \bar{g}_{\mathrm{syn}} H(\bar{\theta})$, so coupling changes the common frequency $\dot{\phi} = \omega_0 + \dot{\psi}_i$ of the units, even when phase locking occurs.

Stability of these phase-locked solutions is determined by the eigenvalues of the 2×2 matrix obtained by linearizing (72) at $\psi_1 - \psi_2 = \bar{\theta}$:

$$\bar{g}_{\mathrm{syn}} \begin{bmatrix} H'(\bar{\theta}) & -H'(\bar{\theta}) \\ -H'(\bar{\theta}) & H'(\bar{\theta}) \end{bmatrix}; \tag{74}$$

these are 0 and $2\bar{g}_{\mathrm{syn}} H'(\bar{\theta}) = \bar{g}_{\mathrm{syn}} G'(\bar{\theta})$, with eigenvectors $(1,1)^{\mathrm{T}}$ and $(1,-1)^{\mathrm{T}}$, respectively. Hence the dynamics is only neutrally stable to perturbations that advance or retard the phases of both units equally, but since $H'(\pi) < 0$ the antiphase solution is asymptotically stable to perturbations that disrupt the relative phase $\psi_1 - \psi_2$.

In [147], to preserve equal net input to all units, it is assumed that ipsilateral synapses from front and rear leg units to middle ones are half the strength of the remaining ipsilateral and contralateral synapses. The six-burster CPG circuit of Fig-

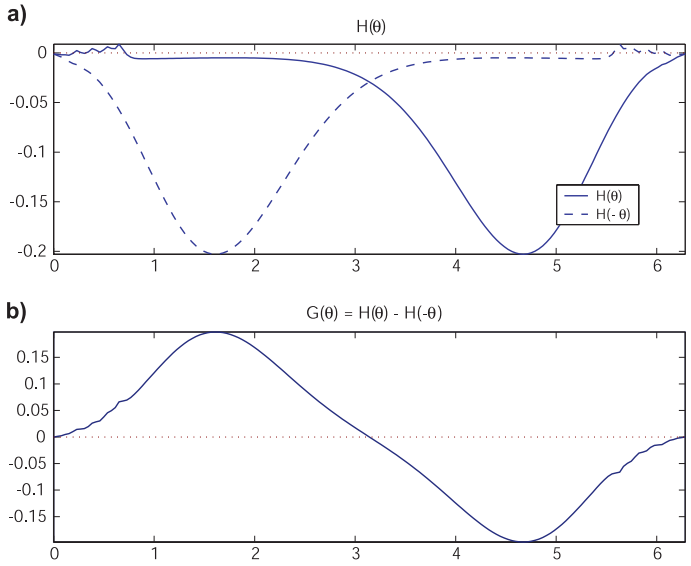

Fig. 36 (a) *The coupling function* $\bar{g}_{syn}H_{ji}(\theta)$ *(solid) for an inhibitory synapse;* $\bar{g}_{syn}H_{ji}(-\theta)$ *also shown (dash-dotted).* (b) *The phase difference coupling function* $\bar{g}G(\theta) = \bar{g}_{syn}[H_{ji}(\theta) - H_{ji}(-\theta)]$. *Note that* $G(0) = G(\pi) = 0$ *and* $\bar{g}_{syn}G'(0) > 0 > \bar{g}_{syn}G'(\pi)$. *From* [147].

ure 33 then reduces to the system

$$
\begin{aligned}
\dot{\psi_1} &= \bar{g}_{\rm syn}H(\psi_1 - \psi_4) + \bar{g}_{\rm syn}H(\psi_1 - \psi_5),\\
\dot{\psi_2} &= \frac{\bar{g}_{\rm syn}}{2}H(\psi_2 - \psi_4) + \bar{g}_{\rm syn}H(\psi_2 - \psi_5) + \frac{\bar{g}_{\rm syn}}{2}H(\psi_2 - \psi_6),\\
\dot{\psi_3} &= \bar{g}_{\rm syn}H(\psi_3 - \psi_5) + \bar{g}_{\rm syn}H(\psi_3 - \psi_6),\\
\dot{\psi_4} &= \bar{g}_{\rm syn}H(\psi_4 - \psi_1) + \bar{g}_{\rm syn}H(\psi_4 - \psi_2),\\
\dot{\psi_5} &= \frac{\bar{g}_{\rm syn}}{2}H(\psi_5 - \psi_1) + \bar{g}_{\rm syn}H(\psi_5 - \psi_2) + \frac{\bar{g}_{\rm syn}}{2}H(\psi_5 - \psi_3),\\
\dot{\psi_6} &= \bar{g}_{\rm syn}H(\psi_6 - \psi_2) + \bar{g}_{\rm syn}H(\psi_6 - \psi_3).
\end{aligned}
\tag{75}
$$

Seeking left–right tripod solutions of the form $\psi_1 = \psi_2 = \psi_3 \equiv \psi_L(t)$, $\psi_4 = \psi_5 = \psi_6 \equiv \psi_R(t)$, (75) collapses to the pair of equations

$$
\dot{\psi}_L = 2\bar{g}_{\rm syn}H(\psi_L - \psi_R) \quad \text{and} \quad \dot{\psi}_R = 2\bar{g}_{\rm syn}H(\psi_R - \psi_L)\,, \tag{76}
$$

and the arguments used above may be applied to conclude that $\psi_R = \psi_L + \pi$ and $\psi_R = \psi_L$ are fixed points of (76), again independent of the form of H. For this argument to hold, note that the sums on the right-hand sides of the first three and last three equations of (75) must be identical when evaluated on the tripod solutions; hence, net inputs must be equal. If all *synaptic strengths* are assumed equal (replacing $\bar{g}_{\rm syn}/2$ by $\bar{g}_{\rm syn}$ in the second and fourth equations of (75)), then to get exact antiphase solutions it is *also* necessary that $H(\pi) = 0$, which does not hold here (Figure 36(a)).

Linearization of (75) at fixed points produces the eigenvalues

$$
\lambda = 0,\ \bar{g}_{\rm syn}H',\ 2\bar{g}_{\rm syn}H',\ 3\bar{g}_{\rm syn}H',\ 4\bar{g}_{\rm syn}H', \tag{77}
$$

the third ($2\bar{g}_{\rm syn}H'$) having algebraic and geometric multiplicity 2. Since $\bar{g}_{\rm syn}H'(\pi) < 0$ (Figure 36), this establishes asymptotic stability with respect to perturbations that disrupt the tripod antiphase relationships, and instability of the in-phase ("pronking") solution. Moreover, the last and largest negative eigenvalue for the antiphase solution has eigenvector $(1, 1, 1, -1, -1, -1)^{\rm T}$, indicating that perturbations that disrupt the relative phasing of the left and right tripods recover fastest, before those that affect phases within a tripod. Hence the most basic element of the gait pattern is its most stable one.

Equations (72) and (75) provide examples of networks that are forced by their symmetries to possess certain steady state solutions regardless of the precise forms of the coupling functions. The stability of the solutions, however, does depend on the coupling. This is a typical situation in equivariant bifurcation theory [153, 156, 155]. In [147] we also study less symmetric networks, in which bilateral symmetry is maintained, but ipsilateral descending and ascending coupling strengths differ. In this situation a phase reduction analogous to (75) accurately predicts the coupling strengths necessary to obtain specified phase relations among the front, middle, and hind leg outputs.

We remark that, while each bursting neuron has been modeled in some biophysical detail in section 5.4.1, the circuit of Figure 33(a) still vastly simplifies the probable architecture of the insect's CPG. A single bursting interneuron represents each "leg oscillator," where several neurons are probably involved. Moreover, in studies of slow walking of stick insects, which use more precise foot placement, there is strong evidence of individual *joint* oscillators within the leg units [20]. For fast running, however, multiple units are likely to be coordinated in a stereotyped fashion, and so even if more units were modeled, the phase reduction and symmetry ideas introduced here may still result in considerable simplification. For example, additional "feedforward" motoneurons could be added without affecting the reduced CPG phase template (75).

5.4.3. Muscles and Legs. Outputs from motoneurons excite muscles, causing contraction. Muscles are complex structures, and muscular contraction and the resulting force production ultimately relies on molecular motors and conformational changes in proteins that have only recently been studied in detail. Fortunately, for our purposes a macroscopic overview will suffice, drawn from sources assembled in the Ph.D. thesis of Ghigliazza [144].

Muscle fibers are comprised of bundles of myofibrils, each in turn containing longitudinal thick and thin myofilaments [242], separated by Z-disks and assembled in cylindrical sarcomeres. The myofibrils lie in the sarcoplasmatic reticulum (SR), which stores calcium. T-tubuli encircle the SR. Upon arrival of a motoneuronal AP at the neuromuscular junction, a second AP is produced that propagates through the T-tubuli, opening gates in the SR to release calcium ions. The calcium ions trigger conformational changes that cause thick myofilaments to slide over the thin ones, thus shortening the muscle. This process, described by Huxley [187], is modeled by a unidirectional cascade of linear processes [174, 198]; see Figure 33(b). First the motoneuron output $u(t)$, either a rapid spike train or a few larger APs, is converted into the T-tubuli response $\beta(t)$ according to

$$\ddot{\beta} + c_1\dot{\beta} + c_2\beta = c_3u(t); \tag{78}$$

this in turn produces SR release $\gamma(t)$ via

$$\ddot{\gamma} + c_4\dot{\gamma} + c_5\gamma = c_6\beta(t); \tag{79}$$

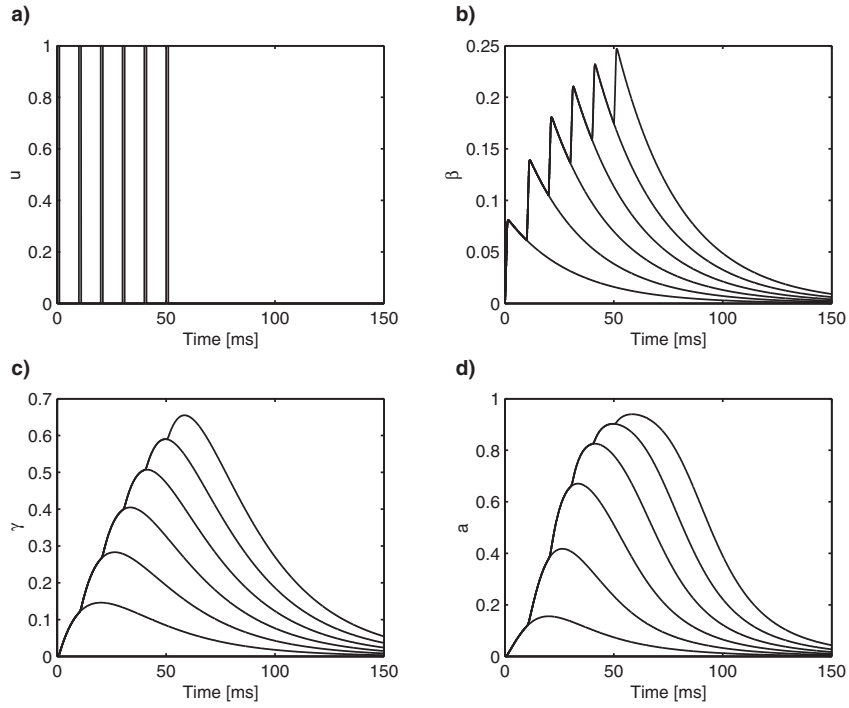

Fig. 37 *Activation dynamics. Panel* (a) *shows the normalized spike train input* $u(t)$ *from a motoneuron, here a train of six APs with* 10 *msec interspike intervals. Panels* (b), (c), *and* (d) *show the T-tubuli depolarizations* $\beta(t)$*, the free calcium concentrations* $\gamma(t)$*, and the resulting activation functions* $a(t)$*. Note linear superposition in* (a)–(c).

finally, the muscle activation is given by the algebraic relation

$$a(t) = \frac{a_0 + (\rho\nu\gamma)^2}{1 + (\rho\nu\gamma)^2}. \tag{80}$$

Muscle fatigue can be accounted for by the fitness variable $\nu(t)$ in (80), itself governed by first-order dynamics [273]:

$$\dot{\nu} = \frac{1}{T_{\rm f}}(\nu_{\min} - \nu)\frac{\gamma}{\gamma_0} + \frac{1}{T_{\rm r}}(1-\nu)\left(1 - \frac{\gamma}{\gamma_0}\right); \tag{81}$$

however, here we shall ignore fatigue and set $\nu(t) \equiv 1$.

The constants $c_j, T_{\rm f}, T_{\rm r}, \nu_{\min}, \gamma_0, a_0$ characterize the muscle properties. Figure 37 shows the result of a train of six fast motoneuron APs fed into this system. Note the linear superposition, with appropriate delays, of the responses to single APs, and the resulting smoothed rising and exponentially decaying activation function $a(t)$. Of course, explicit formulae can be written in terms of the collective impulse response of the linear system (78)–(79).

The mechanical properties of muscle fibers themselves are generally represented by a macroscopic model due to A.V. Hill [178]; cf. [242, 343, 230]. This model, adapted to *Blaberus* hind leg muscle 177c, the major power generator in stance [127, 245], was used in [294] to equip the bipedal LLS model of Figure 26 with agonist–antagonist muscle pairs, and a slightly simpler version will be described here [148].

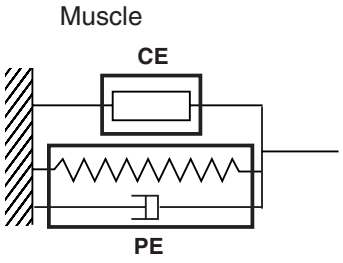

Fig. 38 *The muscle complex model: CE denotes contractile (active) element, PE denotes passive viscoelastic element. See text for description.*

Each muscle complex contains a contractile element (CE) in parallel with passive viscoelastic elements (PE) (Figure 38). Note that, in contrast to other muscle complex models, no additional series spring element is required here, since insect apodemes, the analog of tendons, are relatively stiff [127, 245].

In the Hill model each muscle exerts a force equal to the sum of its passive and active components:

$$F_{\text{Total}} = F_{\text{PE}} + F_{\text{CE}}\,, \tag{82}$$

where F_{PE} takes the form

$$F_{\text{PE}} = c\,\dot{l}_m + \begin{cases} 0\,, & l_m < l_o, \\ k(l_m - l_o)^{\alpha}\,, & l_m \geq l_o. \end{cases} \tag{83}$$

Here $l_m, \dot{l}_m$ denote the muscle length and velocity, respectively, and l_o is the "optimal" length at which the active force is maximum. The second term of (83) vanishes for $l_m < l_o$ because the passive stiffness is effectively zero for contracted muscles. Hence, to maintain nonzero stiffness around equilibrium, muscles typically act in agonist–antagonist (opposing) pairs. The passive stiffness and damping coefficients k, c and exponent α are fitted to data from unactivated muscles [139].

The active force F_{CE} developed in each contractile element is determined by the product of the isometric force-length (F_l) and force-velocity (F_v) relations and the activation, $a(t)$. $F_v(\dot{l}_m)$ takes two forms, depending on whether the muscle is shortening ($\dot{l}_m < 0$) or lengthening ($\dot{l}_m > 0$) [343, 246]:

$$F_{\text{CE}} = \begin{cases} \frac{a(t)\,F_l(l_m)\,b\,[v_{\max}+\dot{l}_m]}{b\,v_{\max}-\dot{l}_m}\,, & \dot{l}_m \leq 0\,, \\ \frac{a(t)\,F_l(l_m)\,[(f-1)\,v_{\max}+f\,(1+b)\,\dot{l}_m]}{(f-1)\,v_{\max}+(1+b)\,\dot{l}_m}\,, & \dot{l}_m > 0\,. \end{cases} \tag{84}$$

Here $v_{\max}$ is the maximal shortening velocity above which no force is produced, f denotes the upper limit of force produced as the lengthening velocity approaches infinity, and b quantifies the "steepness" of dependence on $\dot{l}_m$. In its active range the isometric force-length function can often be modeled as a quartic polynomial:

$$F_l(l_m) = \begin{cases} a_4\,l_m^4 - a_3\,l_m^3 + a_2\,l_m^2 + a_1\,l_m + a_0\,, & l_m \in [\,l_{\min}, l_{\max}], \\ 0\,, & l_m < l_{\min}\,,\ l_m > l_{\max}, \end{cases} \tag{85}$$

where the coefficients a_j are fitted to experimental data. Typically $F_l(l_m)$ drops to zero below $l_{\min} \approx 0.5\,l_o$ and above $l_{\max} \approx 1.5\,l_o$ and rises to a maximum (normalized

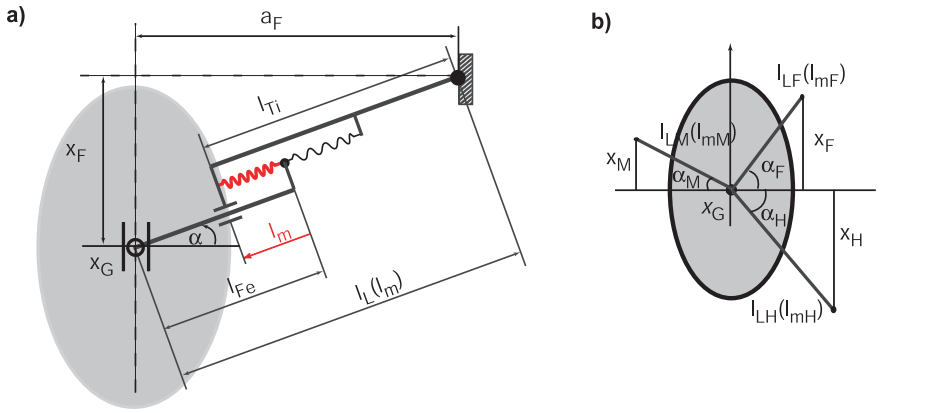

Fig. 39 *An LLS model with telescopic legs actuated by Hill-type muscles.* (a) *Geometry of a single pivoted leg. The "femur" and "tibia" of fixed lengths* $l_{\mathrm{Fe}}, l_{\mathrm{Ti}}$ *are connected by an agonist–antagonist muscle complex of variable length* l_m*, each half of which has the structure of Figure* 38*. Contraction of the extensor, shown bold, lengthens the leg. Given touchdown foot parameters* (x_{F}, α)*, the muscle state* l_m *can be expressed in terms of COM position* x_{G}*.* (b) *Tripod stance model. Adapted from* [148] *with permission from Turpion-Moscow Ltd. Article available online from http://www.turpion.org/php/paper.phtml?journal_id=rd&paper_id=*311*.*

to 1) at $l_m = l_o$. The muscle lengths l_m and velocities $\dot{l}_m$ appearing in (82)–(85) will be determined via the leg geometry and kinematics appearing in the coupled mechanical (force and moment balance) equations. The five constants in (85) allow one to set $F_l(l_{\min}) = F_l(\max) = 0$, $F_l'(l_o) = 0$, to normalize $F_l(l_o) = 1$, and also permit a degree of asymmetry.

5.4.4. Toward a Hexapedal Neuromechanical Model. In [294] it was shown that the results summarized in section 5.2 for the simpler actuated spring LLS of Figure 26—preservation of a branch of stable gaits with the additional property of speed stabilization as per Figures 27–28—persist for an axial spring whose pivot is actuated by an agonist–antagonist Hill muscle pair. As a first step toward a hexapedal model, Ghigliazza studied a single DOF point mass "rail roach," constrained to move along a linear track, with tripods of massless stance legs actuated by simplified extensor and flexor muscles [144, 148]. The geometry is shown in Figure 39. Contraction of the extensor lengthens the leg, and by applying suitable activations $a(t)$ derived from motoneuronal outputs via (78)–(79) as described in section 5.4.3, we can investigate the dynamical effects of different balances of positive and negative work (cf. [134]) among legs and during the stance phase cycle.

Constraining to one DOF allows one to translate COM position and velocity $(x_{\mathrm{G}}, \dot{x}_{\mathrm{G}})$ directly into muscle lengths l_m and shortening velocities $-\dot{l}_m$ for each of the three complexes associated with front (F), middle (M), and hind (H) legs, and thus to write the equations of motion as a planar vector field, albeit with explicit time dependence via the activation function $a(t)$. Details may be found in [148]. By starting with a single leg and first studying unactivated, purely passive muscles, followed by constant activation, and finally by CPG-driven phasic activation and superposition of the three legs, one assembles a reasonable understanding of the existence and stability of periodic gaits using phase plane analysis [144].

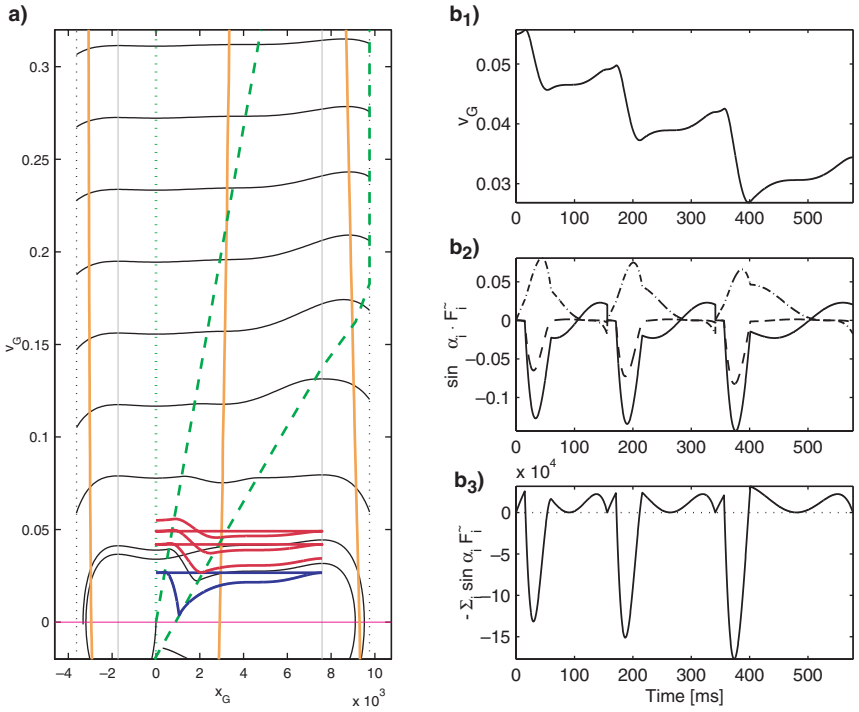

Fig. 40 *Stable gaits under a fixed stretch liftoff protocol.* (a) *Phase portrait with green dashed boundaries indicating region of nonzero muscle activation and the limit cycle (blue). Also shown is a converging trajectory (red).* (b) *Time histories of speed* (b_1)*, individual force profiles for front (dashed), middle (solid), and hind leg (dash-dotted)* (b_2)*, and total fore-aft force on COM* (b_3)*. Reprinted from* [148] *with permission from Turpion-Moscow Ltd. Article available online from http://www.turpion.org/php/paper.phtml?journal_id=rd&paper_id=*311.

A major problem in studying more detailed models of this type is the large number of parameters involved. While those determining the activation and Hill model can be estimated by direct measurements on single muscles [246, 245], these estimates do not apply directly to a simplification such as that of Figure 39 in which several muscles actuating different joints are represented by a single complex, and four limb components (coxa, femur, tibia, and tarsus) are collapsed to a telescopic rod. It is also necessary to choose liftoff and touchdown criteria, involving single legs or collective stance tripod states (some of these are briefly described in the next subsection). In the actuated model described in section 5.2 we took a fixed stance period, implicitly assuming a feedforward signal from the CPG [294]; in that of section 5.3, liftoff and touchdown were assumed to occur when the force in any of the support legs first drops to zero [302]. Leg force, leg stretch or angle, and CPG phase or timing criteria are all considered in [144].

Figure 40 shows an example of a stable gait under a fixed stretch protocol, liftoff and touchdown being indicated by the vertical grey lines on the phase portrait of panel (a). Individual forces are not as smooth as desired (panel (b_2)), but they do exhibit the appropriate patterns, falling near zero at touchdown and liftoff, and the net COM fore-aft force is marginally acceptable (panel (b_3)). However, while stable gaits were relatively easy to find for constant activation, because positive and

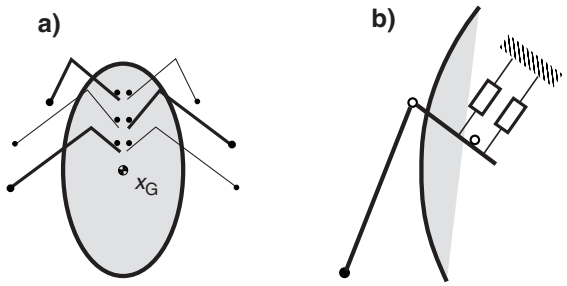

Fig. 41 (a) *Geometry of the hexapedal model with actuated muscles and two-component legs; left stance tripod shown bold.* (b) *A pair of Hill-type muscles (Figure* 38*) represents the depressor muscle complexes active in each leg during stance. The pivots represent the coxa–trochanteral and femur–tibia joints, and passive torsional stiffness and dissipation can be included in both joints.*

negative actuated work and passive elastic effects can be balanced by considering contractive and expansive regions in phase space, we were unable to find stable gaits with reasonable force profiles over a realistic speed range for time-dependent CPG actuations. This may be due to the muscle acting on an oversimplified leg, with fixed, torque-free pivots, or to the COM constraint. The actuated models of [294] and [302] either specified "hip" torques directly, or indirectly via moving pivot positions, and allowed three-DOF coupled translations and rotations in the horizontal plane.

Thus, to properly incorporate muscles we believe that a more realistic model than the abstracted telescopic leg of sections 5.2–5.3 and Figure 39 is required. To avoid excessive complexity, we propose to follow Full and Ahn [127, Figure 2] in simplifying the four-component cockroach limbs to two rigid links, connected to the body at a "hip," representing the coxa–trochanteral joint, and pivoted at a "knee" or "ankle," representing the femur–tibia joint, these being the joints that display the greatest angular variations [214]. Similarly, the depressor musculo-apodeme complexes active during the stance phase are collapsed to an agonist–antagonist pair of Hill-type elements that pull on the "lever" of the femur; see Figure 41. We can also include passive damping and stiffness in the knee and hip joints.

We are currently performing simulations of bipedal and hexapedal models with the jointed leg geometry of Figure 41. Although we anticipate that appropriate leg geometries will be necessary to generate the correct forces and moments at the coxa–trochanteral joints, we shall continue to neglect leg masses, thus obviating swing phase dynamics and restricting to three degrees of freedom (in the horizontal plane).

5.5. On Proprioceptive and Exteroceptive Feedback. The neuromechanical model sketched in section 5.4 lacks reflexive feedback and overall CNS control. In particular, the CPG model is "wired" to produce a stable antiphase tripod gait. (It possesses other periodic gait patterns that are mostly unstable, although the all-in-phase pronking gait can be stabilized by adjusting the timescale of inhibitory coupling among the six CPG interneurons [147].) This is appropriate in the present context, since as we emphasized at the outset and again in section 2.4, this review focuses on rapid running, in which neural reflexes are dominated by preflexive, mechanical feedback. However, if only to indicate a little of what we have omitted, we now briefly discuss some aspects of reflexive feedback in insects.

Tryba and Ritzmann [321, 322] present evidence of different inter- and intralimb (joint) phase relations during slow walking and searching behaviors in cockroaches in which the double-tripod gait characteristic of higher speeds is replaced by more varied patterns. Extensive work on stick insects [92, 93, 20, 91] indicates that proprioceptive feedback from strain sensors (campaniform sensillae) and hair cells and hair plates are important in regulating interlimb motions, load-sharing among legs, and posture control in these regimes [345, 264, 339, 272, 5, 347]. Indeed, as noted earlier in section 2.4, complex models of proprioceptive feedback and the resulting limb kinematics have been formulated based on this work; see [111, 108] for recent reviews.

Cockroach circuitry is not as well known as that of the larger and slower stick insect, but Pearson [261, 257, 263] shows that campaniform sensillae make excitatory connections to slow depressor motoneurons and inhibitory connections to bursting interneurons, thereby reinforcing depressor muscle activity during stance, while tonic inputs from other leg receptors exert the opposite effect. It is also known that overall CNS commands excite both CPG neurons and motoneurons and that, in turn, CPG outputs can significantly modulate reflexive feedback pathways [75]. Zill et al. [346, 222, 347] provide details of these and other sensory pathways in the cockroach, and Pearson's review [259] cites many further references on proprioceptive feedback. The use of body orientation and load direction sensing to change leg phasing for improved hill climbing in the robot RHex is discussed in [209]; cf. [208].

Once our feedforward neuromechanical model is running reliably we intend to add proprioceptive feedback to both motoneurons and CPG (inter)neurons, along with exteroreception from, for example, antennae and vision, as well as higher level, goal-oriented feedback from the CNS. Recent papers from Cowan's lab [221, 90] describe control of a wheeled robot and of a modified LLS model of the type considered in section 5.1 using antennal sensing to evoke wall-following behavior characteristic of cockroaches [64]. Other insect navigation control systems and their role in designing bio-inspired autonomous robots are described in [332].

It will be important to first ensure that proprioceptive feedback does not destabilize preflexively stabilized gaits. Assuming that this is the case, the models will allow us to examine the advantages it affords, especially at low speeds, in increasing flexibility and resistance to large perturbations.

As we have noted, organs called campaniform sensillae detect exoskeletal strain components [263], and this and the multiple and single-leg force measurements of [135, 136, 317] prompted our initial choice to define liftoff of stance and touchdown of swing legs in the LLS model to occur when the force in the stance leg(s) falls to zero. Hair cells or plates [345, 264, 339, 272] and chordotonal organs [222] detect joint angles and angular velocities. The inclusion of such sensors, hexapedal geometry, muscles, and the CPG-motoneuron circuit described in sections 5.4.1–5.4.2 suggests several additional, alternative rules for stance-switching, for example:

1. when leg force magnitudes, or fore-aft or lateral force components, first drop to zero (proprioceptive feedback);
2. when joint angles (leg stretches) first reach prescribed values (proprioceptive feedback);
3. when CPG oscillator phases first reach prescribed values (pure feedforward).

The first two feedback rules may be applied when any leg of the stance tripod first meets the chosen criterion, or when an average over the three legs achieves it. Other criteria, or combinations of the above, are of course possible. The legs may be constrained to lift and set down as two tripods, or allowed to do so independently.

Rules of comparable and greater complexity have been proposed and shown to generate stable gaits in models of stick insect walking [20, 92, 93, 111], although as we have noted these studies are kinematic rather than dynamic: they do not consider the full Newtonian mechanics of body and limbs.

Once a periodic gait is found using, say, a stretch criterion as in Figure 40, liftoff joint angles and CPG phases are thereby determined and thus the same gait must exist under the other criteria and appropriate combinations thereof. Stability may vary, however, much as it can under hard (displacement or rigid) and soft (traction or dead) loading in elasticity theory [316].[13] In fact, the results reported in [144, 148] indicate that the force-sensing protocol seems to lead to stable gaits more readily than the others suggested above, and we note that stride-to-stride feedback to modify actuation onset times was required to stabilize the actuated Hill-type LLS model of [294]. With this and the great variety of possible reflexive feedback modes in mind, studies of different criteria are more likely to be illuminating when informed by experiments on animals with lesioned or otherwise-disrupted sensory pathways.

6. Conclusions: Open Problems and Challenges. In this article we have described several achievements in modeling the dynamics of legged locomotion, and noted some open questions. After reviewing biomechanical, neurobiological, and control-theoretic background and summarizing results of animal studies, in section 3.3 we proposed four hypotheses that guide our approach to experimentation and modeling. The work described in sections 4–5 goes some way toward addressing the first two of these: that locomotive systems are inherently stable with minimal neural feedback, and that the neural and mechanical architectures of animals effectively collapse their potentially high-dimensional dynamical systems into much lower dimensional templates.

Specifically, we showed that passively stabilized SLIP and LLS models, having, respectively, two and three DOFs and describing motions constrained to vertical (saggital) and horizontal planes, can capture key qualitative features of mass center motions during running. We sketched current work on fully three-dimensional coupled dynamics, and on hexapedal models with actuated legs, that provide quantitative matches to data. We then showed that relatively detailed biophysical models of bursting neurons can be assembled into a CPG-motoneuron circuit and reduced to a tractable phase oscillator model that enables the analytical study of gaits and phase relationships among limbs. Using phase response curves and averaging theory, we reduced some sixty ODEs (previously pared from over a hundred by eliminating fast timescales) to six, and then, assuming support tripods in exact antiphase and appealing to symmetry, to a single scalar ODE on the circle with trivially simple dynamics.

We have indicated how fast and slow motoneuron outputs of the CPG model can innervate Hill-type muscle models and thus activate a hexapedal body with jointed legs more representative of the insect than the telescoping springs of sections 5.3 and 5.4.4. Since these spike trains are determined by the CPG and the calcium dynamics steps to muscle activation are linear, the resulting feedforward neuromechanical model may be reducible to a set of six phase oscillators (cf. (75)) that excite, via Hill-type dynamics (82)–(85), a mechanical model with massless legs, thus generating a four-dimensional Poincaré map much as in sections 5.1–5.3. Further reduction may even be possible for stereotyped gaits with fixed phase relationships, although it remains

[13] Soft loading permits a larger class of solutions than hard loading, so in the former, less-constrained case, specific solutions may be unstable even if they are stable under hard loading.

to be seen to what degree the details of spike trains can be ignored and subsumed in phase reductions, especially when proprioceptive feedback is added.

Although models such as these are radically simplified, their hybrid nature makes them resistant to "closed-form" analysis in all but the simplest limiting cases (sections 4.4 and 5.1), and while perturbation methods can extend these results [293, 294], numerical studies remain essential (hence our account of the methods in section 4.3). It is difficult to extract general information on parameter dependence from numerical work alone, but careful nondimensionalization and linearization in appropriate parameter ranges, suggested by comparative studies such as those reviewed in section 3, can be useful. In this regard we are currently using the SLIP approximations proposed in [298, 143] to investigate how gravitational, elastic, and rotational effects interact to produce bouncing frequencies.

In the work described here we made the relatively vague "preflex hypothesis" of Brown, Scott, and Loeb [49] precise by creating passive and actuated models—the latter with predominantly feedforward forcing—and investigating the existence and stability of periodic gaits via analytical, perturbative, and numerical computations of Poincaré maps. Since the models have massless legs, "logical" rather than dynamical liftoff and touchdown criteria must be employed, but this is the only point at which sensory control enters. For simplicity, we have thus far mostly assumed liftoff of stance legs and touchdown of swing legs to occur simultaneously when stance foot forces fall to zero, but, as noted in section 5.5, other criteria may be more realistic. Overall, the formulation of such mathematical models forces one to specify precise mechanisms that, while inevitably idealizing and simplifying the animal's own strategies, reveal key underlying principles. Moreover, we believe that they will allow us to discover the relative importance of factors such as positive and negative work (cf. [134, 4]) vs. dissipative losses in stabilization, and to further elucidate the scaling relations of section 3.

The third and fourth hypotheses of section 3.3—that, depending upon task demands and sensor capabilities, reflexive controls are tuned in a space characterized by centralized/decentralized and feedback/feedforward qualities (Figure 7) and that higher (task) level control operates by assembling goal pursuit dynamics from simpler behavioral primitives—remain as outstanding challenges. They nonetheless suggest an experimental program and will allow us to build at least template-type models of reflexive feedback systems and CNS controls.

In particular, to probe the space of reflexive control architectures, we propose that the dynamic clamp technique of neuroscience should be extended to neuromechanical systems. In dynamic clamp experiments "virtual" ionic currents are added to neurons *in vitro* by running real-time computer simulations of their gating dynamics (cf. (11b)–(12)) in response to digitized intracellular membrane voltage measurements [280, 308, 309]. The resulting currents, after digital-to-analog conversion, are then input to the neuron via the recording microelectrode. In this way precise manipulations of both natural and artificial intracellular dynamics, and of intercellular (synaptic) inputs, can be achieved and used to probe the parameter space [309]. Linux-based software is available for implementation of this and related biological control tasks [104].

We imagine several extensions to this powerful technique. An isolated CPG-motoneuron preparation *in vitro*, deprived of sensory inputs, could have them artificially restored by introducing a mathematical model of muscles and limb–body dynamics "driven" by the motoneuron outputs. More or less rich dynamics and environmental insults could be allowed, and different types of proprioceptive feedback

added. Less radically, one could sever a reflexive pathway and record spike trains from, say, campaniform sensillae or hair cells, manipulate the signals by introducing delays or degrading (or improving) signal-to-noise ratios, and reinject them at the target cells. In both cases, one literally builds a mathematical model into the physical loop and varies its properties in a controlled manner in order to probe less well understood biological components.

Experiments such as these will, we believe, allow us to investigate proprioceptive and central sensory pathways to a degree that will enable the creation of neuromechanical models of freely running insects with at least limited behavioral repertoires. The resulting models—a suite of anchors and templates—will, in turn, further elucidate the path from neural spikes through mechanical work to behavior. Paraphrasing T.S. Eliot [113], we will then have removed a little more of the shadow between intent and action.

Acknowledgments. The work that led to this review was begun in June 1998 at the Institute for Mathematics and Its Applications (Minnesota) Workshop on Animal Locomotion and Robotics, which we all attended, and at which some of us first met; we thank the IMA for inviting us. Since then it has been variously supported by DARPA/ONR: N00014-98-1-0747, DoE: DE-FG02-95ER25238 and DE-FG02-93ER25164, and NSF: DMS-0101208 and EF-0425878. PH thanks the Institute for Advanced Study for its hospitality during spring 2003, when the first drafts of the manuscript were written. Tony Bloch, Raffaele Ghigliazza, Andy Ruina, Justin Seipel, and Francisco Valero-Cuevas offered advice and input, and we thank them, the three referees, and Randy LeVeque, who dealt with this paper as the Survey and Review section editor, for pointing out errors and omissions and for many helpful suggestions. Justin Seipel prepared final versions of the figures.

REFERENCES

[1] L. Abbott, *Single neuron dynamics*, in Neural Modeling and Neural Networks, F. Ventriglia, ed., Pergamon Press, Oxford, UK, 1994, Chap. 4, pp. 57–78.
[2] R. Abraham and J. Marsden, *Foundations of Mechanics*, Addison-Wesley, New York, 1985.
[3] C. Acker, N. Kopell, and J. White, *Synchronization of strongly coupled excitatory neurons: Relating network behavior to biophysics*, J. Comput. Neurosci., 15 (2003), pp. 71–90.
[4] A. Ahn and R. Full, *A motor and a brake: Two leg extensor muscles acting at the same joint manage energy differently in a running insect*, J. Exp. Biol., 205 (2002), pp. 379–389.
[5] T. Akay, U. Bässler, P. Gerharz, and A. Büschges, *The role of sensory signals from the insect coxa-trochanteral joint in controlling motor activity of the femur-tibia joint*, J. Neurophys., 85 (2001), pp. 594–604.
[6] R. Alexander, *Elastic Mechanisms in Animal Movement*, Cambridge University Press, Cambridge, UK, 1988.
[7] R. Alexander, *The mechanics of jumping by a dog (canis familiaris)*, J. Zool. Lond., 173 (1989), pp. 549–573.
[8] R. Alexander, *Principles of Animal Locomotion*, Princeton University Press, Princeton, NJ, 2003.
[9] R. Alexander and A. Jayes, *A dynamic similarity hypothesis for the gaits of quadrupedal mammals*, J. Zool. London, 201 (1983), pp. 135–152.
[10] R. Alexander and A. Vernon, *Mechanics of hopping by kangaroos (macropodidae)*, J. Zool. London, 177 (1975), pp. 265–303.
[11] R. Altendorfer, D. Koditschek, and P. Holmes, *Stability analysis of a clock-driven rigid-body SLIP model for RHex*, Int. J. Robotics Res., 23 (2004), pp. 1001–1012.
[12] R. Altendorfer, D. Koditschek, and P. Holmes, *Stability analysis of legged locomotion models by symmetry-factored return maps*, Int. J. Robotics Res., 23 (2004), pp. 979–999.
[13] R. Altendorfer, A. Moore, H. Komsuoglu, M. Buehler, H. Brown, D. McMordie, U. Saranli, R. Full, and D. Koditschek, *RHex: A biologically inspired hexapod runner*, J. Autonomous Robots, 11 (2001), pp. 207–213.

[14] S. Arimoto, *A challenge to Bernstein's degrees-of-freedom problem in both cases of human and robotic multi-joint movements*, in Proceedings of the 2004 International Symposium on Nonlinear Theory and Its Applications, Research Society of Nonlinear Theory and Its Applications, IEICE, 2004, pp. 1–15 (CD-ROM).
[15] S. Arimoto, *Intelligent control of multi-fingered hands*, Ann. Rev. Control, 28 (2004), pp. 75–85.
[16] V. Arnold, *Mathematical Methods of Classical Mechanics*, Springer-Verlag, New York, 1978.
[17] Y. Arshavsky, T. Deliagina, and G. Orlovsky, *Pattern generation*, Current Opinion in Neurobiology, 7 (1997), pp. 781–789.
[18] K. Autumn, M. Ryan, and D. Wake, *Integrating historical and mechanistic biology enhances the study of adaptation*, Quart. Rev. Biol., 77 (2002), pp. 383–408.
[19] A. Back, J. Guckenheimer, and M. Myers, *A dynamical simulation facility for hybrid systems*, in Hybrid Systems, Lecture Notes in Comput. Sci. 736, Springer-Verlag, Berlin, 1993, pp. 255–267.
[20] U. Bässler and A. Büschges, *Pattern generation for stick insect walking movements—multisensory control of a locomotor program*, Brain Research Rev., 27 (1998), pp. 65–88.
[21] P. Beek, C. Peper, and A. Daffertshofer, *Modeling rhythmic interlimb coordination: Beyond the Haken-Kelso-Bunz model*, Brain and Cognition, 48 (2002), pp. 149–165.
[22] R. Beer, H. Chiel, and J. Gallagher, *Evolution and analysis of model CPGs for walking* II. *General principles and individual variability*, J. Comput. Neurosci., 7 (1999), pp. 119–147.
[23] R. Beer and J. Gallagher, *Evolving dynamical neural networks for adaptive behavior*, Adaptive Behavior, 1 (1992), pp. 91–122.
[24] A. Bernstein, *The Coordination and Regulation of Movements*, Pergamon Press, Oxford, UK, 1967.
[25] A. Bernstein, *On Dexterity and Its Development*, Lawrence Erlbaum Associates, Mahwah, NJ, 1996. Translated from the Russian by M. L. Latash.
[26] A. Biewener and R. Baudinette, *In vivo muscle force and elastic energy storage during steady-speed hopping of tammar wallabies (macropus eugenii)*, J. Exp. Biol., 198 (1995), pp. 1829–1841.
[27] A. Biewener, D. Konieczynski, and R. Baudinette, *In vivo muscle force-length behavior during steady-speed hopping in tammar wallabies*, J. Exp. Biol., 201 (1998), pp. 1681–1694.
[28] A. Biewener and C. Taylor, *Bone strain: A determinant of gait and speed?*, J. Exp. Biol., 123 (1986), pp. 383–400.
[29] G. Birkhoff, *Dynamical Systems*, AMS, Providence, RI, 1927. Reprinted, Colloquium. Publications, Vol. 9, AMS, Providence, RI, 1966.
[30] E. Bizzi, N. Hogan, F. Mussa-Ivaldi, and S. Giszter, *Does the nervous system use equilibrium-point control to guide single and multiple joint movements?*, Behav. Brain Sci., 15 (1992), pp. 603–613.
[31] E. Bizzi, M. Tresch, P. Saltiel, and A. d'Avella, *New perspectives on spinal motor systems*, Nature Reviews Neurosci., 1 (2000), pp. 101–108.
[32] R. Blickhan, *The spring-mass model for running and hopping*, J. Biomechanics, 22 (1989), pp. 1217–1227.
[33] R. Blickhan and R. Full, *Locomotion energetics of the ghost crab:* II. *Mechanics of the centre of mass during walking and running*, J. Exp. Biol., 130 (1987), pp. 155–174.
[34] R. Blickhan and R. Full, *Similarity in multi-legged locomotion: Bouncing like a monopode*, J. Comp. Physiol. A, 173 (1993), pp. 509–517.
[35] R. Blickhan, R. Full, and L. Ting, *Exoskeletal strain: Evidence for a trot-gallop transition in rapid running ghost crabs*, J. Exp. Biol., 179 (1993), pp. 301–321.
[36] A. Bloch, J. Baillieul, P. Crouch, and J. Marsden, *Nonholonomic Mechanics and Control*, Springer-Verlag, New York, 2003.
[37] A. Bloch, H. Chang, N. Leonard, and J. Marsden, *Controlled Lagrangians and the stabilization of mechanical systems:* II. *Potential shaping*, IEEE Trans. Automat. Control, 46 (2001), pp. 1556–1571.
[38] A. Bloch and P. Crouch, *Nonholonomic and vakonomic control systems on Riemannian manifolds*, Fields Inst. Commun., 1 (1993), pp. 25–52.
[39] A. Bloch and P. Crouch, *Nonholonomic control systems on Riemannian manifolds*, SIAM J. Control, 33 (1995), pp. 126–148.
[40] A. Bloch, P. Krishnaprasad, J. Marsden, and R. Murray, *Nonholonomic mechanical systems with symmetry*, Arch. Rational Mech. Anal., 136 (1996), pp. 21–99.

[41] A. Bloch, N. Leonard, and J. Marsden, *Controlled Lagrangians and the stabilization of mechanical systems:* I. *The first matching theorem*, IEEE Trans. Automat. Control, 45 (2000), pp. 2253–2270.

[42] V. Blondel and J. Tsitsiklis, *NP-hardness of some linear control design problems*, SIAM J. Control Optim., 35 (1997), pp. 2118–2127.

[43] N. Borghese, L. Bianchi, and F. Lacquaniti, *Kinematic determinants of human locomotion*, J. Physiol., 494 (1996), pp. 863–879.

[44] G. Bowtell and T. Williams, *Anguilliform body dynamics: Modelling the interaction between muscle activation and curvature*, Phil. Trans. Roy. Soc. B, 334 (1991), pp. 385–390.

[45] G. Bowtell and T. Williams, *Anguilliform body dynamics: A continuum model for the interaction between muscle activation and body curvature*, J. Math. Biol., 32 (1994), pp. 83–91.

[46] E. Brown, J. Moehlis, and P. Holmes, *On the phase reduction and response dynamics of neural oscillator populations*, Neural Comp., 16 (2004), pp. 673–715.

[47] E. Brown, J. Moehlis, P. Holmes, E. Clayton, J. Rajkowski, and G. Aston-Jones, *The influence of spike rate and stimulus duration on noradrenergic neurons*, J. Comput. Neurosci., 17 (2004), pp. 13–29.

[48] I. Brown and G. Loeb, *A reductionist approach to creating and using neuromusculoskeletal movement*, in Biomechanics and Neural Control of Movement, J. Winters and P. Crago, eds., Springer-Verlag, New York, 2000, pp. 148–163.

[49] I. Brown, S. Scott, and G. Loeb, *"Preflexes"—programmable, high-gain, zero-delay intrinsic responses of perturbed musculoskeletal systems*, Soc. Neurosci. Abstr., 21 (1995), p. 562.9.

[50] N. Brunel and X.-J. Wang, *Effects of neuromodulation in a cortical network model of object working memory dominated by recurrent inhibition*, J. Comput. Neurosci., 11 (2001), pp. 63–85.

[51] A. Bryson and Y. Ho, *Applied Optimal Control*, Taylor and Francis, New York, 1975.

[52] J. Buchli and A. Ijspeert, *Distributed central pattern generator model for robotics application based on phase sensitivity analysis*, in Biologically Inspired Approaches to Advanced Information Technology: First International Workshop, BioADIT 2004, Lecture Notes in Comput. Sci. 3141, Springer-Verlag, Berlin, 2004, pp. 333–349.

[53] M. Buehler, D. Koditschek, and P. Kindlmann, *A family of robot control strategies for intermittent dynamical environments*, IEEE Control Systems Mag., 10 (2) (1990), pp. 16–22.

[54] F. Bullo and A. Lewis, *Geometric Control of Mechanical Systems*, Springer-Verlag, New York, 2005.

[55] R. Burke, *Revisiting the notion of "motor unit types,"* Prog. Brain Res., 123 (1999), pp. 167–175.

[56] R. Burke, *Some unresolved issues in motor unit research*, Adv. Exp. Med. Biol., 508 (2002), pp. 171–178.

[57] M. Burrows, *The control of sets of motoneurones by local interneurones in the locust*, J. Physiol., 298 (1980), pp. 213–233.

[58] M. Burrows and M. Siegler, *Networks of local interneurons in an insect*, in Neural Origin of Rhythmic Movements, A. Roberts and B. Roberts, eds., Symposia of the Society for Experimental Biology, Vol. 37, Cambridge University Press, Cambridge, UK, 1983, pp. 29–53.

[59] A. Büschges and A. Manira, *Sensory pathways and their modulation in the control of locomotion*, Current Opinion in Neurobiology, 8 (1998), pp. 733–739.

[60] R. Butera, J. Rinzel, and J. Smith, *Models of respiratory rhythm generation in the pre-Bötzinger complex.* I. *Bursting pacemaker neurons*, J. Neurophys., 81 (1999), pp. 382–397.

[61] R. Butera, J. Rinzel, and J. Smith, *Models of respiratory rhythm generation in the pre-Bötzinger complex.* II. *Populations of coupled pacemaker neurons*, J. Neurophys., 81 (1999), pp. 398–415.

[62] W. Calder, *Size, Function, and Life History*, Harvard University Press, Cambridge, MA, 1984.

[63] A. Calvitti and R. Beer, *Analysis of a distributed model of leg coordination.* I. *Individual coordination mechanisms*, Biol. Cybern., 82 (2000), pp. 197–206.

[64] J. Camhi and E. Johnson, *High frequency steering maneuvers mediated by tactile cues: Antennal wall-following in the cockroach*, J. Exp. Biol., 202 (1999), pp. 631–643.

[65] C. Canavier, R. Butera, R. Dror, D. Baxter, J. Clark, and J. Byrne, *Phase response characteristics of model neurons determine which patterns are expressed in a ring model of gait generation*, Biol. Cybern., 77 (1997), pp. 367–380.

[66] J. Carling, T. Williams, and G. Bowtell, *Self-propelled anguilliform swimming: Simultaneous solution of the two-dimensional Navier-Stokes equations and Newton's laws of motion*, J. Exp. Biol., 201 (1998), pp. 3143–3166.

[67] S. Carver, *Control of a Spring-Mass Hopper*, Ph.D. thesis, Cornell University, Ithaca, NY, 2003.

[68] G. Cavagna, N. Heglund, and C. Taylor, *Mechanical work in terrestrial locomotion: Two basic mechanisms for minimizing energy expenditure*, Amer. J. Physiol., 233 (1977), pp. R243–R261.

[69] G. Cavagna, F. Saibene, and R. Margaria, *Mechanical work in running*, J. Appl. Physiol., 19 (1964), pp. 249–256.

[70] G. Cavagna, H. Thys, and A. Zamboni, *The sources of external work in level walking and running*, J. Physiol. Lond., 262 (1976), pp. 639–657.

[71] H. Chang, A. Bloch, N. Leonard, J. Marsden, and C. Woolsey, *The equivalence of controlled Lagrangian and controlled Hamiltonian systems*, ESIAM Control Optim. Calc. Var., 8 (2002), pp. 393–422.

[72] H. Chiel, R. Beer, and J. Gallagher, *Evolution and analysis of model CPGs for walking* I. *Dynamical modules*, J. Comput. Neurosci., 7 (1999), pp. 99–118.

[73] H. Chiel, R. Beer, R. Quinn, K. Espenschied, and P. Larson, *A distributed neural network architecture for hexapod robot locomotion*, Neural Computation, 4 (1992), pp. 356–365.

[74] C. Chow, J. White, J. Ritt, and N. Kopell, *Frequency control in synchronized networks of inhibitory neurons*, J. Comput. Neurosci., 5 (1998), pp. 407–420.

[75] F. Clarac, D. Cattaert, and D. L. Ray, *Central control components of a "simple" stretch reflex*, Trends in Neurosci., 23 (2000), pp. 199–208.

[76] A. Cohen, P. Holmes, and R. Rand, *The nature of coupling between segmental oscillators of the lamprey spinal generator for locomotion: A model*, J. Math. Biol., 13 (1982), pp. 345–369.

[77] A. Cohen and T. Kiemel, *Intersegmental coordination: lessons from modeling systems of non-linear oscillators*, Amer. Zool., 33 (1993), pp. 54–65.

[78] A. Cohen, R. Rand, and P. Holmes, *Systems of coupled oscillators as models of central pattern generators*, in Neural Control of Rhythmic Movements in Vertebrates, A. Cohen, S. Rossignol, and S. Grillner, eds., Wiley, New York, 1988, pp. 333–367.

[79] A. Cohen, S. Rossignol, and S. Grillner (eds), *Neural Control of Rhythmic Movements in Vertebrates*, Wiley, New York, 1988.

[80] A. Cohen and P. Wallén, *The neuronal correlate of locomotion in fish. "Fictive swimming" induced in an in vitro preparation of the lamprey spinal cord*, Exp. Brain. Res., 41 (1980), pp. 11–18.

[81] M. Coleman, A. Chatterjee, and A. Ruina, *Motions of a rimless spoked wheel: A simple three-dimensional system with impacts*, Dynam. Stability Systems, 12 (1997), pp. 139–159.

[82] M. Coleman, M. Garcia, K. Mombaur, and A. Ruina, *Prediction of stable walking for a toy that cannot stand*, Phys. Rev. E, 64 (2001), article 022901-1-3.

[83] M. Coleman and P. Holmes, *Motions and stability of a piecewise holonomic system: The discrete Chaplygin sleigh*, Regular and Chaotic Dynamics, 4 (1999), pp. 1–23.

[84] M. Coleman and A. Ruina, *An uncontrolled walking toy that cannot stand still*, Phys. Rev. Lett., 80 (1998), pp. 3658–3661.

[85] J. Collins and I. Stewart, *Hexapodal gaits and coupled nonlinear oscillator models*, Biol. Cybern., 68 (1993), pp. 287–298.

[86] S. Collins, A. Ruina, R. Tedrake, and M. Wisse, *Efficient bipedal robots based on passive-dynamic walkers*, Science, 305 (2005), pp. 1082–1085.

[87] S. Collins, M. Wisse, and A. Ruina, *A three-dimensional passive-dynamic walking robot with two legs and knees*, Int. J. Robotics Res., 20 (2001), pp. 607–615.

[88] J. Connor, D. Walter, and R. McKown, *Neural repetitive firing: Modifications of the Hodgkin-Huxley axon suggested by experimental results from crustacean axons*, Biophys. J., 18 (1977), pp. 81–102.

[89] P. Constantin, C. Foias, R. Temam, and B. Nicolaenko, *Integral Manifolds and Inertial Manifolds for Dissipative Partial Differential Equations*, Springer-Verlag, New York, 1989.

[90] N. Cowan, J. Lee, and R. Full, *Dynamical Control of Antennal Wall Following in the American Cockroach*, Society for Integrative and Comparative Biology, San Diego, CA, 2005.

[91] H. Cruse, *The functional sense of central oscillations in walking*, Biol. Cybern., 86 (2002), pp. 271–280.
[92] H. Cruse, T. Kindermann, M. Schumm, J. Dean, and J. Schmitz, *Walknet—a biologically inspired network to control six-legged walking*, Neural Networks, 11 (1998), pp. 1435–1447.
[93] G. Cymbaluk, R. Borisyuk, U. Müller-Wilm, and H. Cruse, *Oscillatory network controlling six-legged locomotion: Optimization of model parameters*, Neural Networks, 11 (1998), pp. 1449–1460.
[94] T. Dawson and C. Taylor, *Energetic cost of locomotion in kangaroos*, Nature, 246 (1973), pp. 313–314.
[95] P. Dayan and L. Abbott, *Theoretical Neuroscience*, MIT Press, Cambridge, MA, 2001.
[96] C. Del Negro, S. Johnson, R. Butera, and J. Smith, *Models of respiratory rhythm generation in the pre-Bötzinger complex.* III. *Experimental tests of model predictions*, J. Neurophys., 86 (2001), pp. 59–74.
[97] F. Delcomyn, *Neural basis of rhythmic behaviours in animals*, Science, 210 (1980), pp. 492–498.
[98] F. Delcomyn, *Walking and running*, in Comprehensive Insect Physiology Biochemistry and Pharmacology, G. Kerkut and L. Gilbert, eds., Pergamon Press, New York, 1985, pp. 439–466.
[99] F. Delcomyn, *Perturbation of the motor system in freely walking cockroaches* II. *The timing of motor activity in leg muscles after amputation of a middle leg*, J. Exp. Biol., 156 (1991), pp. 503–517.
[100] F. Delcomyn, *Insect walking and robotics*, Ann. Rev. Entomol., 149 (2004), pp. 51–70.
[101] M. Dickinson, C. Farley, R. Full, M. Koehl, R. Kram, and S. Lehman, *How animals move: An integrative view*, Science, 288 (2000), pp. 100–106.
[102] E. Doedel, A. Champneys, T. Fairgrieve, B. S. Y. Kuznetsov, and X. Wang, *Auto* 97: *Continuation and Bifurcation Software for Ordinary Differential Equations*, Tech. Report, Concordia University, 1997. Available via FTP from directory /pub/doedel/auto at ftp.cs.concordia.ca; software available from http://indy.cs.concordia.ca/auto/ and http://sourceforge.net/projects/auto2000.
[103] J. Donelan, R. Kram, and A. Kuo, *Simultaneous positive and negative external mechanical work in human walking*, J. Biomech., 35 (2002), pp. 117–124.
[104] A. Dorval, D. Christini, and J. White, *Real-time Linux dynamic clamp: A fast and flexible way to construct virtual ion channels in living cells*, Ann. Biomed. Eng., 29 (2001), pp. 897–907.
[105] P. Drazin and W. Reid, *Hydrodynamic Stability*, Cambridge University Press, Cambridge, UK, 1981.
[106] D. Dudek and R. Full, *Leg function in running insects: Resilience and impedance of legs linked to a body*, Amer. Zool., 41 (2001) (abstract).
[107] D. Dudek and R. Full, *Mechanical properties of the support tripod in running insects*, in Society of Integrative and Comparative Biology Annual Meeting and Exhibition: Final Program and Abstracts, 2004.
[108] V. Dürr, J. Schmitz, and H. Cruse, *Behavior-based modeling of insect locomotion: Linking biology and technical application*, Arthropod Structure and Development, 33 (2004), pp. 237–250.
[109] J. Duysens, F. Clarac, and H. Cruse, *Load-regulating mechanisms in gait and posture: Comparative aspects*, Physiol. Rev., 80 (2000), pp. 83–133.
[110] Ö. Ekeberg, *A combined neuronal and mechanical model of fish swimming*, Biol. Cybern., 69 (1993), pp. 363–374.
[111] O. Ekeberg, M. Blümel, and A. Büschges, *Dynamic simulation of insect walking*, Arthropod Structure and Development, 33 (2004), pp. 287–300.
[112] Ö. Ekeberg and S. Grillner, *Simulations of neuromuscular control in lamprey swimming*, Phil. Trans. Roy. Soc. B, 354 (1999), pp. 895–902.
[113] T. S. Eliot, in "The Hollow Men," *Collected Poems*, Faber and Faber, London, 1964.
[114] G. B. Ermentrout, *Type* I *membranes, phase resetting curves, and synchrony*, Neural Comp., 8 (1996), pp. 979–1001.
[115] G. B. Ermentrout, *Simulating, Analyzing, and Animating Dynamical Systems: A Guide to XPPAUT for Researchers and Students*, SIAM, Philadelphia, 2002.
[116] G. B. Ermentrout and N. Kopell, *Symmetry and phase locking in chains of weakly coupled oscillators*, Comm. Pure Appl. Math., 39 (1986), pp. 623–660.
[117] G. B. Ermentrout and N. Kopell, *Oscillator death in systems of coupled neural oscillators*, SIAM J. Appl. Math., 50 (1990), pp. 125–146.
[118] G. B. Ermentrout and N. Kopell, *Multiple pulse interactions and averaging in systems of coupled neural oscillators*, J. Math. Biol., 29 (1991), pp. 195–217.

[119] C. Farley, J. Glasheen, and T. McMahon, *Running springs: Speed and animal size*, J. Exp. Biol., 185 (1993), pp. 71–86.
[120] C. Farley and C. Taylor, *A mechanical trigger for the trot-gallop transition in horses*, Science, 253 (1991), pp. 306–308.
[121] J. Felsenstein, *Phylogenies and the comparative method*, Amer. Nat., 125 (1985), pp. 1–15.
[122] R. Fitzhugh, *Thresholds and plateaus in the Hodgkin-Huxley nerve equations*, J. General Physiol., 43 (1960), pp. 867–896.
[123] R. Fitzhugh, *Impulses and physiological states in theoretical models of nerve membrane*, Biophys. J., 1 (1961), pp. 455–466.
[124] R. Full, *Mechanics and energetics of terrestrial locomotion: From bipeds to polypeds*, in Energy Transformation in Cells and Animals, W. Weiser and E. Gnaiger, eds., Georg Thieme Verlag, Stuttgart, Germany, 1989, pp. 175–182.
[125] R. Full, *Animal motility and gravity*, Physiologist, 34 (1991), pp. S15–18.
[126] R. Full, *Invertebrate locomotor systems*, in The Handbook of Comparative Physiology, W. Dantzler, ed., Oxford University Press, New York, 1997, pp. 853–930.
[127] R. Full and A. Ahn, *Static forces and moments generated in the insect leg: Comparison of a three-dimensional musculo-skeletal computer model with experimental measurements*, J. Exp. Biol., 198 (1995), pp. 1285–1298.
[128] R. Full, K. Autumn, J. Chung, and A. Ahn, *Rapid negotiation of rough terrain by the death-head cockroach*, Amer. Zool., 38 (1998), p. 81A.
[129] R. Full, R. Blickhan, and L. Ting, *Leg design in hexapedal runners*, J. Exp. Biol., 158 (1991), pp. 369–390.
[130] R. Full and C. Farley, *Musculoskeletal dynamics in rhythmic systems: A comparative approach to legged locomotion*, in Biomechanics and Neural Control of Movement, J. Winters and P. Crago, eds., Springer-Verlag, New York, 2000, pp. 192–205.
[131] R. Full and D. Koditschek, *Templates and anchors: Neuromechanical hypotheses of legged locomotion on land*, J. Exp. Biol., 202 (1999), pp. 3325–3332.
[132] R. Full, T. Kubow, M. Garcia, W. Schwind, and D. Koditschek, *Can a Simple Neural Oscillator Generate Rapid Running in Cockroaches?*, Society for Integrative and Comparative Biology, Toronto, ON, Canada, 2003.
[133] R. Full, T. Kubow, J. Schmitt, P. Holmes, and D. Koditschek, *Quantifying dynamic stability and maneuverability in legged locomotion*, Integ. Comp. Biol., 42 (2002), pp. 149–157.
[134] R. Full, D. Stokes, A. Ahn, and R. Josephson, *Energy absorption during running by leg muscles in a cockroach*, J. Exp. Biol., 201 (1998), pp. 997–1012.
[135] R. Full and M. Tu, *Mechanics of six-legged runners*, J. Exp. Biol., 148 (1990), pp. 129–146.
[136] R. Full and M. Tu, *Mechanics of a rapid running insect: Two-, four- and six-legged locomotion*, J. Exp. Biol., 156 (1991), pp. 215–231.
[137] R. Full, A. Yamauchi, and D. Jindrich, *Maximum single leg force production: Cockroaches righting on photoelastic gelatin*, J. Exp. Biol., 198 (1995), pp. 2441–2452.
[138] M. Garcia, A. Chatterjee, A. Ruina, and M. Coleman, *The simplest walking model: Stability, complexity and scaling*, ASME J. Biomech. Eng., 120 (1998), pp. 281–288.
[139] M. Garcia, A. Kuo, A. Peattie, P. Wang, and R. Full, *Damping and size: Insights and biological inspiration*, International Symposium on Adaptive Motion of Animals and Machines, 2000.
[140] T. Garland, Jr. and S. C. Adolph, *Why not to do two-species comparative studies: Limitations on inferring adaptation*, Physiol. Zool., 67 (1994), pp. 797–828.
[141] T. Garland Jr., P. Harvey, and A. Ives, *Procedures for the analysis of comparative data using phylogenetically independent contrasts*, Sys. Biol., 41 (1992), pp. 18–32.
[142] P. Getting, *Comparative analysis of invertebrate central pattern generators*, in Neural Control of Rhythmic Movements in Vertebrates, A. Cohen, S. Rossignol, and S. Grillner, eds., Wiley, New York, 1988, pp. 101–128.
[143] H. Geyer, A. Seyfarth, and R. Blickhan, *Spring mass running: simple approximate solution and application to gait stability*, J. Theoret. Biol., 232 (2005), pp. 315–328.
[144] R. Ghigliazza, *Neuromechanical Models for Insect Locomotion*, Ph.D. thesis, Princeton University, Princeton, NJ, 2004.
[145] R. M. Ghigliazza, R. Altendorfer, P. Holmes, and D. Koditschek, *A simply stabilized running model*, SIAM J. Appl. Dynam. Systems, 2 (2003), pp. 187–218. Revised and updated version appeared in SIAM Rev., 47 (2005), pp. 519–549.
[146] R. M. Ghigliazza and P. Holmes, *Minimal models of bursting neurons: How multiple currents, conductances, and timescales affect bifurcation diagrams*, SIAM J. Appl. Dynam. Systems, 3 (2004), pp. 636–670.

[147] R. M. Ghigliazza and P. Holmes, *A minimal model of a central pattern generator and motoneurons for insect locomotion*, SIAM J. Appl. Dynam. Systems, 3 (2004), pp. 671–700.
[148] R. Ghigliazza and P. Holmes, *Towards a neuromechanical model for insect locomotion: Hybrid dynamical systems*, Regul. Chaotic Dyn., 10 (2005), pp. 193–225.
[149] C. Gilbert, *Visual control of cursorial prey pursuit by tiger beetles (Cicindelidae)*, J. Comp. Physiol. A, 181 (1997), pp. 217–230.
[150] M. Goldman, J. Golowasch, E. Marder, and L. Abbott, *Global structure, robustness, and modulation of neuronal models*, J. Neurosci., 21 (2001), pp. 5229–5238.
[151] H. Goldstein, *Classical Mechanics*, 2nd ed., Addison Wesley, Reading, MA, 1980.
[152] D. Golomb, J. Guckenheimer, and S. Gueron, *Reduction of a channel based model for a stomatogastric ganglion LP neuron*, Biol. Cybern., 69 (1993), pp. 129–137.
[153] M. Golubitsky and D. G. Schaeffer, *Singularities and Groups in Bifurcation Theory*, Vol. I, Springer-Verlag, New York, 1985.
[154] M. Golubitsky, I. Stewart, P. Buono, and J. Collins, *A modular network for legged locomotion*, Phys. D, 115 (1998), pp. 56–72.
[155] M. Golubitsky, I. Stewart, P. Buono, and J. Collins, *The role of symmetry in locomotor central pattern generators and animal gaits*, Nature, 401 (1999), pp. 693–695.
[156] M. Golubitsky, I. Stewart, and D. G. Schaeffer, *Singularities and Groups in Bifurcation Theory*, Vol. II, Springer-Verlag, New York, 1988.
[157] P. Gove, ed., *Webster's Third New International Dictionary of the English Language Unabridged*, Merriam, Springfield, MA, 1985.
[158] D. Graham, *Pattern and control of walking in insects*, in Advances in Insect Physiology, Vol. 18, Academic Press, London, UK, 1985, pp. 31–140.
[159] M. Graziano, C. Taylor, and T. Moore, *Complex movements evoked by microstimulation of prefrontal cortex*, Neuron, 34 (2002), pp. 841–851.
[160] A. Griewank, *Evaluating Derivatives: Principles and Techniques of Algorithmic Differentiation*, SIAM, Philadelphia, 2000.
[161] A. Griewank, D. Juedes, H. Mitev, J. Utke, O. Vogel, and A. Walther, *Adol-c: A package for the automatic differentiation of algorithms written in C/C++*, ACM Trans. Math. Software, 22 (1996), pp. 131–167, Algor. 755; see also http://www.math.tu-dresden.de/wir/project/adolc/.
[162] S. Grillner, *Neurobiological bases of rhythmic motor acts in vertebrates*, Science, 228 (1985), pp. 143–149.
[163] S. Grillner, *Bridging the gap—from ion channels to networks and behaviour*, Current Opinion in Neurobiol., 9 (1999), pp. 663–669.
[164] S. Grillner, P. Wallén, L. Brodin, and A. Lansner, *Neuronal network generating locomotor behavior in lamprey*, Ann. Rev. Neurosci., 14 (1991), pp. 169–199.
[165] J. Guckenheimer, *Isochrons and phaseless sets*, J. Math. Biol., 1 (1975), pp. 259–273.
[166] J. Guckenheimer and P. Holmes, *Nonlinear Oscillations, Dynamical Systems, and Bifurcations of Vector Fields*, Springer-Verlag, New York, 1983.
[167] J. Guckenheimer and B. Meloon, *Computing periodic orbits and their bifurcations with automatic differentiation*, SIAM J. Sci. Comput., 22 (2000), pp. 951–985.
[168] H. Haken, J. A. S. Kelso, and H. Bunz, *A theoretical model of phase transitions in human hand movements*, Biol. Cybern., 51 (1985), pp. 347–356.
[169] E. Hairer and G. Wanner, *Solving Ordinary Differential Equations* II: *Stiff and Differential Algebraic Problems*, Springer-Verlag, New York, 1991.
[170] J. Hancox and R. Pitman, *Plateau potentials drive axonal impulse bursts in insect motoneurons*, Proc. Roy. Soc. London Ser. B, 244 (1991), pp. 33–38.
[171] D. Hansel and G. Mato, *Phase dynamics for weakly coupled Hodgkin-Huxley neurons*, Europhys. Letters, 23 (1993), pp. 367–372.
[172] D. Hansel, G. Mato, and C. Meunier, *Phase reduction and neural modeling*, Concepts Neurosci., 4 (1993), pp. 192–210.
[173] D. Hansel, G. Mato, and C. Meunier, *Synchrony in excitatory neural networks*, Neural Comp., 7 (1995), pp. 307–337.
[174] H. Hatze, *A myocybernetic control model of skeletal muscle*, Biol. Cybernet., 25 (1977), pp. 103–119.
[175] N. Heglund, G. Cavagna, and C. Taylor, *Energetics and mechanics of terrestrial locomotion* III: *Energy changes of the centre of mass as a function of speed and body size in birds and mammals*, J. Exp. Biol., 97 (1982), pp. 41–56.
[176] N. Heglund and C. Taylor, *Speed, stride frequency and energy cost per stride. How do they change with body size and gait?*, J. Exp. Biol., 138 (1988), pp. 301–318.

[177] N. Heglund, C. Taylor, and T. McMahon, *Scaling stride frequency and gait to animal size: Mice to horses*, Science, 186 (1974), pp. 1112–1113.
[178] A. Hill, *The heat of shortening and the dynamic constants of muscle*, Proc. Roy. Soc. London Ser. B, 126 (1938), pp. 136–195.
[179] J. Hindmarsh and R. Rose, *A model of neuronal bursting using three coupled first order differential equations*, Proc. Roy. Soc. London Ser. B, 221 (1984), pp. 87–102.
[180] A. Hodgkin and A. Huxley, *A quantitative description of membrane current and its application to conduction and excitation in nerve*, J. Physiol., 117 (1952), pp. 500–544.
[181] P. Holmes, *Poincaré, celestial mechanics, dynamical systems theory and "chaos,"* Phys. Rep., 193 (3) (1990), pp. 137–163.
[182] M. Höltje and R. Hustert, *Rapid mechano-sensory pathways code leg impact and elicit very rapid reflexes in insects*, J. Exp. Biol., 206 (2003), pp. 2715–2724.
[183] F. Hoppensteadt and E. Izhikevich, *Weakly Connected Neural Networks*, Springer-Verlag, New York, 1997.
[184] D. Hoyt and C. Taylor, *Gait and the energetics of locomotion in horses*, Nature, 292 (1981), pp. 239–240.
[185] R. Huey, *Phylogeny, history and the comparative method*, in Directions in Ecological Physiology, M. Feder, A. Bennett, W. Burggren, and R. Huey, eds., Cambridge University Press, Cambridge, UK, 1988, pp. 76–97.
[186] G. Hughes, *The co-ordination of insect movements.* I. *The walking movement of insects*, J. Exp. Biol., 29 (1952), pp. 267–284.
[187] A. Huxley, *Muscular contraction*, J. Physiol., 243 (1974), pp. 1–43.
[188] A. Ijspeert, *A connectionist central pattern generator for the aquatic and terrestrial gaits of a simulated salamander*, Biol. Cybern., 84 (2001), pp. 331–348.
[189] A. Ijspeert and J. Kodjabachian, *Evolution and development of a central pattern generator for the swimming of a lamprey*, Artificial Life, 5 (1999), pp. 247–269.
[190] Y. Ivanenko, R. Grasso, V. Macellari, and F. Lacquaniti, *Two-thirds power law in human locomotion: Role of ground contact forces*, Neuroreport, 13 (2002), pp. 1171–1174.
[191] A. Jayes and R. Alexander, *Mechanics of locomotion of dogs (Canis familiaris) and sheep (Ovis aries)*, J. Zool. London, 185 (1978), pp. 289–308.
[192] D. Jindrich and R. Full, *Dynamic stabilization of rapid hexapedal locomotion*, J. Exp. Biol., 205 (2002), pp. 2803–2823.
[193] D. Johnston and S.-S. Wu, *Foundations of Cellular Neurophysiology*, MIT Press, Cambridge, MA, 1995.
[194] C. Jones, *Geometric Singular Perturbation Theory*, Lecture Notes in Math. 1609, C.I.M.E. Lectures, Springer-Verlag, Heidelberg, 1994.
[195] S. Jones, B. Mulloney, T. Kaper, and N. Kopell, *Coordination of cellular pattern-generating circuits that control limb movements: The sources of stable differences in intersegmental phases*, J. Neurosci., 23 (2003), pp. 3457–3468.
[196] R. Josephson, *Contraction dynamics and power output of skeletal muscle*, Ann. Rev. Physiol., 55 (1993), pp. 527–546.
[197] R. Jung, T. Kiemel, and A. Cohen, *Dynamic behavior of a neural network model of locomotor control in the lamprey*, J. Neurophys., 75 (1996), pp. 1074–1086.
[198] E. Kandel, J. Schwartz, and T. Jessel, *Principles of Neuroscience*, 3rd ed., Appleton and Lange, Norwalk, CT, 1991.
[199] M. Kawato, *Internal models for motor control and trajectory planning*, Current Opinion in Neurobiol., 9 (1999), pp. 718–727.
[200] J. Keener and J. Sneyd, *Mathematical Physiology*, Springer-Verlag, New York, 1998.
[201] J. Kelso, P. W. Fink, C. DeLaplain, and R. Carson, *Haptic information stabilizes and destabilizes coordination dynamics*, Proc. Roy. Soc. London Ser. B, 268 (2001), pp. 1207–1213.
[202] T. Kepler, L. Abbott, and E. Marder, *Reduction of conductance-based neuron models*, Biol. Cybern., 66 (1992), pp. 381–387.
[203] T. Kiemel and A. Cohen, *Estimation of coupling strength in regenerated lamprey spinal cords based on a stochastic phase model*, J. Comput. Neurosci., 5 (1998), pp. 267–284.
[204] T. Kindermann, *Behavior and adaptability of a six-legged walking system with highly distributed control*, Adaptive Behavior, 9 (2002), pp. 16–41.
[205] E. Klavins and D. Koditschek, *Phase regulation of decentralized cyclic robotic systems*, Int. J. Robotics Res., 3 (2002), pp. 257–275.
[206] E. Klavins, H. Komsuoglu, D. Koditschek, and R. Full, *Coordination and control for locomotion*, in Neurotechnology for Biomimetic Robots, A. Rudolph, ed., MIT Press, Boston, MA, 2001, pp. 351–382.

[207] D. Koditschek and M. Buehler, *Analysis of a simplified hopping robot*, Int. J. Robotics Res., 10 (1991), pp. 587–605.
[208] D. Koditschek, R. Full, and M. Buehler, *Mechanical aspects of legged locomotion control*, Arthropod Structure and Development, 33 (2004), pp. 251–272.
[209] H. Komsuoglu, D. McMordie, U. Saranli, N. Moore, M. Buehler, and D. Koditschek, *Proprioceptive-based behavioral advances in a hexapod robot*, in Proceedings of the IEEE International Conference on Robotics and Automation, IEEE Press, Piscataway, NJ, 2001, pp. 3650–3655.
[210] N. Kopell, *Toward a theory of modelling central pattern generators*, in Neural Control of Rhythmic Movements in Vertebrates, A. Cohen, S. Rossignol, and S. Grillner, eds., Wiley, New York, 1988, pp. 369–413.
[211] N. Kopell and G. B. Ermentrout, *Phase transitions and other phenomena in chains of coupled oscillators*, SIAM J. Appl. Math., 50 (1990), pp. 1014–1052.
[212] N. Kopell, G. B. Ermentrout, and T. L. Williams, *On chains of oscillators forced at one end*, SIAM J. Appl. Math., 51 (1991), pp. 1397–1417.
[213] N. Kopell and G. LeMasson, *Rhythmogenesis, amplitude modulation, and multiplexing in a cortical architecture*, Proc. Natl. Acad. Sci. USA, 91 (1994), pp. 10586–10590.
[214] R. Kram, B. Wong, and R. Full, *Three-dimensional kinematics and limb kinetic energy of running cockroaches*, J. Exp. Biol., 200 (1997), pp. 1919–1929.
[215] H. Krebs, *For many problems there is an animal on which it can be most conveniently studied*, J. Exp. Zool., 194 (1975), pp. 221–226.
[216] T. Kubow and R. Full, *The role of the mechanical system in control: A hypothesis of self-stabilization in hexapedal runners*, Philos. Trans. Roy. Soc. London Ser. B, 354 (1999), pp. 849–861.
[217] A. Kuo, *Stabilization of lateral motion in passive dynamic walking*, Int. J. Robotics Res., 18 (1999), pp. 917–930.
[218] A. Kuo, *The relative roles of feedforward and feedback in the control of rhythmic movements*, Motor Control, 6 (2002), pp. 129–145.
[219] F. Lacquaniti, R. Grasso, and M. Zago, *Motor patterns in walking*, News Physiol. Sci., 14 (1999), pp. 168–174.
[220] F. Lacquaniti, C. Terzuolo, and P. Viviani, *The law relating the kinematic and figural aspects of drawing movements*, Acta Psychol., 54 (1983), pp. 115–130.
[221] A. Lamperski, O. Loh, B. Kutscher, and N. Cowan, *Dynamical wall-following for a wheeled robot using a passive tactile sensor*, in Proceedings of the IEEE International Conference on Robotics and Automation, 2005.
[222] G. Larsen, S. Frazier, and S. Zill, *The tarso-pretarsal chordotonal organ as an element in cockroach walking*, J. Comp. Physiol., 180 (1997), pp. 683–700.
[223] G. Lauder, *Evolutionary innovations and constraints: Functional analyses and phylogenetic test*, J. Morphology, 248 (2001), p. 201.
[224] A. Lewis, J. Ostrowski, R. Murray, and J. Burdick, *Nonholonomic mechanics and locomotion: The snakeboard example*, in International Conference on Robotics and Automation, IEEE Press, Piscataway, NJ, 1994, pp. 2391–2400.
[225] T. Lewis and J. Rinzel, *Dynamics of spiking neurons connected by both inhibitory and electrical coupling*, J. Comput. Neurosci., 14 (2003), pp. 283–309.
[226] C.-S. Li, C. Padoa-Schioppa, and E. Bizzi, *Neuronal correlates of motor performance and motor learning in the primary motor cortex of monkeys adapting to an external force field*, Neuron, 30 (2001), pp. 593–607.
[227] G. Loeb, I. Brown, and E. Cheng, *A hierarchical foundation for models of sensorimotor control*, Exp. Brain Res., 126 (1999), pp. 1–18.
[228] I. Malkin, *Methods of Poincaré and Linstedt in the Theory of Nonlinear Oscillations*, Gostexisdat, Moscow, 1949 (in Russian).
[229] I. Malkin, *Some Problems in Nonlinear Oscillation Theory*, Gostexisdat, Moscow, 1956 (in Russian).
[230] E. Mallett, G. Yamaguci, J. Birch, and K. Nishikawa, *Feeding motor patterns in Anurans: Insight from biomechanical modeling*, Amer. Zool., 41 (2001), pp. 1364–1374.
[231] C. Mangum and P. Hochachka, *New directions in comparative physiology and biochemistry: Mechanisms, adaptations, and evolution*, Physiol. Zool., 71 (1998), pp. 471–484.
[232] E. Marder, *Motor pattern generation*, Current Opinion in Neurobiol., 10 (2000), pp. 691–698.
[233] R. Margaria, *Biomechanics and Energetics of Muscular Exercise*, Oxford University Press, Oxford, UK, 1976.
[234] J. Marsden, *Lectures on Mechanics*, London Math. Soc. Lecture Note Ser. 174, Cambridge University Press, Cambridge, UK, 1992.

[235] J. Marsden and T. Ratiu, *Introduction to Mechanics and Symmetry*, 2nd ed., Springer-Verlag, New York, 1999.
[236] T. McGeer, *Passive bipedal running*, Proc. Roy. Soc. London Ser. B, 240 (1990), pp. 107–134.
[237] T. McGeer, *Passive dynamic walking*, Int. J. Robotics Res., 9 (1990), pp. 62–82.
[238] T. McGeer, *Passive walking with knees*, in Proceedings of the IEEE International Conference on Robotics and Automation, Cincinnati, OH, 1990, IEEE Press, Piscataway, NJ, pp. 1640–1645.
[239] T. McGeer, *Principles of walking and running*, in Advances in Comparative and Environmental Physiology, Vol. 11: Mechanics of Animal Locomotion, R. Alexander, ed., Springer-Verlag, Berlin, 1992, pp. 113–139.
[240] T. McGeer, *Dynamics and control of bipedal locomotion*, J. Theoret. Biol., 16 (1993), pp. 277–314.
[241] R. McGehee, *Triple collisions in Newtonian gravitational systems*, in Dynamical Systems, Theory and Applications, J. Moser, ed., Lecture Notes in Phys. 38, Springer-Verlag, Berlin, 1975, pp. 550–572.
[242] T. McMahon, *Muscles, Reflexes and Locomotion*, Princeton University Press, Princeton, NJ, 1984.
[243] T. McMahon and J. Bonner, *On Size and Life*, Scientific American Books/W.H. Freeman, New York, 1983.
[244] T. McMahon and G. Cheng, *The mechanics of running: how does stiffness couple with speed?*, J. Biomechanics, 23 (suppl 1) (1990), pp. 65–78.
[245] K. Meijer. *Personal communication*, 2001.
[246] K. Meijer, H. Grootenboer, H. Koopman, B. van der Linden, and P. Huijing, *A Hill type model of rat medial gastrocnemius muscle that accounts for shortening history effects*, J. Biomech., 31 (1998), pp. 555–564.
[247] S. Mochon and T. McMahon, *Ballistic walking*, J. Biomech., 13 (1980), pp. 49–57.
[248] S. Mochon and T. McMahon, *Ballistic walking: An improved model*, Math. Biosci., 52 (1981), pp. 241–260.
[249] K. Mombaur, R. Longman, H. Bock, and J. Schlöder, *Stable one-legged hopping without feedback and with a point foot*, in Proceedings of the IEEE International Conference on Robotics and Automation, Vol. 4, 2002, pp. 3978–3983.
[250] C. Morris and H. Lécar, *Voltage oscillations in the barnacle giant muscle*, Biophys. J., 35 (1981), pp. 193–213.
[251] J. Murray, *Mathematical Biology*, 3rd ed., Springer-Verlag, New York, 2001.
[252] F. Mussa-Ivaldi, *Modular features of motor control and learning*, Current Opinion in Neurobiol., 9 (1999), pp. 713–717.
[253] Y. Nakamura, *Advanced Robotics: Redundancy and Optimization*, Addison-Wesley, Reading, MA, 1991.
[254] J. Nakanishi, T. Fukuda, and D. Koditschek, *A brachiating robot controller*, IEEE Trans. Robotics and Automat., 16 (2000), pp. 109–123.
[255] J. Neĭmark and N. Fufaev, *Dynamics of Nonholonomic Systems*, AMS, Providence, RI, 1972.
[256] J. Ostrowski and J. Burdick, *Gait kinematics for a serpentine robot*, in International Conference on Robotics and Automation, IEEE Press, 1996, Piscataway, NJ, pp. 1294–1299.
[257] K. Pearson, *Central programming and reflex control of walking in the cockroach*, J. Exp. Biol., 56 (1972), pp. 173–193.
[258] K. Pearson, *Common principles of motor control in vertebrates and invertebrates*, Ann. Rev. Neurosci., 16 (1993), pp. 265–297.
[259] K. Pearson, *Proprioceptive regulation of locomotion*, Current Opinion in Neurobiol., 5 (1995), pp. 786–791.
[260] K. Pearson, *Motor systems*, Current Opinion in Neurobiol., 10 (2000), pp. 649–654.
[261] K. Pearson and J. Iles, *Discharge patterns of coxal levator and depressor motoneurones in the cockroach* periplaneta americana, J. Exp. Biol., 52 (1970), pp. 139–165.
[262] K. Pearson and J. Iles, *Innervation of the coxal depressor muscles in the cockroach* periplaneta americana, J. Exp. Biol., 54 (1971), pp. 215–232.
[263] K. Pearson and J. Iles, *Nervous mechanisms underlying intersegmental co-ordination of leg movements during walking in the cockroach*, J. Exp. Biol., 58 (1972), pp. 725–744.
[264] K. Pearson, R. Wong, and C. Fourtner, *Connections between hairplate afferents and motoneurons in the cockroach leg*, J. Exp. Biol., 64 (1976), pp. 251–266.

[265] E. Phipps, *Taylor Series Integration of Differential-Algebraic Equations: Automatic Differentiation as a Tool for Simulating Rigid Body Mechanical Systems*, Ph.D. thesis, Cornell University, Ithaca, NY, 2003.

[266] I. Poulakakis, J. Smith, and M. Buehler, *Experimentally validated bounding models for the Scout* II *quadrupedal robot*, in International Conference on Robotics and Automation, Vol. 3, IEEE Press, Piscataway, NJ, 2004, pp. 2595–2600.

[267] I. Poulakakis, J. Smith, and M. Buehler, *Modeling and experiments of untethered quadrupedal running with a bounding gait: The Scout* II *robot*, Int. J. Robotics Res., 24 (2005), pp. 239–256.

[268] M. Raibert, *Legged Robots that Balance*, MIT Press, Cambridge, MA, 1986.

[269] M. Raibert, M. Chepponis, and H. Brown Jr, *Running on four legs as though they were one*, IEEE J. Robotics and Automat., 2 (1986), pp. 70–82.

[270] M. Reed, *Why is mathematical biology so hard?*, AMS Notices, 51 (2004), pp. 338–342.

[271] M. Richardson and T. Flash, *Comparing smooth arm movements with the two-thirds power law and the related segmented-control hypothesis*, J. Neurosci., 22 (2002), pp. 8201–8211.

[272] A. Ridgel, S. Frazier, R. A. DiCaprio, and S. Zill, *Encoding of forces by cockroach tibial campaniform sensilla: Implications in dynamic control of posture and locomotion*, J. Comp. Physiol. A, 186 (1998), pp. 359–374.

[273] R. Riener and J. Quintern, *A physiologically based model of muscle activation verified by electrical stimulation*, Bioelectrochemistry and Bioenergetics, 43 (1997), pp. 257–264.

[274] J. Rinzel, *A formal classification of bursting mechanisms in excitable systems*, in Mathematical Topics in Population Biology, Morphogenesis, and Neurosciences, E. Teramoto and M. Yamaguti, eds., Lecture Notes in Biomath., Springer-Verlag, New York, 1987, pp. 267–281.

[275] J. Rinzel and G. Ermentrout, *Analysis of excitability and oscillations*, in Methods in Neuronal Modeling: From Ions to Networks, C. Koch and I. Segev, eds., MIT Press, Cambridge, MA, 1999, Chap. 7, pp. 251–291.

[276] J. Rinzel and Y. Lee, *On different mechanisms for membrane potential bursting*, in Nonlinear Oscillations in Biology and Chemistry, H. Othmer, ed., Lecture Notes in Biomath. 66, Springer-Verlag, Berlin, 1986, pp. 19–33.

[277] J. Rinzel and Y. Lee, *Dissection of a model for neuronal parabolic bursting*, J. Math. Biol., 25 (1987), pp. 653–675.

[278] R. Ritzmann, S. Gorb, and R. D. Quinn, eds., *Arthropod locomotion systems: From biological materials and systems to robotics*, Arthropod Structure and Development, 33 (2004), special issue.

[279] A. Rizzi and D. Koditschek, *Further progress in robot juggling: Solvable mirror laws*, in Proceedings of the International Conference on Robotics and Automation, IEEE Press, Piscataway, NJ, 1994, pp. 2935–2940.

[280] H. Robinson and N. Kawai, *Injection of digitally-synthesized synaptic conductance transients to measure the integrative properties of neurons*, J. Neurosci. Methods, 49 (1993), pp. 157–165.

[281] R. Rose and J. Hindmarsh, *The assembly of ionic currents in a thalamic neuron* I: *The three-dimensional model*, Proc. Roy. Soc. London Ser. B, 237 (1989), pp. 267–288.

[282] A. Ruina, *Non-holonomic stability aspects of piecewise holonomic systems*, Rep. Math. Phys., 42 (1998), pp. 91–100.

[283] P. Saltiel, K. Wyler-Duda, A. D'Avella, M. Tresch, and E. Bizzi, *Muscle synergies encoded within the spinal cord: Evidence from focal intraspinal NMDA iontophoresis in the frog*, J. Neurophys., 85 (2001), pp. 605–619.

[284] U. Saranli, M. Buehler, and D. Koditschek, *RHex: A simple and highly mobile hexapod robot*, Int. J. Robotics Res., 20 (2001), pp. 616–631.

[285] U. Saranli and D. Koditschek, *Template based control of hexapedal running*, in Proceedings of the IEEE International Conference on Robotics and Automation, Vol. 1, Taipei, Taiwan, IEEE Press, Piscataway, NJ, 2003, pp. 1374–1379.

[286] U. Saranli, W. Schwind, and D. Koditschek, *Toward the control of a multi-jointed, monoped runner*, in Proceedings of the IEEE International Conference on Robotics and Automation, Leuven, Belgium, IEEE Press, Piscataway, NJ, 1998, pp. 2676–2682.

[287] S. Schaal and D. Sternad, *Origins and violations of the* 2/3 *power law in rhythmic three-dimensional arm movements*, Exp. Brain Res., 136 (2001), pp. 60–72.

[288] S. Schaal, D. Sternad, and C. Atkeson, *One-handed juggling: A dynamical approach to a rhythmic movement task*, J. Motor Behavior, 28 (1996), pp. 165–183.

[289] K. Schmidt-Nielsen, *Scaling: Why Is Animal Size So Important?*, Cambridge University Press, New York, 1984.

[290] J. Schmitt, M. Garcia, R. Razo, P. Holmes, and R. Full, *Dynamics and stability of legged locomotion in the horizontal plane: A test case using insects*, Biol. Cybern., 86 (2002), pp. 343–353.

[291] J. Schmitt and P. Holmes, *Mechanical models for insect locomotion: Dynamics and stability in the horizontal plane—Theory*, Biol. Cybern., 83 (2000), pp. 501–515.

[292] J. Schmitt and P. Holmes, *Mechanical models for insect locomotion: Dynamics and stability in the horizontal plane—Application*, Biol. Cybern., 83 (2000), pp. 517–527.

[293] J. Schmitt and P. Holmes, *Mechanical models for insect locomotion: Stability and parameter studies*, Phys. D, 156 (2001), pp. 139–168.

[294] J. Schmitt and P. Holmes, *Mechanical models for insect locomotion: Active muscles and energy losses*, Biol. Cybern., 89 (2003), pp. 43–55.

[295] A. Schwartz and D. Moran, *Motor cortical activity during drawing movements: Population representation during lemniscate tracing*, J. Neurophys., 82 (1999), pp. 2705–2718.

[296] W. Schwind, *Spring Loaded Inverted Pendulum Running: A Plant Model*, Ph.D. thesis, University of Michigan, Ann Arbor, MI, 1998.

[297] W. Schwind and D. Koditschek, *Characterization of monoped equilibrium gaits*, in Proceedings of the IEEE International Conference on Robotics and Automation, Albuquerque, NM, IEEE Press, Piscataway, NJ, 1997, pp. 1986–1992.

[298] W. Schwind and D. Koditschek, *Approximating the stance map of a 2 DOF monoped runner*, J. Nonlinear Sci., 10 (2000), pp. 533–568.

[299] J. Seipel and P. Holmes, *Running in three dimensions: Analysis of a point-mass springy-leg model*, Int. J. Robotics Res., 24 (2005), pp. 657–674.

[300] J. Seipel and P. Holmes, *Three-dimensional dynamics and stability of multi-legged runners*, Int. J. Robotics Res., submitted.

[301] J. Seipel and P. Holmes, *Three-dimensional running is unstable but easily stabilized*, in Climbing and Walking Robots: Proceedings of the 7th International Conference CLAWAR 2004, M. A. Armada and P. González de Santos, eds., Springer-Verlag, Berlin, 2005, pp. 585–592.

[302] J. Seipel, P. Holmes, and R. Full, *Dynamics and stability of insect locomotion: A hexapedal model for horizontal plane motions*, Biol. Cybern., 91 (2004), pp. 76–90.

[303] A. Selverston, R. Elson, M. Rabinovich, R. Huerta, and H. Abarbanel, *Basic principles for generating motor output in the stomatogastric ganglion*, in Neuronal Mechanisms for Generating Locomotor Activity, O. Kiehn, R. M. Harris-Warrick, L. M. Jordan, H. Hultborn, and N. Kudo, eds., Ann. New York Acad. Sci. 860, New York Academy of Sciences, New York, 1998, pp. 35–50.

[304] A. Seyfarth and H. Geyer, *Natural control of spring-like running—optimized self-stabilization*, in Proceedings of the Fifth International Conference on Climbing and Walking Robots (CLAWAR 2002), Professional Engineering Publishing Limited, 2002, pp. 81–85.

[305] A. Seyfarth, H. Geyer, R. Blickhan, and H. Herr, *Does leg retraction simplify control in running?*, in the Fourth World Congress of Biomechanics, Calgary, Canada, Omnipress, 2002 (CD-ROM).

[306] A. Seyfarth, H. Geyer, M. Günther, and R. Blickhan, *A movement criterion for running*, J. Biomech., 35 (2002), pp. 649–655.

[307] A. Seyfarth, H. Geyer, and H. Herr, *Swing leg retraction: A simple control model for stable running*, J. Exp. Biol., 206 (2003), pp. 2547–2555.

[308] A. Sharp, M. O'Neil, L. Abbott, and E. Marder, *Dynamic clamp: Computer-generated conductances in real neurons*, J. Neurophys., 69 (1993), pp. 992–995.

[309] A. Sharp, F. Skinner, and E. Marder, *Mechanisms of oscillation in dynamic clamp constructed two-cell half-center circuits*, J. Neurophys., 76 (1996), pp. 867–883.

[310] Y. Sinai, *Hyperbolic billiards*, in Proceedings of the International Congress of Mathematicians, Kyoto, 1990, Vol. I, Springer-Verlag, Berlin, 1991, pp. 249–260.

[311] D. Singer, *Stable orbits and bifurcations of maps of the interval*, SIAM J. Appl. Math., 35 (1978), pp. 260–267.

[312] P. Swanson, R. Burridge, and D. Koditschek, *Global asymptotic stability of a passive juggler: A parts feeding strategy*, Math. Probab. Engrg., 1 (1995), pp. 193–224.

[313] S. P. Swinnen, *Intermanual coordination: From behavioural principles to neural-network interactions*, Nature Neurosci., 3 (2002), pp. 348–359.

[314] F. Theunissen and J. Miller, *Temporal encoding in nervous systems—a rigorous definition*, J. Comput. Neurosci., 2 (1995), pp. 149–162.

[315] F. Theunissen, J. Roddey, S. Stufflebeam, H. Clague, and J. Miller, *Information theoretic analysis of dynamical encoding by four primary sensory interneurons in the cricket cercal system*, J. Neurophys., 75 (1996), pp. 1345–1359.
[316] J. Thompson, *Instabilities and Catastrophes in Science and Engineering*, Wiley, New York, 1982.
[317] L. Ting, R. Blickhan, and R. Full, *Dynamic and static stability in hexapedal runners*, J. Exp. Biol., 197 (1994), pp. 251–269.
[318] E. Todorov, *Direct cortical control of muscle activation in voluntary arm movements: A model*, Nature Neurosci., 3 (2000), pp. 391–398.
[319] E. Todorov and M. Jordan, *Smoothness maximization along a predefined path accurately predicts the speed profiles of complex arm movements*, J. Neurophys., 80 (1998), pp. 696–714.
[320] E. Todorov and M. Jordan, *Optimal feedback control as a theory of motor coordination*, Nature Neurosci., 5 (2002), pp. 1226–1235.
[321] A. Tryba and R. Ritzmann, *Multi-joint coordination during walking and foothold searching in the Blaberus cockroach.* I. *Kinematics and electromyograms*, J. Neurophys., 83 (2000), pp. 3323–3336.
[322] A. Tryba and R. Ritzmann, *Multi-joint coordination during walking and foothold searching in the Blaberus cockroach.* II. *Extensor motor patterns*, J. Neurophys., 83 (2000), pp. 3337–3350.
[323] V. Utkin, *Variable structure systems with sliding modes*, IEEE Trans. Automat. Control, AC-22 (1977), pp. 212–231.
[324] F. Valero-Cuevas, *Large index-fingertip forces are produced by subject-independent patterns of muscle excitation*, J. Biomech., 31 (1998), pp. 693–703.
[325] F. Valero-Cuevas, *Predictive modulation of muscle coordination pattern magnitude scales fingertip force magnitude over the voluntary range*, J. Neurophys., 83 (2000), pp. 1469–1479.
[326] F. Valero-Cuevas, *An integrative approach to the biomechanical function and neuromuscular control of the fingers*, J. Biomech., 38 (2005), pp. 673–684.
[327] F. Valero-Cuevas, N. Smaby, M. Venkadesan, M. Peterson, and T. Wright, *The strength-dexterity test as a measure of dynamic pinch performance*, J. Biomech., 36 (2003), pp. 265–270.
[328] K. Waldron, *Force and motion management in legged locomotion*, IEEE J. Robotics and Automat., RA-2 (1986), pp. 214–220.
[329] K. J. Waldron and V. J. Vohnout, *Configuration design of the adaptive suspension vehicle*, Int. J. Robotics Res., 3 (1984), pp. 37–48.
[330] J. Watson and R. Ritzmann, *Leg kinematics and muscle activity during treadmill running in the cockroach, blaberus discoidalis.* I. *Slow running*, J. Comp. Physiol. A, 182 (1998), pp. 11–22.
[331] J. Watson and R. Ritzmann, *Leg kinematics and muscle activity during treadmill running in the cockroach, blaberus discoidalis.* II. *Transition to fast running*, J. Comp. Physiol. A, 182 (1998), pp. 23–33.
[332] B. Webb, R. Harrison, and M. Willis, *Sensorimotor control of navigation in arthropod and artificial systems*, Arthropod Structure and Development, 33 (2004), pp. 301–329.
[333] J. Weingarten, R. Groff, and D. Koditschek, *A framework for the coordination of legged robot gaits*, in Proceedings of the IEEE Conference on Robotics, Automation and Mechatronics, IEEE Press, Singapore, 2004, pp. 679–686.
[334] E. Westervelt, J. Grizzle, and D. Koditschek, *Hybrid zero dynamics of planar biped walkers*, IEEE Trans. Automat. Control, 48 (2003), pp. 42–56.
[335] S. Wickl, D. Hoyt, E. Cogger, and G. Myers, *The energetics of the trot-gallop transition*, J. Exp. Biol., 206 (2003), pp. 1557–1564.
[336] D. Wilson, *Insect walking*, Ann. Rev. Entomol., 7 (1966), pp. 103–122.
[337] D. Wilson, *An approach to the problem of control of rhythmic behavior*, in Invertebrate Nervous System, C. Wiersma, ed., The University of Chicago Press, Chicago, IL, 1967, Chap. 17, pp. 219–229.
[338] A. Winfree, *The Geometry of Biological Time*, Springer-Verlag, New York, 2001.
[339] R. Wong and K. Pearson, *Properties of the trochanteral hair plate and its function in the control of walking in the cockroach*, J. Exp. Biol., 64 (1976), pp. 233–249.
[340] C. Woolsey and N. Leonard, *Stabilizing underwater vehicle motion using internal rotors*, Automatica, 38 (2002), pp. 2053–2062.
[341] P. Wriggers, *Computational Contact Mechanics*, Wiley, New York, 2002.

[342] X. Xu, W. Cheng, D. Dudek, M. Cutkosky, M. Hatanaka, and R. Full, *Material modeling for shape deposition manufacturing of biomimetic components*, in ASME Proceedings, DETC/DFM 2000, Baltimore, MD, 2000.

[343] F. Zajac, *Muscle and tendon: Properties, models, scaling, and application to biomechanics and motor control*, Critical Rev. Biomed. Eng., 17 (1989), pp. 359–411.

[344] E. Zehr and R. Stein, *What functions do reflexes serve during human locomotion?*, Prog. Neurobiol., 58 (1999), pp. 185–205.

[345] S. Zill, *Proprioceptive feedback and the control of cockroach walking*, in Feedback and Motor Control in Invertebrates and Vertebrates, W. Barnes and M. Galden, eds., Croom Helm, London, 1985, pp. 187–208.

[346] S. Zill, *Mechanoreceptors: Exteroceptors and proprioceptors*, in Cockroaches as Models for Neurobiology: Applications in Biomedical Research, Vol. 2, I. Huber, E. P. Masler, and B. R. Rao, eds., CRC Press, Boca Raton, FL, 1990, Chap. 25, pp. 247–267.

[347] S. Zill, J. Schmitz, and A. Büschges, *Load sensing and control of posture and locomotion*, Arthropod Structure and Development, 33 (2004), pp. 273–286.